Novel Molecular Insights into Stimulus-secretion Coupling in the Adrenal Medulla

by

Alina Chapman-Morales

A dissertation submitted in partial fulfillment
of the requirements for the degree of
Doctor of Philosophy
(Pharmacology)
in the University of Michigan
2021

Doctoral Committee:

Associate Professor Arun Anantharam, Chair
Professor Lori L. Isom
Assistant Professor Paul Jenkins
Professor Alan Smrcka
Associate Professor Sarah Veatch

Alina J. Chapman-Morales
alinamor@umich.edu

ORCID iD: 0000-0002-3627-9205

Acknowledgements

First, I would like to thank my undergraduate research mentor, Dr. Rachel Powers, who sparked my passion for research and helped nurture my confidence to pursue a PhD. Without your leadership, kindness, and infectious passion for research, I would not have had the opportunities I have today. I would also like to thank my current mentor, Dr. Arun Anantharam, for giving me the opportunity for independence, leadership and responsibility while conducting my graduate studies. My perception of what I am capable of has improved dramatically during my time in the lab. I would like to also thank Dr. Mounir Bendahmane, who was my first post-doc mentor in the Anantharam lab. Thank you for teaching me to be a rigorous scientist, critical of my research and always being willing to help me, whether it was with my experiments or with life advice. Your continued support, mentorship and friendship are so appreciated.

Next, I would like to thank Shreeya Bakshi, Maha Hamed and Chante Liu, with whom I have shared many lab experiences. Without your friendship, support, kindness, and constant laughter you brought to my life during graduate school, I do not think I would have made it this far.

Finally, I would like to thank my family and friends. To my parents, Cristina and Gabriel Morales, thank you for giving me the example of hard work and self-discipline which was of particular importance on my journey to becoming a scientist. I would also like to thank my best friends, Teresa Scerback, RoseMary Margarites and Sophia Benedetto, for your understanding, love and support and being a constant in my life since we met.

Table of Contents

Acknowledgements **ii**

List of Figures **iv**

List of Abbreviations **vi**

Abstract **viii**

Chapter I: General Introduction **1**

References 15

Chapter II: Synaptotagmin-7 Enhances Calcium-sensing of Chromaffin Cell Granules and Slows Discharge of Granule Cargos **21**

Materials and methods 24
Results 41
Discussion 48
References 71

Chapter III: Acetylcholine and PACAP Activate Chromaffin Cell Secretion by Signaling Through Unique and Parallel Pathways, Resulting in Phenotypically Different Fusion Events **76**

Materials and methods 79
Results 84
Discussion 91
References 104

Chapter IV: General Discussion **108**

References 118

List of Figures

2.1 Endogenous Syt-7 is co-localized with PAI-1, a protein of the granule dense core 55

2.2 Syt-7 slows release of lumenal cargos 56

2.3 Syt-7 endows granules with an increased fusion probability 57

2.4 Syt-7 slows release of over-expressed NPY in cells stimulated with ACh. WT and Syt-7 KO cells over-expressing NPY were stimulated with 100 μM ACh for 2 min 58

2.5 Granules in Syt-7 KO cells stimulated by ACh evince a lower fusion probability than those in WT cells. WT and Syt-7 KO cells over-expressing GFP-tagged NPY were stimulated with 100 μM ACh for 2 min 59

2.6 Syt-7 is necessary to sustain secretion during prolonged ACh stimulation 60

2.7 In vitro fusion of Syt-7 and Syt-1 granules on planar supported bilayers 61

2.8 Chromaffin cells require Syt-7 for sustained secretory activity during cholinergic stimulation 62

2.1s Mouse chromaffin cells 24 hours after plating on Matrigel coated glass bottom dishes 63

2.2s Validation of immunocytochemical-staining method using two primary antibodies raised in rabbit 64

2.3s Sub-cellular fractionation results 65

2.4s Expression of Syt-1, TH, NPY and tPA transcripts in WT and Syt-7 KO chromaffin cells 66

2.5s NPY-pHl was overexpressed in WT and Syt-7 KO chromaffin cells 67

2.6s An analysis of granule motion in WT and Syt-7 KO cells 68

2.7s Cholinergic currents and depolarization-evoked Ca^{2+} currents are similar in WT and KO cells 69

2.8s Images from individual NPYmRuby release events 70

3.1 PACAP stimulation prolongs fusion time compared to ACh stimulation 96

3.2 PACAP stimulation led to more cavicapture events than ACh stimulation 97

3.3 PACAP-stimulated calcium influx utilizes low voltage gated T-type channels 98

3.4 PACAP stimulated increase in calcium levels rely on extracellular calcium influx and EPAC signaling 99

3.5 PLCε is required for PACAP stimulated calcium influx and ultimately, chromaffin cell exocytosis 100

3.6 Expression levels and cAMP production of WT and PLCε KO cells 102

3.7 Lack of Syt-7 hinders cholinergic and PACAP-stimulated secretion 103

4.1 Signaling summary figure 117

List of Abbreviations

ACh: acetylcholine

BSA: Bovine serum albumin

cAMP: cyclic AMP

DAG: Diacylglycerol

DTT: Dithiothreitol

EPAC: exchange protein activated by cAMP

FFN: fluorescent false neurotransmitter

GPCR: G-protein coupled receptor

NSF: N-ethylmaleimide-sensitive factor

IP_3: Inositol triphosphate

KO: knock out

nACh: nicotinic acetylcholine

NPY: neuropeptide Y

PACAP: pituitary adenylate cyclase activating polypeptide

PIP_2: Phosphatidylinositol 4,5-bisphosphate

PLCε: phospholipase C epsilon

SNAP: Soluble NSF attachment proteins

SNARE: SNAP receptor

SSR: sympathetic stress response

Syt: synaptotagmin

TIRF: total internal reflection fluorescence

tPA: tissue plasminogen activator

VMAT: vesicular monoamine transporter

WT: wild type

Abstract

The adrenal medulla is an important branch of the sympathetic nervous system. Chromaffin cells, which serve as the secretory units of the medulla, receive direct sympathetic innervation via the splanchnic nerves. Secretion from the medulla is primarily caused by two neurotransmitters – acetylcholine (ACh) and pituitary adenylate cyclase activating polypeptide (PACAP) – released from splanchnic nerve terminals. ACh-stimulated secretion is associated with basal sympathetic tone; on the other hand, secretion stimulated by PACAP is associated with heightened sympathetic tone and the fight-or-flight response.

The overarching goal of this dissertation was to test the hypothesis that the different intracellular mechanisms activated by ACh and PACAP regulate chromaffin cell fusion characteristics. The experiments described in this thesis sought to further characterize the intracellular signaling pathways of PACAP stimulated secretion and the mechanisms underlying regulation of granule cell secretion in adrenomedullary chromaffin cells by the calcium sensing proteins, synaptotagmins. Specifically, these studies used TIRF microscopy and primary mouse chromaffin cells from transgenic mouse lines to determine differences in fusion characteristics and identify intracellular proteins involved in exocytosis. Fluorescent cargo proteins and calcium indicators were utilized to monitor dense core granule fusion and intracellular calcium levels after stimulation with endogenous secretagogues, ACh and PACAP.

The synaptotagmins syt-1 and syt-7 are the two major calcium sensors for exocytosis in adrenal chromaffin cells and are important in triggering calcium mediated exocytosis in chromaffin cells. Though the importance of synaptotagmins in the adrenomedullary

system is appreciated, there are questions remaining as to the localization and function in mediated discharge of dense core granule cargos in response to physiological stimulation. To assess the subcellular localization of synaptotagmins in chromaffin cells, we used immunocytochemistry and subcellular fractionation, which showed that syt-7 is distributed in organelles, including dense core granules. TIRF imaging demonstrated that syt-7 -/- cells stimulated by ACh had lower probability of release and rapid fusion kinetics compared to WT chromaffin cells. The use of a reconstituted system employing cell-derived granules expressing either syt-1 or syt-7 allowed us to observe kinetic properties and calcium sensitivities of the synaptotagmins. In these studies, syt-7 had a greater calcium sensitivity and slowed the rate at which cargos are released compared to syt-1. Altogether, this study demonstrated that the high calcium sensitivity of syt-7 and its effects on fusion pore expansion are necessary for chromaffin cells to secrete normally to cholinergic stimulation.

Chapter III of this thesis centered on determining the intracellular signaling components of PACAP-stimulated secretion. It is known that PACAP elicits secretion from chromaffin cells by binding to PAC1 receptors and activating a Gαs-coupled signaling pathway. However, the specific role of proteins downstream of Gαs in causing exocytosis are not well understood. This study was undertaken to fill this gap in our understanding. Using a combination of genetic animal models and TIRF-based imaging of secretion, it is shown that cells lacking phospholipase C epsilon (PLCε) – a protein whose activity is stimulated by the small GTPase Rap – exhibit neither PACAP-stimulated increases in intracellular Ca^{2+} nor exocytosis. These data establish a novel role for PLCε in a signaling cascade that couples PAC1 receptor activation to chromaffin cell secretion.

Overall, the work presented in this thesis suggests that the differing intracellular signaling mechanisms between ACh and PACAP stimulation regulate fusion characteristics from chromaffin cells. Additionally, that synaptotagmins endow dense core granules with distinct fusion properties.

Chapter I

General Introduction

The utility of the sympathetic stress response (SSR) is to protect and regulate bodily functions that are necessary to sustain life when in the presence of a perceived threat. The SSR have evolved over time as such physical stressors that existed in previous history, like predatory animals and lack of ready food accessibility, have subsided. Natural selection and the beneficial outcomes has allowed the SSR to remain a response of the autonomic nervous system. (Flinn, Nepomnaschy et al. 2011) Though the SSR is often looked at in a negative light due to the uncomfortable feelings associated with stress, there is a reason that this complex, highly regulated process has adapted and advanced over time (Gray 1987). The SSR increases blood pressure, heart rate, respiratory rate, and physical activity and allows for other physiological changes necessary to maintain bodily functions and processes (Del Giudice, Ellis et al. 2011). Arguably, the most important branch of the nervous system that regulates the stress response is the adrenal gland.

The adrenal gland is part of the endocrine system and functions in the peripheral nervous system. The adrenal gland is responsible for releasing hormones and neuro-active peptides upon stimulation via the sympathetic nerves. The outer layer of the adrenal gland, the cortex, is responsible for the release of corticosteroids, including cortisol, known as the stress hormone. (Dallman 2005). The release of cortisol is initiated by neural signals that originate from the hypothalamus. The hypothalamus releases corticotrophin releasing hormone (CRH). CRH release results in adrenocorticotropic hormone from the pituitary gland, which then prompts the

synthesis and release of cortisol from the cortex. This response is known to increase anxiety and prepares the body for action. (Goldstein and McEwen 2002) During the SSR, the endocrine system not only initiates hormone release from the cortex, but also the adrenal medulla, which is the inner portion of the adrenal gland. The medulla is responsible for releasing catecholamines into circulation as well as neuropeptides, interleukins and other molecules that are indispensable for normal bodily function. The catecholamine, epinephrine, also known as adrenaline, is solely released, and synthesized within the medulla. This arguably makes the adrenal gland the most important branch of the SSR in our bodies to combat changes in homeostasis. Adrenaline has a profound action on the body, known as the fight-or-flight response, and is necessary for the body to regulate cardiovascular and respiratory output during stress. Though the importance of the system has been recognized for over 100 years, the regulation, and intracellular pathways within the adrenomedullary synapse are still under investigation.

Adrenomedullary Synapse

The adrenomedullary synapse was initially defined roughly 70 years ago by Rex Coupland. He used electron microscopy to image golden hamster adrenal chromaffin cells and described their innervation by sympathetic pre-ganglionic fibers of the splanchnic nerve (Coupland 1965). The biological characteristics of chromaffin cells were later determined. This included the observation that granules within the cells housed epinephrine and chromogranin and are released into the extracellular space in a calcium dependent manner (Douglas and Rubin 1961, Douglas 1968). Since its initial discovery, more has been elucidated about the synapse, including the neurotransmitters released from the splanchnic nerve. The two major neurotransmitters secreted by the splanchnic nerve are acetylcholine (ACh) and pituitary adenylate cyclase activating polypeptide (PACAP). Upon neurotransmitter release from the

splanchnic nerve, ACh and PACAP bind to receptors on chromaffin cells and prompt chromaffin cell secretion of catecholamines and vasoactive neuropeptides into circulation. This allows for a whole-body physiological response, which is necessary for the body to react appropriately to disturbances that threaten survival such as hypothermia, injury, and hypoglycemia. The pre-synaptic release of ACh from splanchnic nerves is well-established in biology; however, the determination of PACAP as the main stress transmitter in this system has only recently been made.

Neurotransmitters of the Adrenomedullary synapse

After the initial discovery of the function of the adrenomedullary synapse, it was quickly determined that the transmitter released form the splanchnic nerve was ACh. Cellular depolarization and chromaffin cell exocytosis occurred via ACh binding and activation to nicotinic cholinergic receptors (Marley 1988). The idea that there may be the presence of another neurotransmitter in the sympathetic nervous system arose in the 1970s. Arun Wakade observed that catecholamine secretion from the medulla continued over the course of several hours after 10Hz splanchnic nerve stimulation (Wakade, Malhotra et al. 1986). Though they hypothesized that the prolonged secretion of catecholamines would empty the entire store of epinephrine, this is not what occurred. After secreting continuously, the medulla contained equal levels of epinephrine as before stimulation, which shows that there must be a mechanism that allows chromaffin cells to re-synthesize the store of epinephrine at a fast rate (Wakade, Wakade et al. 1988). Responsible for the rapid resynthesis of epinephrine were transcriptional and post-translational activation mechanisms that induced tyrosine hydroxylase (TH) to biosynthesize catecholamines. The use of ACh muscarinic receptor blockers did not hinder the ability for TH to re-synthesize catecholamines, suggesting that there must be a non-cholinergic transmitter

responsible for this phenomenon (Thoenen, Mueller et al. 1969, Chuang and Costa 1974). By 1988, the existence of a non-cholinergic transmitter was recognized, however the role of the transmitter was unknown. Arun Wakade performed experiments involving different firing frequencies to study how varying the level of splanchnic nerve activation affected chromaffin cell secretion. To maintain basal sympathetic tone, the splanchnic nerve releases ACh at a firing frequency under 1Hz. When the stress response is activated, the splanchnic nerve increases the firing frequencies to 10-20Hz (de Diego, Arnaiz-Cot et al. 2008, Gorman 2013).Wakade and colleagues stimulated splanchnic nerves with 1Hz and 10Hz stimulation and measured the amount of catecholamines released from chromaffin cells. They then compared the levels of catecholamine release to the amount of catecholamines released after direct ACh perfusion onto chromaffin cells. The level of catecholamine secretion after ACh stimulation declined rapidly which confirmed the idea that the nicotinic ACh receptors desensitized over a short period of time. When they applied the 1Hz firing frequency to splanchnic nerve terminals, they saw similar amounts of catecholamine secretion as during ACh stimulation. However, when the firing frequency increased to 10Hz, the chromaffin cells were able to maintain secretion of catecholamines over the course of hours. This experiment determined that the non-cholinergic transmitter was the main driver of the body's ability to maintain the release of catecholamines in circulation during conditions of high splanchnic nerve activity (Wakade 1988).

Interestingly, one year after this study was published, the discovery of PACAP was made by Miyata and colleagues (Miyata, Arimura et al. 1989). It was determined that PACAP was not only present in splanchnic nerve fibers, but ubiquitously through the brain. In subsequent years, it was shown that release of PACAP stimulated epinephrine secretion from the adrenal gland *in vivo* (Edwards and Jones 1993, Geng, Gaspo et al. 1997, Lamouche, Martineau et al. 1999*)* .

Eiden and colleagues then showed that PACAP was responsible for both increased plasma epinephrine levels as well as increased adrenomedullary TH activity by using PACAP deficient mice (Hamelink, Tjurmina et al. 2002).

ACh and PACAP receptor activation result in chromaffin cell exocytosis

Acetylcholine receptor types

The receptor-stimulus coupling and intracellular actions of ACh and PACAP on chromaffin cells differ due to the receptors that are activated upon binding. ACh binds to both metabolic and ionotropic receptors. Muscarinic receptors comprise five isoforms within mammals and are part of the Class A rhodopsin type G-protein coupled receptors (GPCRs). M1,3 and 5 receptors are coupled with Gq type G proteins, which activate PLCβ, while M2 and 4 are coupled with a Gi type G proteins which inhibit adenylate cyclase. The identification of which muscarinic ACh receptor (mAChr) isoforms are expressed in chromaffin cells has been studied, however results vary and are controversial due to the lack of specific ligands and antibodies for receptor subtypes (Guo and Schofield 2003). Having said this, it is widely accepted that M1 and M5 receptors are highly expressed in chromaffin cells while M2, M3 and M4 may be expressed within chromaffin cells, though the level of expression is most likely low (Harada, Matsuoka et al. 2011). The involvement of mAChr in catecholamine secretion has been studied in both rat and mouse chromaffin cells. Using gene knockdown experiments, it was determined that the M1 receptor may be involved in catecholamine secretion. However, activation of the M5 receptor does not allow for sufficient cation influx to depolarize the cell and elicit chromaffin cell exocytosis. Although activation of M1 ACh receptor activation can result in catecholamine secretion, the efficiency rate and amount of catecholamines secreted is not

substantial enough to be considered the main driver of cholinergic-stimulated chromaffin cell exocytosis. (Harada, Matsuoka et al. 2015)

Ionotropic ACh receptors, such as nicotinic ACh receptors (nAChR) are largely accepted to be responsible for ACh-stimulated chromaffin cell secretion (Douglas and Rubin 1961). Nicotinic AChRs are ligand gated ion channels, which means that upon ligand binding, the receptors undergo a conformational change which allows for the influx of cations into the chromaffin cell. These cationic channels are non-selective, meaning that they are permeable to sodium, potassium, and calcium ions. If the cation influx results in a sufficient depolarization of the cell, then voltage-gated calcium channels will open, allowing calcium to enter the cell, which then triggers chromaffin cell exocytosis (Garcia, Garcia-De-Diego et al. 2006). Measurement of calcium levels using intracellular microelectrodes were taken by Kidokoro and colleagues in 1982 which showed that nAChr activation by ACh or other agonists resulted in repetitive cell membrane depolarization (Kidokoro, Miyazaki et al. 1982).

PACAP receptor types

Due to the importance of PACAP-receptor coupling within the central and peripheral nervous system, the receptor types and signaling cascades that lead to release of neurotransmitters after PACAP stimulation are of great interest (Arimura, Somogyvári-Vigh et al. 1991). PACAP receptors are class B GPCRs and have three main receptor types: PAC1, VPAC1 and VPAC2 (Sreedharan, Patel et al. 1993, Adamou, Aiyar et al. 1995, Harmar, Arimura et al. 1998, Kumar, Pioszak et al. 2011). GPCRs are the most targeted receptor types for current therapeutics and so, PACAP receptors have received attention for potential therapeutic uses. PACAP receptor genes are highly spliced, with nine isoforms being identified in humans and 11 in rodents. All three receptor types are selective for PACAP, however the affinity to the PACAP

isoforms present within the body vary. PACAP27 and PACAP38 are both expressed in the central and peripheral nervous system. They differ in the amino acids that comprise the peptide which results in different affinities to the receptor subtypes (Dickson and Finlayson 2009). The work of Lee Eiden and colleagues have demonstrated that the PAC1 receptor is present at high levels at the adrenomedullary synapse. It is also required to maintain catecholamine release and replenish catecholamine stores in chromaffin cells after high intensity splanchnic nerve firing (Stroth, Kuri et al. 2013, Eiden, Emery et al. 2018). The ability to maintain and replenish catecholamine release is due to the effect of PACAP on gene expression of catecholamine biosynthetic enzymes, TH, dopamine β-hydroxylase (DBH) and phenyl ethanolamine N-methyltransferase (PNMT). Therefore, PACAP is considered the stress-signaling hormone in the adrenomedullary system (Hamelink, Tjurmina et al. 2002, Smith and Eiden 2012, Stroth, Kuri et al. 2013). Although much has been elucidated in recent years about the role of PACAP in the SSR, the intracellular proteins involved in the signaling cascade that lead to an influx of calcium and trigger chromaffin cell secretion is yet to come to light. The PAC1 receptor is the dominant receptor type expressed by chromaffin cells, though the G-protein that is responsible for activating downstream effectors is unknown. Therefore, my thesis focuses on exploring the intracellular pathway that leads to PACAP-stimulated chromaffin cell calcium influx and ultimately, chromaffin cell exocytosis.

Brief History of Exocytosis

The neuron doctrine, which was introduced in the late 1800s, is foundational to our understanding of neuronal signaling. (His 1886, Nansen 1886, Forel 1887, Waldeyer 1891). This theory stated that information in the brain is relayed through a network of different cells that communicate with one another, rather than one single cell. Closely following this theory was the

introduction of the term “synapses” which were identified as the connection points between neurons (Sherrington 1897). The functionality of the synapse was then later established as the location of signal transmission from cell to cell (Loewi 1921, Dale 1934). After this point, scientists postulated a variety of theories to explain how cell-cell communication occurred within the synapses. It was not clear if neurotransmitters were released as single molecules or perhaps as a mixture of a variety of molecules. It was also unknown how these transmitters were housed in the cell and what controlled their release.

The lack of technology to visualize the synapse at this time caused difficulty in further illumination of synaptic secretion. However, even without the ability to visualize the cell, Sir Bernard Katz postulated a model of what he thought was occurring at the synapse, which was later confirmed experimentally. This idea was called quantal theory which stated that transmitters are housed in quanta, which were small all-or-none units that are released after stimulation (Del Castillo and Katz 1954). This was an important discovery because it was previously debated as to how transmitters were stored within the cell. For example, it was unknown whether transmitters were contained in a large pool within the cells or individually packaged. In the same publication, Drs. Katz and Castillo also showed that the potential changes that allowed for exocytosis were directly linked to the calcium concentration present at the neuromuscular junction. As such, these experiments were also the foundation of knowledge that we have of calcium-dependent exocytosis.

It wasn’t until the 1970s, when a collection of electron microscopic studies done by Dr. John Heuser finally allowed visualization of exocytosis in the cell (Heuser and Reese 1981). These experiments involved quick freezing of neuromuscular junctions at different intervals of stimulation to the nerve. They were able to capture an image of the synapse which showed

compartments fusing to the membrane. The ability to visualize exocytosis during a step in the process confirmed quantal theory and the existence of individual components that house the transmitters, which are currently known as synaptic vesicles. After this series of discoveries, there were still important unanswered questions as to how the link between the calcium influx into the cell and the release of the chemical transmitters were so tightly concerted.

Calcium-Dependent Exocytotic Release Machinery

Throughout the late 1980s and 1990s Drs. Scheller, Rothman, and Sudhof led the studies that established the soluble N-ethylmaleimide sensitive factor attachment protein receptor (SNARE) hypothesis. Dr. Rothman and his group were the first to purify soluble NSF attachment protein (SNAP) and determine that this protein played a role in synaptic vesicle membrane fusion (Block, Glick et al. 1988, Malhotra, Orci et al. 1988). Meanwhile in 1988, Dr. Scheller used a polyclonal antibody raised against cholinergic synaptic vesicles that he named vesicle-associated membrane protein 1 (VAMP-1) (Trimble, Cowan et al. 1988). Not a year later, Dr. Sudhof cloned the same protein and called it synaptobrevin (Sudhof, Baumert et al. 1989). Future studies showed that cleaving VAMP/synapbovrevin substantially delayed neurotransmission, which pointed to their role in synaptic vesicle exocytosis (Link, Edelmann et al. 1992, Schiavo, Benfenati et al. 1992). During Sudhof's past experiments, he came across a protein which had previously been called p65, after its initial identification by Reichardt and colleagues, and was known to have a wide distribution in neuronal tissue (Matthew, Tsavaler et al. 1981). It was not until later that he unveiled the functionality of this protein, later called synaptotagmin. Sudhof and Jahn showed that the cytoplasmic domains of this protein bound calcium at physiological concentrations and that the protein was located on the vesicle surface (Brose, Petrenko et al. 1992). Then, in 1993 Scheller used PC12 cells and demonstrated that

regulated secretion was decreased when synaptotagmin was blocked with antibodies (Elferink, Peterson et al. 1993). However, arguably the most important breakthrough in understanding regulated synaptic vesicle fusion was the purification of the SNARE complex, including SNAP, VAMP and syntaxin (Sollner, Bennett et al. 1993, Sollner, Whiteheart et al. 1993) These results showed that the SNARE complex is a universal component of vesicular fusion.

These studies by Drs. Rothman, Sudhof, Scheller, and Jahn essentially provided the basis of understanding of the molecular machinery and interactions that were required to tightly regulate the stimulus-secretion coupling of neurotransmitter exocytosis. Although this rich history of exocytotic discoveries shows a major step forward in understanding synaptic transmission, there are still many gaps in understanding the fine details of regulation.

Synaptotagmins

Our current knowledge of synaptotagmins has expanded dramatically since Reichardt's initial identification of the protein and the determination of its function by Scheller and Sudhof. Synaptotagmins are a family of calcium sensing proteins with currently 17 known isoforms. The protein is a vesicular transmembrane protein with an N-terminus that extends into the vesicle lumen and two cytosolic C2 domains that contain calcium binding loops (Perin, Fried et al. 1990). Synaptotagmins are located on vesicle membranes throughout the body and in different systems. For example, synaptotagmins are present in pancreatic β-cells where they are involved in insulin secretion. They are also expressed in neurons and involved in a form of short term synaptic plasticity called facilitation. Synaptotagmins are also present in cardiac nerve terminals and the stress hormone secretion system of the sympathetic nervous system (Fukuda, Kanno et al. 2004, Li, Wang et al. 2007, Bacaj, Wu et al. 2013, Shih, Varghese et al. 2016).

As previously mentioned, synaptotagmins are involved in facilitation and asynchronous release in neurons in the central nervous system (Jackman and Regehr 2017). Facilitation is a type of synaptic plasticity that can be observed when post synaptic potentials are evoked by impulses that are paired in a short time interval, typically under 500 milliseconds. In facilitating synapses, the second postsynaptic potential is larger in amplitude than the first. This phenomenon is thought to be caused by the slow clearance of "residual calcium" from the cytosol (Cooper, Winslow et al. 1996, Zucker and Regehr 2002). After the first impulse, the cell has not had enough time to restore baseline calcium levels. Therefore, the higher calcium levels present in the cell when the second impulse occurs causes enhanced neurotransmitter release (Zucker and Regehr 2002). It has been observed that facilitation occurs in the adrenomedullary synapse, however it is still unknown what is mediating the facilitation (Wang, Wang et al. 2016). It is possible that synptotagmin-7 (syt-7) may mediate plasticity of peripheral synapses in the same way it mediates plasticity of central synapses (Jackman and Regehr, 2017) and there are groups working to answer these questions.

The adrenomedullary system is partially responsible for basal sympathetic tone and the fight-or-flight response when one undergoes a highly stressful situation. The two synaptotagmin isoforms most highly expressed in chromaffin cell are syt-1 and syt-7 (Bhalla, Chicka et al. 2008, Schonn, Maximov et al. 2008). These calcium sensing proteins, though topologically similar, have slight differences in the calcium binding loops that affect the calcium sensitivity or affinity of that protein to bind calcium. Syt-1 has one of the lowest affinities for calcium, whereas syt-7 has one of the highest affinities. Strikingly, these synaptotagmins have been shown to be differentially sorted to populations of vesicles (Rao, Passmore et al. 2014). When studied in bovine chromaffin cells over-expressing either syt-1 or syt-7, the synaptotagmins endow the

vesicles with distinct fusion properties. When a mild stimulus occurs and there is only a low level of calcium influx, syt-7 is still able to drive membrane fusion. Because the lower calcium affinity of syt-1, syt-1 requires a stronger stimulus and greater increase in intracellular calcium to drive fusion. The intrinsic differences in calcium affinities of syt-1 and syt-7 allow for a level of regulation and control of the secretory response that can be varied to match the strength of cell stimulation. (Rao, Rodriguez et al. 2017). However, it is important to note that these observations were not made in a system that expresses endogenous levels of synaptotagmins, but by electroporation and overexpression. My thesis explores the role of synaptotagmin as a regulator in the adrenomedullary system using tissue with endogenous expression of either syt-1 or the full complement of syt-1 and syt-7.

Experimental Objectives

The experiments described in this thesis sought to further explore regulators involved in controlling chromaffin cell secretion in the adrenomedullary synapse. Specifically, these studies focused on determining the level of regulation that synaptotagmins expressed on dense core granules have on the secretory process in response to cholinergic stimulation. Also, to determine the intracellular components involved in PACAP-secreted exocytosis.

Aim 1: Characterize the role of syt-1 and syt-7 in regulating chromaffin cell secretion after cholinergic stimulation

Chapter II investigates the location and function of synaptotagmins after cholinergic stimulation in chromaffin cells. TIRF microscopy was used to compare release rates, probability of release and times of fusion after ACh stimulation in WT and syt-7 KO primary mouse chromaffin cells. Previous work in the lab using overexpressed synaptotagmins in bovine chromaffin cells showed that synaptotagmins have different calcium affinities and binding

kinetics, which resulted in varying fusion properties depending on the synaptotagmin responsible (Rao, Passmore et al. 2014, Rao, Rodriguez et al. 2017). Chapter II expands on those findings by evaluating the effects that syt-1 and syt-7 have on dense core granule exocytosis in primary chromaffin cells expressing endogenous levels of synaptotagmins; also, after stimulation with an endogenously secreted secretagogue from the splanchnic nerve, such as ACh. Differences in fusion characteristics were measured using TIRF microscopy and transfection of primary mouse chromaffin cells with the fluorescent cargo proteins NPY and tPA. Immunocytochemistry was also utilized to determine localization of syts and level of colocalization for syt-1 and syt-7. The results from this work show that synaptotagmins are differentially expressed on dense core granules and endow granules with distinct fusion mechanisms. In addition, the full complement of synaptotagmins is required for normal levels of chromaffin cell secretion after cholinergic stimulation.

Aim 2: Investigate the intracellular mechanism of PACAP stimulated exocytosis in chromaffin cells

Chapter III investigates the intracellular proteins involved in PACAP-mediated rise of intracellular calcium levels, which triggers a unique, long-lasting form of chromaffin cell secretion. During imaging experiments, we observed that PACAP-elicited events were long lived, and some seemed to move laterally after initial fusion. We hypothesized that the metabolic signaling cascade, which is distinctly different from ACh-ligand gated ion channel activation, must be responsible for prompting such unique fusion types. We also hypothesized that Epac and PLCε were involved in the signaling mechanism, based on previous studies done by Lee Eiden in the same system (Emery, Xu et al. 2017), and by Alan Smrcka in cardiomyocytes (Oestreich, Wang et al. 2007, Oestreich, Malik et al. 2009). To evaluate the critical signaling proteins in this

process, we used pharmacological approaches and TIRF microscopy to evaluate differences in calcium levels, fusion characteristics, and probability in WT and PLCε KO primary mouse chromaffin cells. Cells were transfected with calcium indicator, rescue proteins, and fluorescent cargo proteins. This study demonstrated that both EPAC and PLCε are required for PACAP stimulated exocytosis from chromaffin cells, that increased intracellular calcium levels after stimulation is from the extracellular space, and that the PAC1R receptor is most likely Gs coupled.

References

Adamou, J. E., N. Aiyar, S. Van Horn and N. A. Elshourbagy (1995). "Cloning and functional characterization of the human vasoactive intestinal peptide (VIP)-2 receptor." Biochem Biophys Res Commun **209**(2): 385-392.

Arimura, A., A. Somogyvári-Vigh, A. Miyata, K. Mizuno, D. H. Coy and C. Kitada (1991). "Tissue Distribution of PACAP as Determined by RIA: Highly Abundant in the Rat Brain and Testes." Endocrinology **129**(5): 2787-2789.

Bacaj, T., D. Wu, X. Yang, W. Morishita, P. Zhou, W. Xu, R. C. Malenka and T. C. Sudhof (2013). "Synaptotagmin-1 and synaptotagmin-7 trigger synchronous and asynchronous phases of neurotransmitter release." Neuron **80**(4): 947-959.

Bhalla, A., M. C. Chicka and E. R. Chapman (2008). "Analysis of the synaptotagmin family during reconstituted membrane fusion. Uncovering a class of inhibitory isoforms." J Biol Chem **283**(31): 21799-21807.

Block, M. R., B. S. Glick, C. A. Wilcox, F. T. Wieland and J. E. Rothman (1988). "Purification of an N-ethylmaleimide-sensitive protein catalyzing vesicular transport." Proceedings of the National Academy of Sciences of the United States of America **85**: 7852-7856.

Brose, N., A. G. Petrenko, T. C. S• dhof and R. Jahn (1992). "Synaptotagmin: a calcium sensor on the synaptic vesicle surface." Science **256**: 1021-1025.

Chuang, D. M. and E. Costa (1974). "Biosynthesis of tyrosine hydroxylase in rat adrenal medulla after exposure to cold." Proc Natl Acad Sci U S A **71**(11): 4570-4574.

Cooper, R. L., J. L. Winslow, C. K. Govind and H. L. Atwood (1996). "Synaptic structural complexity as a factor enhancing probability of calcium-mediated transmitter release." J Neurophysiol **75**(6): 2451-2466.

Coupland, R. E. (1965). "(ELECTRON MICROSCOPIC OBSERVATIONS ON THE STRUCTURE OF THE RAT ADRENAL MEDULLA. I. THE ULTRASTRUCTURE AND ORGANIZATION OF CHROMAFFIN CELLS IN THE NORMAL ADRENAL MEDULLA.)." Journal of anatomy **99**(Pt 2): 231-254.

Dale, H. (1934). "The chemical transmission of nerve impulses." Science **80**(2081): 450-450.

Dallman, M. F. (2005). "Fast glucocorticoid actions on brain: Back to the future." Frontiers in Neuroendocrinology **26**(3): 103-108.

de Diego, A. M., J. J. Arnaiz-Cot, J. M. Hernandez-Guijo, L. Gandia and A. G. Garcia (2008). "Differential variations in Ca^{2+} entry, cytosolic Ca^{2+} and membrane capacitance upon steady or

action potential depolarizing stimulation of bovine chromaffin cells." Acta Physiol (Oxf) **194**(2): 97-109.
Del Castillo, J. and B. Katz (1954). "Quantal components of the end-plate potential." J.Physiol.(Lond) **124**: 560-573.

Del Giudice, M., B. J. Ellis and E. A. Shirtcliff (2011). "The Adaptive Calibration Model of stress responsivity." Neuroscience & Biobehavioral Reviews **35**(7): 1562-1592.

Dickson, L. and K. Finlayson (2009). "VPAC and PAC receptors: From ligands to function." Pharmacol Ther **121**(3): 294-316.

Douglas, W. W. (1968). "Stimulus-secretion coupling: the concept and clues from chromaffin and other cells." Br J Pharmacol **34**(3): 451-474.

Douglas, W. W. and R. P. Rubin (1961). "The role of calcium in the secretory response of the adrenal medulla to acetylcholine." J Physiol **159**(1): 40-57.

Edwards, A. V. and C. T. Jones (1993). "Adrenal cortical and medullary responses to acetylcholine and vasoactive intestinal peptide in conscious calves." J Physiol **468**: 515-527.

Eiden, L. E., A. C. Emery, L. Zhang and C. B. Smith (2018). "PACAP signaling in stress: insights from the chromaffin cell." Pflugers Arch **470**(1): 79-88.

Elferink, L. A., M. R. Peterson and R. H. Scheller (1993). "A role for synaptotagmin (p65) in regulated exocytosis." Cell **72**: 153-159.

Emery, A. C., W. Xu, M. V. Eiden and L. E. Eiden (2017). "Guanine nucleotide exchange factor Epac2-dependent activation of the GTP-binding protein Rap2A mediates cAMP-dependent growth arrest in neuroendocrine cells." J Biol Chem **292**(29): 12220-12231.

Flinn, M. V., P. A. Nepomnaschy, M. P. Muehlenbein and D. Ponzi (2011). "Evolutionary functions of early social modulation of hypothalamic-pituitary-adrenal axis development in humans." Neuroscience & Biobehavioral Reviews **35**(7): 1611-1629.

Forel, A. (1887). "Einige hirnanatomische betrachtungen und ergebnisse." Archiv für Psychiatrie und Nervenkrankheiten **18**(1): 162-198.

Fukuda, M., E. Kanno, M. Satoh, C. Saegusa and A. Yamamoto (2004). "Synaptotagmin VII is targeted to dense-core vesicles and regulates their Ca^{2+} -dependent exocytosis in PC12 cells." J Biol Chem **279**(50): 52677-52684.

Garcia, A. G., A. M. Garcia-De-Diego, L. Gandia, R. Borges and J. Garcia-Sancho (2006). "Calcium signaling and exocytosis in adrenal chromaffin cells." Physiol Rev **86**(4): 1093-1131.

Geng, G., R. Gaspo, F. Trabelsi and N. Yamaguchi (1997). "Role of L-type Ca^{2+} channel in PACAP-induced adrenal catecholamine release in vivo." Am J Physiol **273**(4): R1339-1345.
Goldstein, D. S. and B. McEwen (2002). "Allostasis, homeostats, and the nature of stress." Stress **5**(1): 55-58.
Gorman, L. S. (2013). "The adrenal gland: common disease states and suspected new applications." Clin Lab Sci **26**(2): 118-125.

Gray, J. A. (1987). The psychology of fear and stress, 2nd ed. New York, NY, US, Cambridge University Press.

Guo, J. and G. G. Schofield (2003). "Activation of muscarinic m5 receptors inhibits recombinant KCNQ2/KCNQ3 K+ channels expressed in HEK293T cells." Eur J Pharmacol **462**(1-3): 25-32.

Hamelink, C., O. Tjurmina, R. Damadzic, W. S. Young, E. Weihe, H. W. Lee and L. E. Eiden (2002). "Pituitary adenylate cyclase-activating polypeptide is a sympathoadrenal neurotransmitter involved in catecholamine regulation and glucohomeostasis." Proc Natl Acad Sci U S A **99**(1): 461-466.

Harada, K., H. Matsuoka, H. Miyata, M. Matsui and M. Inoue (2015). "Identification of muscarinic receptor subtypes involved in catecholamine secretion in adrenal medullary chromaffin cells by genetic deletion." Br J Pharmacol **172**(5): 1348-1359.

Harada, K., H. Matsuoka, T. Sata, A. Warashina and M. Inoue (2011). "Identification and role of muscarinic receptor subtypes expressed in rat adrenal medullary cells." J Pharmacol Sci **117**(4): 253-264.

Harmar, A. J., A. Arimura, I. Gozes, L. Journot, M. Laburthe, J. R. Pisegna, S. R. Rawlings, P. Robberecht, S. I. Said, S. P. Sreedharan, S. A. Wank and J. A. Waschek (1998). "International Union of Pharmacology. XVIII. Nomenclature of receptors for vasoactive intestinal peptide and pituitary adenylate cyclase-activating polypeptide." Pharmacol Rev **50**(2): 265-270.

Heuser, J. E. and T. S. Reese (1981). "Structural changes after transmitter release at the frog neuromuscular junction." The Journal of Cell Biology **88**(3): 564-580.

His, W. (1886). Abhandlung der matematisch-physischen classe der königl. Sächsichen Gesellschaft der Wissenshcaften [in German]. **13:** 479-513.

Jackman, S. L. and W. G. Regehr (2017). "The Mechanisms and Functions of Synaptic Facilitation." Neuron **94**(3): 447-464.

Kidokoro, Y., S. Miyazaki and S. Ozawa (1982). "Acetylcholine-induced membrane depolarization and potential fluctuations in the rat adrenal chromaffin cell." J Physiol **324**: 203-220.

Kumar, S., A. Pioszak, C. Zhang, K. Swaminathan and H. E. Xu (2011). "Crystal structure of the PAC1R extracellular domain unifies a consensus fold for hormone recognition by class B G-protein coupled receptors." PLoS One **6**(5): e19682.

Lamouche, S., D. Martineau and N. Yamaguchi (1999). "Modulation of adrenal catecholamine release by PACAP in vivo." Am J Physiol **276**(1): R162-170.
Li, Y., P. Wang, J. Xu, F. Gorelick, H. Yamazaki, N. Andrews and G. V. Desir (2007). "Regulation of insulin secretion and GLUT4 trafficking by the calcium sensor synaptotagmin VII." Biochem Biophys Res Commun **362**(3): 658-664.

Link, E., L. Edelmann, J. H. Chou, T. Binz, S. Yamasaki, U. Eisel, M. Baumert, T. C. Sudhof, H. Niemann and R. Jahn (1992). "Tetanus Toxin Action: Inhibition of Neurotransmitter Release Linked to Synaptobrevin Proteolysis." Biochem.Biophys.Res.Commun. **189**: 1017-1023.

Loewi, O. (1921). "Über humorale übertragbarkeit der Herznervenwirkung." Pflüger's Archiv für die gesamte Physiologie des Menschen und der Tiere **189**(1): 239-242.

Malhotra, V., L. Orci, B. S. Glick, M. R. Block and J. E. Rothman (1988). "Role of an N-ethylmaleimide-sensitive transport component in promoting fusion of transport vesicles with cisternae of the Golgi stack." Cell **54**: 221-227.

Marley, P. D. (1988). "Desensitization of the nicotinic secretory response of adrenal chromaffin cells." Trends Pharmacol Sci **9**(3): 102-107.

Matthew, W. D., L. Tsavaler and L. F. Reichardt (1981). "Identification of a synaptic vesicle-specific membrane protein with a wide distribution in neuronal and neurosecretory tissue." Journal of Cell Biology **91**: 257-269.

Miyata, A., A. Arimura, R. R. Dahl, N. Minamino, A. Uehara, L. Jiang, M. D. Culler and D. H. Coy (1989). "Isolation of a novel 38 residue-hypothalamic polypeptide which stimulates adenylate cyclase in pituitary cells." Biochem Biophys Res Commun **164**(1): 567-574.

Nansen, F. (1886). "XXIII.—Preliminary communication on some investigations upon the histological structure of the central nervous system in the Ascidia and in Myxine glutinosa." Journal of Natural History **18**(105): 209-226.

Oestreich, E. A., S. Malik, S. A. Goonasekera, B. C. Blaxall, G. G. Kelley, R. T. Dirksen and A. V. Smrcka (2009). "Epac and phospholipase Cepsilon regulate Ca^{2+} release in the heart by

activation of protein kinase Cepsilon and calcium-calmodulin kinase II." J Biol Chem **284**(3): 1514-1522.

Oestreich, E. A., H. Wang, S. Malik, K. A. Kaproth-Joslin, B. C. Blaxall, G. G. Kelley, R. T. Dirksen and A. V. Smrcka (2007). "Epac-mediated activation of phospholipase C(epsilon) plays a critical role in beta-adrenergic receptor-dependent enhancement of Ca^{2+} mobilization in cardiac myocytes." J Biol Chem **282**(8): 5488-5495.

Perin, M. S., V. A. Fried, G. A. Mignery, R. Jahn and T. C. Sudhof (1990). "Phospholipid binding by a synaptic vesicle protein homologous to the regulatory region of protein kinase C." Nature **345**: 260-263.

Rao, T. C., D. R. Passmore, A. R. Peleman, M. Das, E. R. Chapman and A. Anantharam (2014). "Distinct fusion properties of synaptotagmin-1 and synaptotagmin-7 bearing dense core granules." Mol Biol Cell **25**(16): 2416-2427.

Rao, T. C., Z. S. Rodriguez, M. M. Bradberry, A. H. Ranski, P. J. Dahl, M. W. Schmidtke, P. M. Jenkins, D. Axelrod, E. R. Chapman, D. R. Giovannucci and A. Anantharam (2017). "Synaptotagmin isoforms confer distinct activation kinetics and dynamics to chromaffin cell granules." Journal of General Physiology **149**(8): 763-780.

Schiavo, G., F. Benfenati, B. Poulain, O. Rossetto, P. Polverino de Laureto, B. DasGupta and C. Montecucco (1992). "Tetanus toxin and botulinum-B neurotoxins block neurotransmitter release by proteolytic cleavage of synaptobrevin." Nature **359**: 832-835.

Schonn, J. S., A. Maximov, Y. Lao, T. C. Sudhof and J. B. Sorensen (2008). "Synaptotagmin-1 and -7 are functionally overlapping Ca^{2+} sensors for exocytosis in adrenal chromaffin cells." Proc Natl Acad Sci U S A **105**(10): 3998-4003.

Sherrington, C. S. (1897). "Double (antidrome) conduction in the central nervous system." Proceedings of the Royal Society of London **61**(369-377): 243-246.

Shih, A. M., L. Varghese, A. Bittar, S. H. Park, J. M. Chung and O. H. Shin (2016). "Dysregulation of norepinephrine release in the absence of functional synaptotagmin 7." Journal of cellular biochemistry **117**(6): 1446-1453.

Smith, C. B. and L. E. Eiden (2012). "Is PACAP the major neurotransmitter for stress transduction at the adrenomedullary synapse?" J Mol Neurosci **48**(2): 403-412.

Sollner, T., M. K. Bennett, S. W. Whiteheart, R. H. Scheller and J. E. Rothman (1993). "A protein assembly-disassembly pathway in vitro that may correspond to sequential steps of synaptic vesicle docking, activation and fusion." Cell **75**: 409-418.

Sollner, T., S. W. Whiteheart, M. Brunner, H. Erdjument-Bromage, S. Geromanos, P. Tempst and J. E. Rothman (1993). "SNAP receptors implicated in vesicle targeting and fusion." Nature **362**: 318-324.

Sreedharan, S. P., D. R. Patel, J. X. Huang and E. J. Goetzl (1993). "Cloning and functional expression of a human neuroendocrine vasoactive intestinal peptide receptor." Biochem Biophys Res Commun **193**(2): 546-553.

Stroth, N., B. A. Kuri, T. Mustafa, S. A. Chan, C. B. Smith and L. E. Eiden (2013). "PACAP controls adrenomedullary catecholamine secretion and expression of catecholamine biosynthetic enzymes at high splanchnic nerve firing rates characteristic of stress transduction in male mice." Endocrinology **154**(1): 330-339.

Sudhof, T. C., M. Baumert, M. S. Perin and R. Jahn (1989). "A synaptic vesicle membrane protein is conserved from mammals to Drosophila." Neuron **2**: 1475-1481.
Thoenen, H., R. A. Mueller and J. Axelrod (1969). "Trans-synaptic induction of adrenal tyrosine hydroxylase." J Pharmacol Exp Ther **169**(2): 249-254.

Trimble, W. S., D. M. Cowan and R. H. Scheller (1988). "VAMP-1: a synaptic vesicle-associated integral membrane protein." Proceedings of the National Academy of Sciences **85**(12): 4538-4542.

Wakade, A. R. (1988). "Noncholinergic transmitter(s) maintains secretion of catecholamines from rat adrenal medulla for several hours of continuous stimulation of splanchnic neurons." J Neurochem **50**(4): 1302-1308.

Wakade, A. R., R. K. Malhotra and T. Wakade (1986). "Phorbol ester facilitates 45 Ca accumulation and catecholamine secretion by nicotine and excess K + but not by muscarine in rat adrenal medulla." Nature **321**: 698-700.

Wakade, A. R., T. D. Wakade and R. K. Malhotra (1988). "Restoration of catecholamine content of previously depleted adrenal medulla in vitro: importance of synthesis in maintaining the catecholamine stores." J Neurochem **51**(3): 820-829.

Waldeyer, W. (1891). "Ueber einige neuere Forschungen im Gebiete der Anatomie des Centralnervensystems1." DMW-Deutsche Medizinische Wochenschrift **17**(44): 1213-1218.

Wang, M., Q. Wang and M. D. Whim (2016). "Fasting induces a form of autonomic synaptic plasticity that prevents hypoglycemia." Proc Natl Acad Sci U S A **113**(21): E3029-3038.

Zucker, R. S. and W. G. Regehr (2002). "Short-term synaptic plasticity." Annu Rev Physiol **64**: 355-405.

Chapter II

Synaptotagmin-7 Enhances Calcium-sensing of Chromaffin Cell Granules and Slows Discharge of Granule Cargos

Mounir Bendahmane*, Alina Morales*, Alex Kreutzberger, Noah Schenk, Ramkumar Mohan, Shreeya Bakshi, Julie M. Philippe, Shuang Zhang, Volker Kiessling, Lukas K. Tamm, David R. Giovannucci, Paul M. Jenkins, Arun Anantharam

This chapter was published in the Journal of Neurochemistry in 2020.

* indicates equal contribution

Introduction

Adrenomedullary chromaffin cells serve as a key effector arm of the sympathetic nervous system. In response to stimulation by preganglionic sympathetic nerves, they secrete a number of important hormones, including epinephrine, norepinephrine, neuropeptide Y (NPY), and tissue plasminogen activator (tPA) directly into the circulation (Carmichael & Winkler, 1985; Guerineau, 2019). The trigger for stimulus-evoked exocytosis in adrenal chromaffin cells is a rise in intracellular Ca^{2+}. The level to which intracellular Ca^{2+} is elevated varies with the stimulus intensity and secretagogue (Augustine & Neher, 1992; Fulop, Radabaugh, & Smith, 2005; Fulop & Smith, 2007). Ca^{2+} regulates release by acting on the Ca^{2+}-binding Syt-protein family (Chapman, 2008; Geppert et al., 1994; Sudhof, 2013) to drive its penetration into

membranes that harbor anionic lipids (Bai, Earles, Lewis, & Chapman, 2000; Bai, Tucker, & Chapman, 2004). These actions result in subsequent zippering of the SNARE complex and opening of a fusion pore to permit diffusion or discharge of granule luminal contents into the extracellular space (Murthy & De Camilli, 2003).

Two Syts in particular—Syt-1 and Syt-7—account for the vast majority of Ca^{2+}-triggered release from chromaffin cells (Schonn, Maximov, Lao, Sudhof, & Sorensen, 2008). Although these proteins share a similar topology, they exhibit a number of biochemical differences. For example, in vitro, Syt-7 has a much higher affinity for Ca^{2+} in the presence of phospholipid membranes than Syt-1 (Bhalla, Tucker, & Chapman, 2005; Sugita, Shin, Han, Lao, & Sudhof, 2002). In fact, Syt-7 stimulation of SNARE-mediated liposome fusion occur with a 400-fold higher sensitivity to Ca^{2+} than Syt-1 (Bhalla et al., 2005). Once bound to Ca^{2+}, Syt-7 also releases membranes at rates that are orders of magnitude faster than Syt-1(Bendahmane et al., 2018; Bhalla et al., 2005; Hui et al., 2005; Sugita et al., 2002). The biochemical distinctions between Syt-1 and Syt-7 have a strong bearing on their actions during chromaffin cell exocytosis. The much lower affinity of Syt-1 for Ca^{2+} compared to Syt-7 explains why small elevations in cytosolic Ca^{2+} levels from baseline are generally ineffective in driving fusion of granules bearing Syt-1, but much more effective at driving fusion of granules bearing Syt-7 (Rao et al., 2017). Differences in the Ca^{2+} sensitivities of Syt isoforms, as well as their membrane association and dissociation rates, may also underlie the fast and slow kinetic components of the secretory response (Schonn et al., 2008). These components, revealed through Ca^{2+} uncaging in combination with capacitance measurements, are differentially reliant on Syt-1 and Syt-7. The rapid phase of release is eliminated in the absence of Syt-1 (Schonn et al., 2008). The remaining delayed component exhibits a Ca^{2+}-threshold that closely mirrors the low, micromolar-range

sensitivity of Syt-7 for binding to phospholipids in the presence of Ca^{2+}. Furthermore, deletion of Syt-7 in a Syt-1 knockout (KO) background, almost completely eliminates the slow phase of release (Schonn et al., 2008).

Thus, stimulation paradigms that elevate intracellular Ca^{2+} to varying degrees allow the impact of biochemical differences in the function of Syt-1 and Syt-7 on exocytosis to be readily appreciated. The purpose of this study was to delineate how such differences impinge on the release kinetics of cargos stored within dense core granules harboring Syt-7 and affect the secretory response to native, cholinergic stimulation. In order to define the localization and function of Syt isoforms—especially Syt-7—in chromaffin cell exocytosis, multiple experimental preparations were employed. This includes primary chromaffin cells and an assay in which fusion of dense core granules with a planar membrane has been reconstituted (Kreutzberger, Kiessling, Liang, Seelheim, et al., 2017; Kreutzberger, Kiessling, Liang, Yang, et al., 2017; Kreutzberger et al., 2019). Immunolabeling of endogenous Syt proteins in mouse chromaffin cells as well as subcellular fractionation demonstrate that both Syt-1 and Syt-7 are principally sorted to intracellular organelles (including dense core granules). The role of Syt-7 in regulating the characteristics of exocytosis was ascertained by monitoring the discharge of fluorescently labeled lumenal cargo proteins in cells lacking endogenous Syt-7 (Syt-7 KO cells) using TIRF microscopy. These experiments revealed that cargos are discharged from Syt-7 KO cells at significantly faster rates than they are from WT cells, consistent with the idea that endogenous Syt-7 constrains fusion pore expansion (Brahmachari et al., 1998; Jaiswal, Chakrabarti, Andrews, & Simon, 2004; Rao et al., 2014, 2017; Zhang et al., 2011).

The absence of Syt-7 has a pronounced detrimental effect on the secretory response to prolonged cholinergic stimulation. In fact, the likelihood of observing exocytosis at all declines

sharply in KO cells after the first few seconds of perfusion with acetylcholine (ACh). In contrast, exocytotic events are evident throughout the stimulation period in WT cells, albeit with a lessening frequency as stimulation proceeds. Exocytosis is sustained in WT cells because of the high affinity of Syt-7 for Ca^{2+}. This idea is underscored by reconstitution studies in which dense core granules consisting of only Syt-1 or Syt-7 were triggered to fuse with synthetic bilayers. Even in this setting, Syt-7-bearing granules fuse at significantly lower Ca^{2+} concentrations than Syt-1-bearing granules, with fusion pores that dilate at slower rates. Taken together, the data highlight clear functional distinctions in the roles of synaptotagmins. These properties have a direct bearing on the regulation of Ca^{2+}-triggered exocytosis in cells and are likely to play a role in controlling adrenomedullary output, in situ.

Materials and Methods for chromaffin cell studies

Animals

Litters of adult male and female Syt-7 -/- (Catalog #004950, Jackson labs) (gift of Dr Joel Swanson; (Chakrabarti et al., 2003) and Syt-7 +/+ (from a C57BL/6J background and obtained from Jackson Labs, Catalog #000664) were used in these studies. Animals were group housed (2–5 per ventilated cage) with 24 hr (12/12 dark/ light cycle) access to food and water. All animal procedures and experiments were conducted in accordance with the University of Michigan Institutional Animal Care and Use Committee protocol (PRO00007247). No randomization was performed to allocate subjects in the study.

Below, we describe a novel method for the isolation and culture of adult mouse chromaffin cells from the adrenal medulla. Although the protocol was adapted from previous studies (Kolski-Andreaco, Cai, Currle, Chandy, & Chow, 2007), it is different enough to warrant a more detailed description. Catalog numbers and vendors of materials used arepresented in Table 1. Six- to

sixteen-week-old animals (male and female; 18–25 g) were gas anesthetized using an isoflurane drop jar technique and sacrificed by guillotine decapitation.

Chromaffin cells are responsible for releasing catecholamines in response to stress, including hypoxia. Isoflurane is used to induce a faster loss of consciousness compared to CO2 euthanasia (30 s to 1 min vs. several minutes) and reduce animal stress. 3–4 mice are euthanized per plate to ensure proper cell density and health. Adrenal glands as per condition were rapidly isolated and moved to dishes containing ice-cold dissection buffer (148 mM NaCl, 2.57 mM KCl, 2.2 mM K2HPO4•3H2O, 6.5 mM KH2PO4, 10 mM glucose, 5 mM HEPES free acid, 14.2 mM mannitol). Under a dissection microscope, the cortex was rapidly and carefully removed using thin forceps (Dumont Swissmade, Switzerland Cat. # 72891-Bx) and thin micro scissors (World Precision Instruments, 14124-G). The isolated medullas were washed three times in 150 µl drops of enzyme solution containing (450 units/ml Papain (Worthington Biochemical. #LS003126), 250 µg/ml bovine serum albumin (BSA), and 75 µg/ml dithiothreitol). The medullas were then digested for 15 min in 0.5 ml of the enzyme solution at 37°C. After 15 min, the digesting solution was carefully removed and replaced by 0.5 ml of fresh enzyme solution and left for a maximum of 15 extra minutes at 37°C. The digestion was stopped by transferring the glands into an antibiotic-free culture medium (Dulbecco's modified Eagle's medium (DMEM) (ThermoFisher Scientific) supplemented with 10% fetal bovine serum (FBS) (ThermoFisher Scientific). The digested glands were then triturated by a push-pull movement through a 1 ml pipette tip (10–12 times). The suspension of digested and broken glands was spun at 1,300 g for 2.5 min. The supernatant was discarded, and the pellet was re-suspended in antibiotic-free medium and triturated again in a 200 µl pipette tip for a better cell dissociation (10–12 times). The suspension was spun again at 1,300 g for 2.5 min. After discarding the

supernatant, the pellet was re-suspended in resuspension buffer (Invitrogen, Thermofisher Scientific) for transfection. The cells were rapidly counted and the desired plasmid was added (15 ng/106 cells). The suspended cells were then transiently transfected by electroporation with a single pulse (1,050 mV, 40 ms) using the Neon transfection system (Invitrogen, Thermofisher Scientific). In parallel, 35 mm diameter dishes with 14 mm diameter glass-bottom dishes (MatTek Corporation, #P35G-1.5-14-C) were pre-coated with Matrigel (Cat. #356230) diluted in DMEM (1 : 7) for 2 hr after which the dishes were washed with DMEM and let to dry. After electroporation, an antibiotic-free medium was added to cells to obtain a final concentration of 1 million cells per ml. Three hundred microliters of the final solution containing the electroporated cells were then deposited in each dish. The cells were stored in an incubator (37°C, 5% CO2) for 3–5 hr. Culture medium with antibiotics was then added to a final volume of 2 ml (DMEM supplemented with 10% FBS, 9.52 unit/ml Penicillin, 9.52 μg/ml Streptomycin, and 238 μg/ml Gentamicin (ThermoFisher Scientific). The media was changed daily, and cells were used within 48 hr after plating. The method we describe here provides consistently healthy cells (Figure S1) which exhibit a high probability of secretion upon stimulation. As a matter of course, cell preps and experiments were usually performed during normal working hours (9 a.m.–5 p.m.).

Chromaffin cells were transfected with rat myc-Syt-7 or cargo proteins, including human Neuropeptide Y (NPY) and human tissue plasminogen activator (tPA). The myc-Syt-7 plasmid was a gift from Dr Thomas Sudhof. The fluorescent tag was located following the C-terminal region of the cargo proteins. NPY and tPA constructs (originally in pEGFP-N1 vectors) were provided by Dr Ronald W. Holz.

Approximate numbers of animals used per experimental group are listed below:

Immunocytochemistry (Syt-7 + Syt-1): 4 KO and 4 WT

Immunocytochemistry (Syt-7 + PAI-1): 8 KO and 8 WT

Secretion (KCl): 46 KO and 46 WT

Secretion (ACh): 32 KO and 32 WT

Ca^{2+} imaging: 12 KO and 12 WT

Electrophysiology: 12 KO and 12 WT

Total: 114 KO and 114 WT (males and females, mixed)

Western blotting

Catalog numbers, vendors of materials used, and appropriate dilutions are presented in Table 1. Lysis buffer containing 8 M urea, 5% SDS, and 5 mM N-ethylmaleimide in water was heated to 65°C. Six- to sixteen-week-old animals (male and female; 18–25 g) were gas anesthetized using an isoflurane drop jar technique and sacrificed by guillotine decapitation. Adrenal glands were dissected from five-months old mice and immediately frozen in liquid nitrogen, then handed over to a colleague blinded to the genotype of the mice to complete the western blot. Four total adrenal glands from two mice of each genotype were dissolved into 200 µl of warm lysis buffer, and homogenized using a handheld, battery-operated homogenizer. The homogenate was incubated at 65°C for 20 min and mixed 1 : 1 with 5× PAGE buffer (5% (wt/vol) SDS, 25% (wt/vol) sucrose, 50 mM Tris pH 8, 5 mM EDTA, & bromophenol blue). The lysates were stored at −20°C until use. Samples (10 µl/well) were separated on a 4%–12% NuPAGE Bis-Tris Gel in 1× NuPAGE MOPS SDS Running Buffer, for 1 hr at 175 mV. Transfer to nitrocellulose membrane occurred at 120 mV for 1.5 hr, on ice, in 1× NuPAGE transfer buffer. The membrane was blocked with blocking buffer containing 5% BSA and 0.1% tween in TBS (TBS-T) for 1 hr, before incubation with primary antibodies (Rabbit anti Synaptotagmin-7 1 : 1,000, Synaptic Systems, and Mouse anti alpha-tubulin, 1 : 10,000, Cedarlane; RRID:AB_10060319) at 4°C,

overnight. The membrane was washed 3× 15 min with TBS-T and incubated for 1 hr with LiCor fluorescent secondaries (1 : 10,000) in blocking buffer (multiplexed). After washing 3× 15 min in TBS-T, the membrane was imaged using LiCor Odyssey Clx imager. Chromaffin cells are isolated from bovine adrenal glands as described previously (Holz, Senter, & Frye, 1982). Briefly, adrenal glands were obtained from a slaughterhouse and delivered to the lab. Surrounding fat and connective tissues were removed carefully and adrenal glands were perfused with physiological saline solution (PSS) through adreno-lumbar vein to remove residual blood. Glands were then digested at 37°C by perfusing with enzymatic solution A (Liberase TH) for 30–40 min. Digested medullas were collected and digested again at 37°C in enzymatic solution B (Liberase TH and TL mixture) for 30 min under constant agitation. This is then passed through 400 μm filter to obtain chromaffin cells. Subcellular fractionation of chromaffin cells was performed following a published protocol (Kreutzberger et al., 2019) with slight modifications. The fractions (400 μl) were collected for western blotting. Blots containing the transferred proteins were blocked in 5% milk and incubated overnight at 4°C with the following primary antibodies: Rabbit anti Synaptotagmin-7 (1 : 1,000, Synaptic Systems, Cat.no. 105173; RRID: AB_887838), Mouse anti Synaptotagmin-1 (1 : 1,000, Synaptic Systems, Cat #105 011, 1 : 1,200; RRID: AB_887832), Rabbit anti PAI-1 (1 : 500, Abcam, Cat. no. ab66705; RRID: AB_1310540), Rabbit anti LAMP-1 (1 : 1,000, Abcam, Cat. no. ab24170; RRID: AB_775978). Following primary antibody incubation, blots were washed with TBS-T and incubated with HRP conjugated secondary antibodies (anti-mouse HRP 1 : 5,000, Cat. no. NXA931V; RRID: AB_2721110 or anti-rabbit HRP 1 : 5,000, Cat. no NA934V; RRID: AB_772206) diluted in 5% milk. Chemiluminescent substrate (Thermofisher) was used to visualize blots on iBright Imager (Invitrogen). Protein band intensity was quantified using Fiji software.

Reverse transcription and quantitative PCR

Reverse transcription was performed on mouse adrenal medullas dissected from adrenal glands and homogenized. Adrenal medullas from two animals in each WT and Syt-7 KO group are considered as one experiment. Specifically, four adrenal medullas from two animals were homogenized in one 1.5-ml Eppendorf tube on ice for ~ 45 s with motorized pestle mixer (Argos Technologies, Inc.). More than three experiments were performed for each target. RNeasy Mini (Qiagen) was used to isolate the RNAs. The first strand cDNA synthesis was performed with 400 ng of RNAs using the qScript cDNA SuperMix kit (Quanta Biosciences). The reverse transcription product was kept at −20°C until qPCR was performed. qPCR primers for the target genes were designed with online tools (GenScript PCR Primer Design and NCBI primer designing tool). The forward (fw) and reverse (rv) primer sequences are as follows:

GAPDH fw CTGACGTGCCGCCTGGAGAA

GAPDH rv CCCGGCATCGAAGGTGGAAGA

Syt−1 fw GGCGCGATCTCCAGAGTGCT

Syt−1 rv GCCGGCAGTAGGGACGTAGC

Syt−7 fw CCAGACGCCACACGATGAGTC

Syt−7 rv CCTTCCAGAAGGTCTGCATCTGG

NPY fw GTGTGTTTGGGCATTCTGGC

NPY rv TGTCTCAGGGCTGGATCTCT

tPA fw CTCGGCCTGGGCAGACACAA

tPA rv AGGCCACAGGTGGAGCATGG

TH fw GCGCCGGAAGCTGATTGCAG

TH rv CCGGCAGGCATGGGTAGCAT

Glyceraldehyde 3-phosphatedehydrogenase (GAPDH) was used as an endogenous control run in parallel with target genes. Each assay was performed in triplicate. For the qPCR, we used the PerfeCTa SYBR Green SuperMix (Quanta Biosciences). Ten microliters of reverse transcription product was added to the master mix with 10 μM of each primer. The directions for the PCR protocol were followed as per the manufacturer's instructions. The qPCR was performed using the CFX96 TouchTM Real-Time PCR Detection System (Bio-Rad). Melting curves were analyzed to verify that no primer dimers were produced.

TIRF microscopy for observation of exocytosis

TIRF imaging was performed using an Olympus cellTIRF-4Line microscope (Olympus) equipped with a TIRF oil-immersion objective (NA 1.49) and an additional 2x lens in the emission path between the microscope and the cooled electron-multiplying charge-coupled device Camera (iXon 897; Andor Technology). The final pixel size of the images was 80 nm. Series of images were acquired at ~ 20 Hz using CellSense software with an exposure time of 30 ms and an EM gain of 100. pHl and GFP were excited using a 488 nm laser.

Cell stimulation

All TIRF experiments were performed at room temperature ~ 24°C. The culture medium was replaced by pre-warmed (37°C) physiological salt solution (PSS) (145 mM NaCl, 5.6 mM KCl, 2.2 mM CaCl2, 0.5 mM MgCl2, 5.6 mM glucose, and 15 mM HEPES, pH 7.4). Chromaffin cells were individually stimulated using a needle (100- μm inner diameter) connected to a perfusion system under positive pressure ALA-VM4 (ALA Scientific Instruments). To trigger exocytosis,

cells were first perfused with PSS for 5–10 s and then stimulated with high potassium containing solution (100 mM KCl) for 70–75 s. For the acetylcholine experiment, 100 μM acetylcholine (Sigma- Aldrich) diluted in PSS was perfused for 120 s.

Image analysis

Fusion sites of granules containing GFP or pHl-tagged proteins undergoing exocytosis were identified. The abruptness with which NPY-GFP puncta disappear is taken as indication that fusion and release has occurred. In the event of slower cargo release, an increase in fluorescence often precedes the disappearance of GFP puncta as the granule moves closer to the brightest part of the evanescent field and the lumenal pH of the granule becomes more neutral (Taraska, Perrais, Ohara-Imaizumi, Nagamatsu, & Almers, 2003). Regions of interest (ROIs) measuring 0.8 μm diameter were manually selected at fusion sites and image sequences were analyzed using the Time Series Analyzer v3.0 plugin on Fiji software. For each ROI, the fluorescence intensity was measured for each frame. A nearby ROI of the same size where no fusion events were observed was selected for background subtraction. Using a custom program written in Interactive Data Language (IDL; ITT, Broomfield, CO) by Dr. Daniel Axelrod (University of Michigan), background subtracted intensity versus time curves were plotted and the duration of cargo release was calculated (Abbineni, Bittner, Axelrod, & Holz, 2019; Bohannon, Bittner, Lawrence, Axelrod, & Holz, 2017). Briefly, after a user selects fusion events from blinded files, the program generates fluorescence-versus-time curves for each one. A user selects a start time, tstart, just before fluorescence begins and an end time, tend, when fluorescence returns to baseline. The program determines the time of the maximum fluorescence tmax within this time window. The intervals (tstart, tmax) and (tmax, tend) are defined as the rise phase and fall phase, respectively. Each phase is fit with a fifth-degree polynomial function, and a weighted average

slope is calculated (upward for the rising phase, and downward for the falling phase). The time period between the baseline intercept of the rising phase straight line and the falling phase straight line is considered to be the duration of the event (Bohannon et al., 2017). Each fusion event was further analyzed by the user to confirm that only events in which cargos were completely released were used in the analysis. Illustrations of the output of the curve-fitting procedure and examples of release durations calculated by the program, are reported in Bohannon et al. (2017) and in Bendahmane et al. (2018).

Cells transfected with GCaMP5G (Akerboom et al., 2012) were analyzed to determine the relative amount of calcium influx into the cell. Three ROIs measuring 1.68 μm diameter were manually selected at different points within each cell and fluorescence was measured for each ROI for each frame. The equation ΔF/F was applied to each ROI for each frame, then the values were averaged between the three ROIs to determine the overall ΔF/F for the whole cell. The values determined were plotted versus time. The exclusion criteria used to select which cells to analyze were based on proper fixation to the dish, no response to the control stimulation, and single response tracings that indicated calcium influx in response to the stimulus trigger.

As a matter of routine, imaging and analysis were performed by an experimenter who was blinded to the genotype of the cell. The individual who euthanized the mice assigned numbers to each groups and then handed over said groups to the experimenter who continued with the preparation. Whether the cells were harvested from WT or KO mice was revealed after analysis was completed. Chromaffin cells that appeared healthy in brightfield (Figure S1) with at least 10 docked granules, and responded to KCl or ACh stimulation with at least 1 fusion event, were included in data sets. No sample calculation was used.

Immunocytochemistry

Immunofluorescence imaging was performed to assess the distribution of endogenous Syt-1, Syt-7, LAMP-1 (Abcam cat# 25630; RRID: AB_470708), and PAI-1 in chromaffin cells. Mouse chromaffin cells were plated on the same Matrigel-precoated 14 mm glass-bottom dishes used for TIRF imaging. All incubations and washing steps were performed on ice unless otherwise stated. Twenty-four hours after plating, the cells were fixed with 4% paraformaldehyde in phosphate buffered solution (PBS) for 30 min. The fixed cells were quickly rinsed with PBS and quenched with 50 mM NH4Cl solution in PBS for 30 min. After a brief wash from the NH4Cl solution with PBS, the cells were permeabilized with methanol for 7 min at −20°C. Following the permeabilization, the cells were washed in Tris-buffered saline (TBS) and blocked in 0.01% gelatin solution for 30 min followed by another 30 min incubation in 4% donkey serum and 0.2% BSA prepared in TBS. Primary and secondary antibodies were diluted in TBS at 0.2%. Cells were incubated for 2 hr with a combination of polyclonal rabbit anti-Syt-7 antibody (Synaptic Systems, Göttingen, Germany. Cat # 105 173, 1 : 1,200; RRID: AB_887838), and monoclonal mouse anti-Syt-1 (Synaptic Systems, Göttingen, Germany. Cat # 105 011, 1 : 1,200; RRID: AB_887832). The cells were then washed and incubated for 70 min at room temperature with Alexa 488/561-conjugated anti-rabbit and anti-mouse secondary antibodies (Molecular Probes, Invitrogen). The double-labeled cells were then washed and kept at 4°C until confocal imaging.

For co-labeling of endogenous PAI-1 and Syt-7, both the polyclonal anti-Syt-7 and polyclonal anti-PAI-1 (Abcam cat# 66705; RRID: AB_1310540) antibodies were made in rabbit. In this experiment, to avoid cross-labeling, the cells were first labeled with anti-Syt-7 following the protocol described above. Cells labeled for Syt-7 were then incubated for 60 min with polyclonal cross-adsorbed unconjugated F(ab')2-Goat anti-Rabbit IgG (Invitrogen,

ThermoFisher, Cat. # A24539, 1 : 300; RRID: AB_2536007) diluted in TBS-0.2% BSA solution to bind the possibly remaining free primary antibody sites (anti-Syt-7) not bound by the Alexa 488conjugated donkey anti-rabbit.

Labeling for PAI-1 was performed separately. Briefly, the primary and secondary antibodies (anti-PAI-1, 1 : 600 – Alexa 561-conjugated anti rabbit, 1 : 600) were incubated for 70 min in reaction tube pre-adsorbed in dry milk 1% diluted in TBS (Kroeber, Schomerus, & Korf, 1998). After incubation, normal rabbit serum (Invitrogen, ThermoFisher Scientific, Cat. # 016101; RRID: AB_2532937) was added to the tube (10% volume/volume dilution) to bind the free secondary antibody for 60 min. The mix was then added in the Syt-7 labeled dishes for 2 hr. In control dishes, either the Syt-7 or PAI-1 antibodies were omitted (Figure S2) to verify the absence of cross-labeling. Cells were subsequently imaged using a Zeiss 880 confocal microscope (Zeiss) with a 3x oil immersion objective in airyscan mode. Images were analyzed using Imaris Software (Bitplane, Zurich, Switzerland) using the 'spot' function module for puncta detection and colocalization analysis (Rao et al., 2017). Catalog numbers, vendors of materials used, and appropriate dilutions are presented in Table 1.

Electrophysiological recordings

Primary cultures of mouse chromaffin cells were maintained on glass bottom dishes and mounted onto the stage of a Nikon Eclipse TE2000, as described previously (Rao et al., 2017). A micro-manifold and polyamide-coated capillary was positioned in the field of view and bath solutions were exchanged through using a pressure driven reservoir system. Standard whole-cell patch clamp methods were used record currents evoked by acetylcholine or by step depolarizations using an Axopatch 200B amplifier and Pulse Control/ Igor Pro software. Patch pipettes were constructed out of 1.5 mm o.d. borosilicate glass (#TW150F-4; WPI), coated with

Sylgard elastomer (#24236-10, EMS) and fire polished to resistances of 2.5–7 MΩ. The standard intracellular recording solution contained (in mM): 128 N-methyl-d-glucamine-Cl, 40 HEPES, 10 NaCl, 4 MgATP, 0.2 GTP, 0.1 Tris-EGTA, and pH adjusted to 7.2. IACh were induced by 10 s to 300 s applications of 100 μM ACh and recorded in physiological saline (125 mM NaCl, 2.5 mM KCl, 2 mM CaCl2, 1 mM MgCl2, 1.25 mM NaH2PO4, 26 mM NaHCO3, and 25 mM glucose, pH 7.4). For recording of ICa, the superfusion solution was changed to a solution containing (in mM): 137 tetraethylammonium chloride, 5 CaCl2, 2 MgCl2, 10 HEPES, and 19 glucose, and pH adjusted to 7.2 with Tris. ICa current-voltage relationship was obtained in response to step depolarizations (30 ms) from a holding membrane potential of −90 mV. Pulses were applied in a randomized series to membrane potentials between −80 and + 60 mV. All recordings were performed at room temperature. Cells with leak current greater than −80 pA or access resistance greater than 45 MΩ were excluded from our analysis.

Materials and methods for single granule/ supported membrane fusion assay

The following materials were purchased and used without further purification:

porcine brain L-α-phosphatidylcholine (bPC), porcine brain L- α-phosphatidylethanolamine (bPE), porcine brain L- α-phosphatidylserine (bPS), and L- α-phosphatidylinositol (liver, bovine) (PI), and porcine brain phosphatidylinositol 4,5bisphosphate (bPIP2) were from Avanti Polar Lipids; cholesterol, sodium cholate, EDTA, calcium Opti-Prep Density Gradient Medium, sucrose, MOPS, glutamic acid potassium salt monohydrate, potassium acetate, and glycerol were from Sigma; CHAPS and DPC were from Anatrace; HEPES was from Research Products International; chloroform, ethanol, Contrad detergent, all inorganic acids and bases, and hydrogen peroxide were from Fisher Scientific. Water was purified first with deionizing and organic-free 3 filters (Virginia Water Systems) and then with a

NANOpure system from Barnstead to achieve a resistivity of 18.2 MΩ/cm. Antibodies for synaptotagmin-1 (mouse monoclonal), synaptotagmin- 7 (rabbit polyclonal) are from Synaptic Systems.

PC12 cell culture

Pheochromocytoma cells (PC12), gifted from Tom Martin, with endogenous synaptotagmin-1 and −9 knocked down, as described previously (Kreutzberger, Kiessling, Liang, Seelheim, et al., 2017), were cultured on 10-cm plastic cell culture plates at 37°C in 10% CO2 in 1x Dulbecco's modified Eagle's medium, high glucose (Gibco) supplemented with 10% horse serum (CellGro), 10% calf serum (Fe+) (HyClone), 1% penicillin/ streptomycin mix, and 2 µg/ml of puromycin. Medium was changed every 2–3 days and cells were passed after reaching 90% confluency by incubating for 5 min in Hank's balanced salt solution and replating in fresh medium. Cells were passed no more than 30 times in total. Cells were transfected by electroporation using ECM 830 Electro Square Porator (BTX). After harvesting and sedimentation, cells were suspended in a small volume of sterile cytomix electroporation buffer (120 mM KCl, 10 mM KH2PO4, 0.15 mM CaCl2, 2 mM EGTA, 20 mM HEPES-KOH, 5 mM MgCl2, 2 mM adenosine triphosphate, and 5 mM glutathione (pH 7.6), then diluted to ~ 14 × 106 cells/ml. Cell suspensions (~10 × 106 cells in ~ 700 µl volume) and 30 µg of NPY-mRuby DNA and 30 µg of synaptotagmin-1 or −7 DNA added and placed in an electroporator cuvette with a 4-mm gap. Then two 255-V, 8-ms electroporation pulses were applied. Cells were immediately transferred to a 10-cm cell culture dish with 10 ml of normal growth medium. Cells were cultured under normal conditions for 3 days prior to fractionation.

Dense core granule purification

Dense core granules from PC12 cells were purified as described previously (Kreutzberger, Kiessling, Liang, Seelheim, et al., 2017). PC12 cells with shRNA mediated knockdowns of endogenous synaptotagmin-1 and −9 were transfected with NPY-mRuby (~20 10-cm plates) and plasmids for synaptotagmin-1 or −7 (Kreutzberger, Kiessling, Liang, Seelheim, et al., 2017; Kreutzberger et al., 2019). Cells were scraped into PBS and pelleted by centrifugation and then suspended and washed in homogenization medium (0.26 M sucrose, 5 mM MOPS, 0.2 mM EDTA) by pelleting and resuspending. Following re-suspension in 3 ml of medium containing protease inhibitor (Roche Diagnostics), the cells were cracked open using a ball bearing homogenizer with a 0.2507-inch bore and 0.2496-inch diameter ball. The homogenate was spun at 1,500 g for 10 min at 4°C in fixed angle micro-centrifuge to pellet nuclei and larger debris. The post-nuclear supernatant was collected and spun at 11,000 rpm (8,000 g) for 15 min at 4°C to pellet mitochondria. The post-mitochondrial supernatant was then collected, adjusted to a final concentration of 5 mM EDTA, and incubated for 10 min on ice. A working solution of 50% Optiprep (iodixanol) (5 vol 60% Optiprep: 1 vol 0.26M sucrose, 30 mM MOPS, 1 mM EDTA) and homogenization medium were mixed to prepare solutions for discontinuous gradients in Beckman SW55 tubes: 0.5 ml of 30% iodixanol on the bottom and 3.8 ml of 14.5% iodixanol, above which 1.2 ml EDTA-adjusted supernatant was layered. Samples were spun at 45,000 rpm (190,000 g) for 5 hr. A clear white band at the interface between the 30% iodixanol and the 14.5% iodixanol was collected as the dense core granule sample. The dense core granule sample was then extensively dialyzed in a cassette with 10,000 kDa molecular weight cutoff (24–48 hr, 3 × 5L) into the fusion assay buffer (120 mM potassium glutamate, 20 mM potassium acetate, 20 mM HEPES, pH 7.4).

Protein purification

Syntaxin-1a (constructs of residues 1–288), SNAP-25, Munc18, and Munc13 (construct of residues 529–1407 containing the C1C2MUN region), and complexin-1 from Rattus norvegicus were expressed in Escherichia coli s train B L21(DE3) cells as d escribed previously (Kreutzberger, Kiessling, Liang, Seelheim, et al., 2017; Kreutzberger, Kiessling, Liang, Yang, et al., 2017; Zdanowicz et al., 2017).

Formation of planar supported bilayers with reconstituted plasma membrane SNAREs

Planar supported bilayers with reconstituted plasma membrane SNAREs were prepared by Langmuir–Blodgett/vesicle fusion technique as described in previous studies (Domanska, Kiessling, Stein, Fasshauer, & Tamm, 2009; Kalb, Frey, & Tamm, 1992; Wagner & Tamm, 2001). Quartz slides were cleaned by dipping in 3 : 1 sulfuric acid:hydrogen peroxide for 15 min using a Teflon holder. Slides were then rinsed in milli-Q water. The first leaflet of the bilayer was prepared by Langmuir–Blodgett transfer onto the quartz slide using a Nima 611 Langmuir–Blodgett trough (Nima) by applying the lipid mixture of 70 : 30 : 3 bPC:Chol:DPS from a chloroform solution. Solvent was allowed to evaporate for 10 min, the monolayer was compressed at a rate of 10 cm2/ min to reach a surface pressure of 32 mN/m. After equilibration for 5 min, a clean quartz slide was rapidly (68 mm/min) dipped into the trough and slowly (5 mm/min) withdrawn, while a computer maintained a constant surface pressure and monitored the transfer of lipids with head groups down onto the hydrophilic substrate.

Plasma membrane SNARE containing proteoliposomes with a lipid composition of PC:bPE:bPS:Chol:PI:PI(4,5)P2 (25 : 25 : 15 : 30 : 4 : 1) were prepared by mixing the lipids and evaporating the organic solvents under a stream of N2 gas f ollowed by vacuum desiccation for at least 1 hr. The dried lipid films were dissolved in 25 mM sodium cholate in a buffer (20 mM HEPES, 150 mM KCl, pH 7.4) followed by the addition of an appropriate volume of synatxin-1a

and SNAP-25 in their respective detergents to reach a final lipid/protein ratio of 3,000 for each protein. After 1 hr of equilibration at room temperature, the mixture was diluted below the critical micellar concentration by the addition of more buffer to the desired final volume. The sample

was then dialyzed overnight against 1 L of buffer, with one buffer change after ~4 hr with Biobeads included in the dialysis buffer. To complete formation of the SNARE containing supported bilayers, proteoliposomes were incubated with the Langmuir–Blodgett monolayer with the proteoliposome lipids forming the outer leaflet of the planar supported membrane and most SNAREs oriented with their cytoplasmic domains away from the substrate and facing the bulk aqueous region. A concentration of ~77 mM total lipid in 1.2 ml total volume was used. Proteoliposomes were incubated for 1 hr and excess proteoliposomes were removed by perfusion with 5 ml of buffer (120 mM potassium glutamate, 20 mM potassium acetate (20 mM potassium sulfate was used in buffers with acridine orange-labeled granules), 20 mM HEPES, 100 mM EDTA, pH 7.4).

TIRF microscopy for single granule/supported membrane fusion assay

Dense core granule to planar supported bilayer fusion assay experiments were performed on a Zeiss Axio Observer 7 fluorescence microscope (Carl Zeiss), with a 63x water immersion objective (Zeiss, N.A. 0.95) and a prism-based TIRF illumination. Laser light at 514 nm from an argon ion laser (Innova 90C, Coherent), controlled through an acousto-optic modulator (Isomet), and at 640 nm from a diode laser (Cube 640, Coherent) were used as excitation sources. The characteristic penetration depths were between 90 and 130 nm. An OptoSplit (Andor Technology) was used to separate two spectral bands (540 nm – 610 nm, and 655 nm – 725 nm). Fluorescence signals were recorded by an EMCCD (iXon DV887ESC-BV, Andor Technology).

Calcium-triggered single granule – planar supported membrane fusion assay

As described previously (Kreutzberger, Kiessling, Liang, Seelheim, et al., 2017), planar supported bilayers containing syntaxin-1a (1-288): dodecylated (d) SNAP-25 (bulk phasefacing leaflet lipid composition of 25 : 25 : 15 : 30 : 4 : 1 bPC:bPE:bPS:Chol:PI:bPIP2) were incubated with 0.5 μM Munc18 and 2 μM complexin-1. Secretory granules were then injected while keeping the concentrations of Munc18 and complexin- 1 constant. Dense core granule docking was allowed to occur for ~ 20 min before the chamber was placed on the TIRF microscope and the microscope was focused on the planar supported membrane. Fluorescent images were recorded every 200 ms while buffer containing 100 μM calcium and a soluble Alexa647 dye to monitor the arrival of calcium at the observation site was injected.

Movies were analyzed as described previously (Domanska, Kiessling, & Tamm, 2010; Kreutzberger, Kiessling, Liang, Seelheim, et al., 2017; Kreutzberger, Kiessling, Liang, Yang, et al., 2017). Fusion efficiencies are reported as the percentage of granules in the field of view that fuse within 15 s. Fluorescent line shapes are presented as average from 20 single events as described previously Kreutzberger, Kiessling, Liang, Yang, et al., 2017).

Statistical analysis

Graphpad Prism 7 was used for analysis of data collected from TIRF studies, Immunocytochemistry, electrophysiological data and qPCR. Igor was used to fit and analyze data collected from single granule/supported membrane fusion assays. Data collected for studies utilizing primary chromaffin cell culture were collected using at least three different cell preparations. Specifically, co-localization studies include the average and standard error of the mean (SEM). Imaging studies on the release of cargos were analyzed using non-linear regressions and Tukey's multiple comparisons tests ($p < .05$) to determine if there were

significant differences between groups. Fusion probability and release data were statistically analyzed using a non-parametric Mann–Whitney test, $p < .05$. The choice of using a parametric o r n on-parametric test was determined by an F-test or a Brown–Forsythe test which determines if variances are significantly different; values are reported in results section if non-parametric tests were used. No sample calculation was performed to determine appropriate sample sizes. The ROUT method was used to identify outliers (Graphpad Prism).

Results

The localization of Syt-7 in mouse chromaffin cells

Fluorescent labeling of endogenous Synaptotagmin-1 and −7 in bovine adrenal chromaffin cells revealed these proteins to exhibit a punctate intracellular distribution, with a low degree of co-localization (Rao et al., 2014). A similar pattern is observed in chromaffin cells harvested from the mouse adrenal medulla. As shown in Figure 2.1, endogenous Syt-1 and Syt-7 fluorescence is largely nonoverlapping (in the range of 3%–5%), punctate, and intracellular (Figure 2.1a and b). It was previously reported that Syt-7 is sorted to the plasma membrane in PC12 cells and rat chromaffin cells (Sugita et al., 2001). However, the punctate pattern of staining observed here is most consistent with the protein being sorted to organelles. The co-localization of Syt-7 with plasminogen activator inhibitor-1 (PAI-1) (Figure 2.1c and d)—a ubiquitous dense core marker in chromaffin cells (Abbineni et al., 2019; Bohannon et al., 2017)—shows that Syt-7 is present in secretory granules. Confocal imaging of immunolabeled Syt-7 demonstrates that it is co-localized with lysosome associated membrane protein-1 (LAMP-1), in the range of 14%—18% (Figure 2.1e and f). LAMP-1 and PAI-1 exhibited a roughly 10%—11% co-localization frequency (Figure 2.1g and h). LAMP-1 has been previously shown to label both granules and lysosomes in chromaffin cells (Hao et al., 2015).

To further characterize the subcellular distribution of Syt-7, bovine chromaffin cell lysates were layered on an iodixanol gradient and centrifuged to separate organelles by density (see Methods). Sequential fractions of 400 μl were collected and run on a polyacrylamide gel for western blotting. Immunoreactive bands corresponding to PAI-1, Syt-7, Syt-1, and LAMP-1 are evident in Figure S3. Given the intensity of the PAI-1 reactivity, fraction 13 likely contains dense core granule constituents. Less dense fractions (4–6) presumably contain lysosomes or endosomes. Syt-7 and Syt-1 also appear in these lighter fractions, in addition to those that contain PAI-1.

Endogenous Syt-7 slows dense core granule cargo release

A major goal of this study was to delineate the ways in which the chromaffin cell secretory system depends on the presence of Syt-7. To avoid the potential ambiguities associated with over-expression of synaptotagmins in cells already expressing a full complement of endogenous proteins, most of the experiments in this study instead rely on cells harvested from Syt-7 KO mice. Figure S4a shows that compared to WT cells, expression of Syt-1 transcript remains unchanged in KO cells, while Syt-7 transcript is undetectable. Western blotting was also performed on adrenal gland lysates to verify the loss of Syt-7 protein in the KO. The alpha variant of Syt-7 (403 amino acids), targeted by Andrews and colleagues when generating the original Syt-7KO mouse, has been reported to run at approximately 45 kDa (marked by arrow) (Martinez et al., 2000). That band is absent in the KO (Figure S4b).

Our first objective was to determine the release rate of NPY-pHl in Syt-7 KO cells compared to WT cells. Cells expressing fluorescent protein were identified by a brief exposure to 10 mM NH_4Cl (Anantharam, Onoa, Edwards, Edwards, & Axelrod 2010). Single cells were then depolarized by local perfusion of 100 mM KCl while exocytosis was imaged with a TIRF

microscope. Figure 2.2a, b, and d show that the time necessary for NPY to be completely released from fused chromaffin granules is broadly distributed in WT cells (times ranged from 0.049 s to 8.10 s; the data are not normally distributed). In Syt-7 KO cells, NPY release durations were shifted to shorter times (ranging from 0.084 s to 1.17 s) (Figure 2.2c and d). A cumulative frequency distributions representing the time at which granules fused with respect to the start of stimulation, are plotted in Figure 2.5s.

To assess if Syt-7 is responsible for slower rates of NPY release, myc-tagged Syt-7 and NPY-pHl (myc expression was verified post hoc) were co-expressed in Syt-7 KO cells. Cells were stimulated with KCl and the rate of NPY release determined, as above. In cells expressing myc-Syt-7, a slow population of NPY release times was again observed (times ranged from 0.076 s to 8.05 s) (Figure 2.2d).

Certain lumenal cargo proteins, such as tissue Plasminogen Activator (tPA), exhibit intrinsically slower release or 'discharge' times during exocytosis (Perrais, Kleppe, Taraska, & Almers, 2004; Weiss, Anantharam, Bittner, Axelrod, & Holz 2014). In the case of tPA, this has been attributed to the protein's ability to stabilize the curvature of the fusion pore and thereby limit its rate of expansion (Bohannon et al., 2017). Here, the goal was to address whether tPA release from fused granules may be hastened by the abrogation of Syt-7 expression—a protein which imposes its own constraints on fusion pore expansion (Rao et al., 2014; Rao et al., 2017). As described previously, the rate of release of tPA-pHl was measured in both WT and Syt-7 KO cells depolarized with KCl. The average rate at which tPA is released is considerably slower than it is for NPY (tPA: 6.57 ± 0.59 s, NPY: 0.67 ± 0.13 s, Mann–Whitney test, $p < .0001$, Brown–Forsythe test, $p < .05$) (Figure 2.2e). Transfection with tPA yielded secretion events from WT cells with a large distribution of release times ranging from 68 ms to 30.67 s (average time =

6.57 ± 0.59 s; n = 103 events). In Syt-7 KO cells, the distribution of the release time was somewhat narrower, and ranged from 84 ms to 17.44 s (average time = 3.16 ± 0.38 s; n = 120 events). The over-expression of myc-Syt-7 in the Syt-7 KO cells again restored the broader distribution of release times, which ranged from 100 ms to 33.4 s (average time = 7.00 ± 0.62 s; n = 89 events). * $p < .05$, ** $p < .005$ Tukey's multiple comparison test.

Granule fusion probability and mobility in WT and Syt-7 KO cells

The number of NPY-GFP-labeled, docked granules that fused in response to 100 mM KCl depolarization in WT and KO cells was determined and used to calculate a granule fusion probability (Figure 2.3a; see also Movie S1). The criterion for 'docked' in this case, is that the granule is resident in the evanescent field at the start of KCl stimulation. The absence of Syt-7 severely disrupts the secretory response to KCl-based depolarization. This is evidenced by the fact that fusion probability of granules in KO cells is approximately 5-fold lower than that of granules in WT cells (Figure 2.3b).

In a previous study, we had reported that the frame-to-frame displacement (ΔR) of granules in bovine chromaffin cells harboring GFP-Syt-7 was, on average, lower than that of granules harboring GFP-Syt-1 (Rao et al., 2017). Thus, we also set out to determine whether granule mobility varies as a function of Syt-7 expression. NPY-GFP-labeled granules in WT and KO cells were tracked over a minimum of 200 frames (10 s in duration) (Figure S6a and b). From those tracks, ΔR of individual granules was calculated (Figure S6c) (Rao et al., 2017). The distribution of ΔRs for granules from both cell-types, WT and KO, were best fit to a sum of two gaussians. The average ΔR from the slower WT population was 29.32 ± 1.41 nm, and 48.39 ± 1.13 nm for the faster population, with 53.58 ± 30.67% of granules residing in the slower population. The differences between the slower and faster populations of

KO granules were less pronounced, with a slow population ΔR of 27.82 ± 0.59, a fast population ΔR of 39.97 ± 3.76 nm, and 47.84 ± 59.77% of granules residing in the slower population. Thus, the mobility of chromaffin granules labeled with NPY-GFP was not significantly different between WT and Syt-7 KO groups.

Stimulation of secretion in WT and SYT-7 KO cells with a physiological agonist

Chromaffin cell secretion, in situ, is triggered by the activation of nicotinic receptors and subsequent Ca^{2+} influx (Douglas, 1968; Douglas & Rubin, 1963). Therefore, to understand how the lack of Syt-7 might disrupt secretion in a physiological setting, WT and KO cells were stimulated with ACh delivered locally via a perfusion pipet. ACh triggered release kinetics of NPY-pHl was measured first (Figure 2.4a– d). As with elevated KCl stimulation, the range of NPY release times in response to ACh stimulation was broader in WT cells (0.06 s to 24.05 s) than in Syt-7 KO cells (0.07 s to 2.93 s). On average, the rate at which NPY is released was slower in WT cells compared to Syt-7 KO cells (WT: 1.47 ± 0.34 s, KO: 0.44 ± 0.1 s, Mann–Whitney test, $p < .05$, Brown–Forsythe, $p < .05$) (Figure 2.4d). Moreover, the overall fusion probability of NPY-GFP-labeled granules in Syt-7 KO cells was substantially lower than WT cells (Movie S2) following cholinergic stimulation (3.2 ± 0.7% in KO vs. 19.1 ± 3.4% in WT) (Figure 2.5a and b).

One potential explanation for the difference in granule fusion probability observed between the two cell types is that Ca^{2+} signaling is compromised in cells lacking Syt-7. Therefore, qualitative changes in intracellular Ca^{2+} in response to ACh stimulation were monitored using the fluorescent Ca^{2+} indicator, GCaMP5G (Akerboom et al., 2012). Neither the kinetics nor the peak amplitude of the GCaMP5G signal differed between WT and Syt-7 KO cells (Figure 2.5c and d). The possibility that differences in the magnitude of cholinergic or Ca^{2+}

currents might underlie differences in the secretory phenotype of WT and KO cells was also tested. However, these were not different between the two groups (Figures S7a–d).

Sustained chromaffin cell secretory output relies on the presence of SYT-7

During the course of the experiments described in Figure 2.4, it became evident that the times at which NPY-pHl-labeled granules fused with respect to the start of stimulation varied depending on the genotype of the cell. To examine this issue more closely, WT and KO cells expressing NPY-pHl were stimulated for 2 min with 100 μM ACh while images were continuously acquired. The secretory response of a single WT and Syt-7 KO cell to prolonged ACh stimulation (beginning at 5 s after imaging begins) is shown in Figure 2.6a and b. Each of the vertical lines (blue for WT and red for KO) corresponds to the time of an individual NPY fusion event during the period of stimulation. In contrast to WT cells, the secretory response of KO cells rapidly wanes after an initial burst of fusion events.

The cumulative distribution of all fusion events in WT and Syt-7 KO cells (n = 7 cells for each group) occurring after ACh stimulation is plotted in Figure 2.6c. A distinctive feature of the cumulative time course for Syt-7 KO events is that the curve plateaus. Such a result would be expected if the absence of Syt-7 prevents a sustained response to cholinergic stimulation. The cumulative time course for WT cells stimulated with ACh does not plateau; secretion is observed for as long as the cell is stimulated although the frequency with which events occur does decline at later times. The curves were fit by the sum of two exponential (Figure 2.6c). Interestingly, over the first approximately 20 s of ACh stimulation, there is more secretory activity in the Syt-7 KO than in the WT cell (see inset, Figure 2.6c).

SYT-7 endows dense core granules with distinct Ca^{2+}-sensing and fusion properties

To better assign mechanistic roles to Syt-1 and Syt-7 in exocytosis, we utilized a previously characterized purified secretory granule to planar supported bilayer fusion assay (Figure 2.7a). PC12 cells lacking endogenous synaptotagmin (Kreutzberger, Kiessling, Liang, Seelheim, et al., 2017) were transfected to over-express either Syt-1 or Syt-7 protein ((Kreutzberger et al., 2019) and Figure 2.7b). In the presence of SNARE regulatory proteins Munc18 and complexin-1, these granules will bind in an arrested state to planar supported bilayers (lipid composition of 70 : 30 bPC:Chol in the extracellular mimicking leaflet and 25 : 25 : 15 : 30 : 4 : 1 bPC:bPE:bPS:Chol:PI:PIP2) containing the plasma membrane SNARE proteins (syntaxin-1a and dSNAP-25). Injection of Ca^{2+} into this system readily stimulates fusion of dense core granules with the planar bilayer. Increasing the level of Ca^{2+} in the chamber containing docked dense core granules, triggers fusion with different efficiencies depending on the sensitivity to Ca^{2+} of the expressed synaptotagmin isoform (Figure 2.7c). Syt-7 containing dense core granules consistently fused at lower Ca^{2+} concentrations than those bearing Syt-1. The higher sensitivity of Syt-7-bearing granules to Ca^{2+} is consistent with the observations previously made in bovine chromaffin cells stimulated to secrete with elevated KCl (Bendahmane et al., 2018; Rao et al., 2014, 2017).

The intensity time course of NPY-mRuby fluorescence during release has noteworthy characteristics. Initially, a decrease in fluorescence is observed as NPY-mRuby begins to diffuse out of the early fusion pore and away from the fusion site (note dip in fluorescence in Figure 2.7d and e). After a brief delay, a sharp increase in fluorescence intensity is observed as the fusion pore expands and the granule membrane collapses (Kreutzberger, Kiessling, Liang, Yang, et al., 2017).

Previously, the delay time from the onset of NPY-mRuby release was shown to be sensitive to the presence of lipids with geometries that promote or inhibit fusion pore stability (Kreutzberger, Kiessling, Liang, Yang, et al., 2017). Here, we show this feature is also sensitive to the synaptotagmin isoform expressed. A close examination of the fluorescence intensity profile of Syt-1 granules shows that there is approximately a 0.4 s delay time from the initial decrease in fluorescence until the collapse of the granule into the supported bilayer (Figure 2.7d). In Syt-7 granules, the delay is lengthened to approximately 1 s (Figure 2.7e). An overlay of averaged release profiles of NPY from Syt-1 and Syt-7 granules is shown in Figure S8c. Images of individual NPY-mRuby release events from Syt-1 and Syt-7-bearing granules are also shown in Figure S8.

Discussion

Despite the broad interest in Syt-7 as a regulator of exocytosis (MacDougall et al., 2018), surprisingly basic aspects of its function remain unresolved, including its intracellular localization and role in regulating fusion pore expansion. Using a combination of subcellular fractionation and immunolabeling methods, we report that endogenous Syt-7 is colocalized with markers of the lysosome and dense core granule (LAMP-1 and PAI-1, respectively). The marker used in this study to identify granules, PAI-1, is ubiquitously expressed in chromaffin cells (Bohannon et al., 2017) and exhibits a high degree of co-localization with other markers of the dense core, tPA and dopamine β-hydroxylase (Abbineni et al., 2019; Bohannon et al., 2017). The conclusion that fraction 13 (Fr-13, Figure S3) contained the majority of dense core granule constituents is based on the strong PAI-1 signal. Syt-7 was most abundant in fractions 13 and 4-6. Approximately 20% of the total amount of Syt-7 in the cell can be found in fraction 13 (i.e., granules)—a number that is also consistent with the immunocytochemical data (Figure 2.1).

Fractions 4-6 represent less dense organelles, including lysosomes. Immunoreactivity for LAMP-1 is greatest in fractions 4-6, but is also detected in fraction 13. This suggests that dense core granules house LAMP1 in addition to Syts 1 and 7 – a conclusion which is supported by immunocytochemical data (Figure 2.1) and published reports (Hao et al., 2015).

We presume that membrane proteins, such as Syt-7, are turned over more slowly than secreted proteins (Winkler, 1971). The recycling of synaptotagmin isoforms (e.g., after fusion) would account for their higher abundance in lighter organelles which may form part of the endolysosomal system. Interestingly, Syt-1 is more abundant in fraction 13, as a percentage of total protein, than is Syt-7. This may reflect differences in the steady-state turnover of granules to which Syt-1 and Syt-7 are sorted.

The basic finding that Syt-7 is sorted to chromaffin granules corroborates what has been previously published in PC12 cells and chromaffin cells (Fukuda, Kanno, Satoh, Saegusa, & Yamamoto, 2004; Rao et al., 2014; Tsuboi & Fukuda, 2007; Zhang et al., 2011). In contrast, neuronal Syt-7 has been reported to exist primarily as a plasma membrane bound protein (Jackman, Turecek, Belinsky, & Regehr, 2016; Sugita et al., 2001; Weber, Toft-Bertelsen, Mohrmann, Delgado-Martinez, & Sorensen, 2014) (Jackman et al., 2016; Sugita et al., 2001; Weber et al., 2014). The reason for differences in Syt-7 localization between neurons and neuroendocrine cells is unclear at this time.

A second key unresolved issue concerning the function of Syt-7 in chromaffin cells is whether it constrains (Rao et al., 2014), or alternatively, promotes (Zhang et al., 2019) fusion pore expansion. Here, two distinct experimental preparations were used to address this issue: (1) primary mouse chromaffin cells lacking Syt-7; and, (2) a reconstituted single granule fusion assay employing PC12 granules only expressing either Syt-1 or Syt-7. Data gathered from both

experimental preparations provide support for the principle that Syt-7 imposes limits on the rate at which cargos are discharged during exocytosis. In the case of cargos that exhibit an intrinsically slow release profile (e.g., tPA), the effect of Syt-7 is additive. The findings are also consistent with TIRF-based measurements of secretion in other systems, including PC12 cells (Zhang et al., 2011) and mouse embryonic fibroblasts (Jaiswal et al., 2004), where it has been shown that Syt-7 restricts post-fusion soluble content release and diffusion of granule membrane proteins into the plasma membrane.

Although the mechanism by which Syt-7 acts at the pore to slow discharge is not resolved, the protein's high affinity for anionic phospholipids likely plays a key role. According to this model, the tight binding of the Syt-7 C2 domains to lipids constituting the fusion pore is a determining factor of pore stabilization (Bendahmane et al., 2018; Tran, Anderson, & Knight, 2019; Voleti, Tomchick, Sudhof, & Rizo, 2017). In support of this hypothesis, a mutant of Syt-1, whose C2B domain Ca^{2+}/phospholipid-binding loops were exchanged for those of Syt-7, exhibited a higher intrinsic affinity for phospholipids and a slower dissociation from phospholipids in the presence of Ca^{2+}, than the WT Syt-1 protein (Bendahmane et al., 2018). When expressed in cells, this Syt-1 mutant also stabilized membrane curvature associated with the fused granule/plasma membrane domain, thereby slowing the discharge of NPY-pHl (Bendahmane et al., 2018). It should be noted here that fluorescent peptide hormone release observed by TIRF microscopy is likely to represent a slower process than the transition from pre-spike foot to burst of neurotransmitter release captured by amperometry recordings, which occurs in a matter of milliseconds (Albillos et al., 1997; Ales et al., 1999; Chow, Ruden, & Neher, 1992; Lindau & Alvarez de Toledo, 2003; Segovia et al., 2010; Wightman et al., 1991). Although both phenomena have been interpreted as expansion of the fusion pore, they are likely

to represent temporally distinct kinetic steps in the process of exocytosis. Therefore, a clear distinction between fusion pore dynamics as described by imaging and electrochemical methods should be made.

This study shows that Syt-7 and Syt-1 are both necessary for a robust secretory response to native stimuli that elevate intracellular Ca^{2+} level (Figure 2.6). The number of fusion events, and the rate at which those fusion events occur, are significantly lower in Syt-7 KO cells than in WT cells. The decreased likelihood of observing fusion events in cells that do not express Syt-7 is not due to impaired Ca^{2+} 'handling' or excitability. There is also no difference in the magnitude of Ca^{2+} or cholinergic current in Syt-7 KO cells compared to WT cells (Figure S7). Based on the data shown in Figures 6 and 7, a mechanism is proposed to explain why the secretory response to prolonged cholinergic stimulation is disrupted in Syt-7 KO cells. Over the course of a 2-min exposure to ACh, nicotinic receptors (nAChRs) undergo desensitization (Figure 2.7s ba). Free cytosolic Ca^{2+}, initially elevated as a result of Ca^{2+} influx through nAChRs, and also possibly Cavs, is rapidly sequestered, buffered, or extruded (Neher & Augustine, 1992). Despite the collapse of the Ca^{2+} gradient, fusion persists in WT cells throughout the period of ACh perfusion (Figure 2.8b and c). In Syt-7 KO cells, secretory activity quickly ceases after an initial burst of fusion. Thus, expression of Syt-7 is necessary for sustained activity in the setting of rapidly declining levels of intracellular free Ca^{2+} following nAChR desensitization. Presumably, the residual Ca^{2+} that remains is effective at triggering fusion only when Syt-7 is present (Figure 2.8c). The stark differences in Ca^{2+} affinities between Syt-1 and Syt-7 are likely sufficient to account for this phenomenon (Bhalla et al., 2005; Sugita et al., 2002). Dose–response curves (Figure 2.7c) show that there is at least a 6-fold difference in the

[Ca^{2+}]1/2 for fusion of purified dense core granules bearing Syt-1 (63 μM) versus Syt-7 (10 μM). In fact, at 10 μM Ca^{2+}, there is no appreciable fusion of Syt-1 granules.

Interestingly, the time course of the cumulative frequency distribution of fusion events in Syt-7 KO cells stimulated by ACh and KCl is different (Figure 2.5s compare to Figure 2.6). This can be explained by the fact that Ca^{2+} elevations evoked by ACh stimulation (Figure 2.5) decay more rapidly in the subplasmalemma than those evoked by KCl secretion (Fulop & Smith, 2007; Rao et al., 2014), which in the absence of Syt-7, results in a more rapid inhibition of the secretory response. The rate at which NPY was released as a result of fusion in WT cells differed depending on whether KCl or ACh was used to trigger release (compare Figures 2 and 4). It may be that ACh-based stimulation relies to a greater extent on activation of granules bearing Syt-7 than does KCl-based stimulation, or such variability may simply reflect the fact that experiments were performed in different groups of cells at different times. Irrespective of the manner of stimulation, the absence of Syt-7 has the consistent effect of speeding NPY cargo release.

We note that no significant difference in the mobility of NPYGFP-labeled chromaffin granules in WT and Syt-7 KO cells was observed in this study. A previous study, in which fluorescently-tagged Syts were over-expressed in cells, revealed that the frame-to-frame movement of granules harboring Syt-1 was greater than those harboring Syt-7 (Rao et al., 2017). Therefore, the degree to which the molecular identity of a chromaffin granule regulates its mobility and whether this depends on the expression of a particular Syt isoform, all remain open questions for future work. We also note that the absence of Syt-7 inhibits the secretory response to a greater extent in these TIRF-based studies than what had been previously reported in studies that measured secretion by capacitance or amperometry (Schonn et al., 2008; Segovia et al., 2010). One can speculate as to the reasons why. What is reported here is the probability of

fusion, which requires over-expression of NPY-GFP in order to identify docked granules. It is only the fusion of these labeled granules, which likely constitute a minority of the total fusion-competent population of granules within the cell, that is documented. The manner in which secretion was elicited in these studies, and previous ones in which capacitance was measured, is also different. Here, cells were stimulated via local perfusion of elevated KCl or ACh. In studies employing capacitance measurements, cells were stimulated by either directly depolarizing the membrane potential via the patch pipet, or by uncaging Ca^{2+} to concentrations in the range of tens of micromolar (Schonn et al., 2008). Secretion elicited by a strong stimulus and associated with a greater increase in intracellular Ca^{2+}, may be less likely to rely on fusion mediated by Syt-7.

To conclude, the experiments in this study demonstrate that the absence of Syt-7 has a profound impact on Ca^{2+}-triggering of exocytosis and the discharge rate of peptide hormones. A key result is that the delayed kinetic component of the secretory response to cholinergic stimulation, during which subplasmalemmal Ca^{2+} elevations have collapsed to near baseline levels, is impaired in Syt-7 KO cells. This is shown in cumulative frequency histograms of the time course of fusion events, which can be fit by the sum of two exponentials representing the fast and slow/sustained phases of secretion. The fast phase, in WT cells, is a minor component of the curve (0.66%), whereas the slow phase dominates. In the Syt-7 KO, the fast phase of release constitutes a greater proportion of the span of the curve (58.08%) than the slow phase. The idea that the initial and later phases of exocytosis have different Ca^{2+} sensitivities is supported by previous work performed in permeabilized bovine chromaffin cells (Bittner & Holz, 1992). By measuring [3H] norepinephrine in the medium after cells were exposed to different levels of Ca^{2+}, Bittner and Holz (1992) concluded that an early phase of release (i.e., occurring with 5 s of

stimulation) must correspond to a lower affinity process ($[Ca^{2+}]1/2 \approx 100$ μM) than a later phase of release (i.e., occurring between 5 and 10 s ($[Ca^{2+}]1/2 \approx 10$ μM)). In this study, we propose a molecular mechanism to account for these observations—a mechanism that relies on the sequential activation of specialized low and high affinity Ca^{2+} sensors.

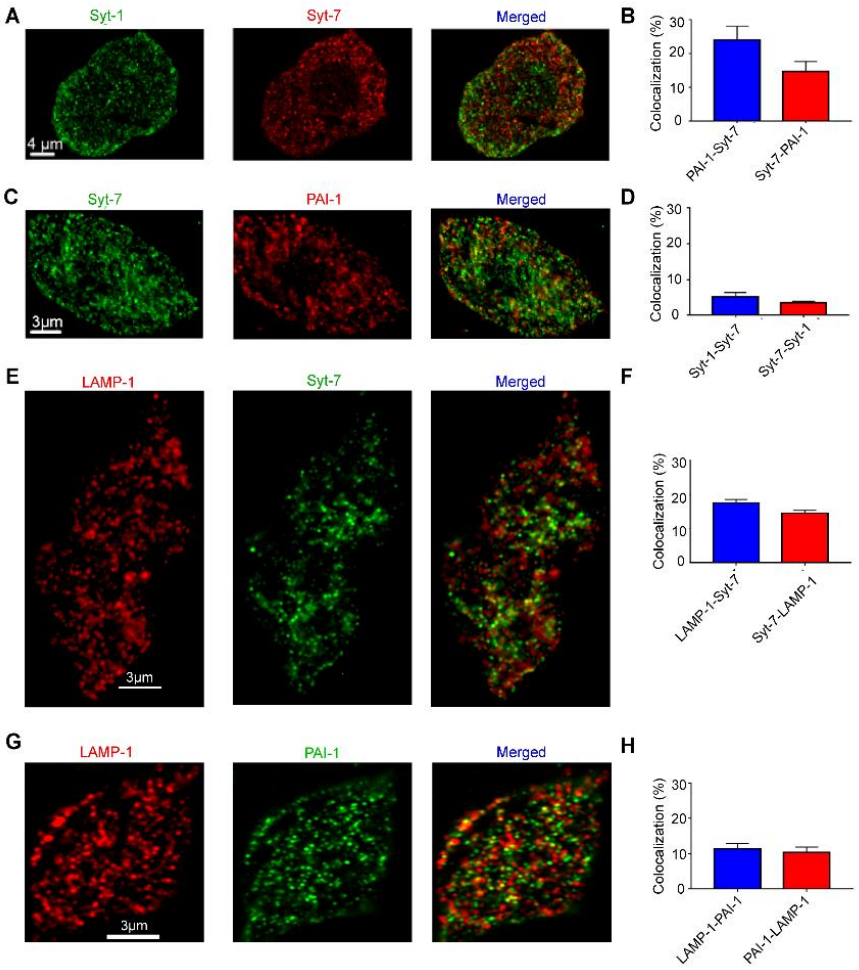

F I G U R E 2.1 Endogenous Syt-7 is co-localized with PAI-1, a protein of the granule dense core. (a) Immunolabeling was performed in WT cells for endogenous Syt-7 (red) and Syt-1 (green). Images from a representative cell showing Syt-7 fluorescence, Syt-1 fluorescence, and fluorescence of the merged channels. (b) Box plot indicates the percentage of Syt-1 puncta that harbor Syt-7 (5.18 ± 1.03%; *n* = 8 cells; 3 primary cell preparations) and Syt-7 puncta that harbor Syt-1 (3.36 ± 0.43%; *n* = 8 cells; 3 primary cell preparations). (c) Immunolabeling was performed in WT cells for Syt-7 (green) and PAI-1, a dense core granule marker (red). (d) Box plot showing the percentage of PAI-1 puncta that are co-localized with Syt-7 (24.06 ± 1.41%; *n* = 8 cells; 3 primary cell preparations) and the percentage of Syt-7 puncta that are colocalized with PAI-1 (14.65 ± 1.075%; *n* = 8 cells; 3 primary cell preparations). (e) Immunolabeling was performed in WT cells for endogenous LAMP-1 (red) and Syt-7 (green). Images from two representative cells showing LAMP-1 fluorescence, Syt-7 fluorescence, and fluorescence of the merged channels. (f) Box plot shows the percentage of LAMP-1 staining that harbor Syt-7 puncta (17.59 ± 2.28%; *n* = 6 cells; 2 primary cell preparations) and Syt-7 puncta that harbor LAMP-1 staining (14.58 ± 1.83%; *n* = 6 cells: 2 primary cell preparations). (g) Immunolabeling was performed in WT cells for endogenous LAMP-1 (red), a lysosomal marker, and PAI-1 a dense core granule marker (green). (h) Box plot shows the percentage of LAMP-1 staining that are co-localized with PAI-1 puncta (11.42 ± 3.44%; *n* = 6 cells; 2 primary cell preparations) and the percentage of PAI-1 puncta that are co-localized with LAMP-1 (10.31 ± 3.47%; *n* = 6 cells; 2 primary cell preparations). For all box-plots, box dimensions extend from the 25th to the 75th percentiles; whiskers represent the minimum and maximum values; line represents median

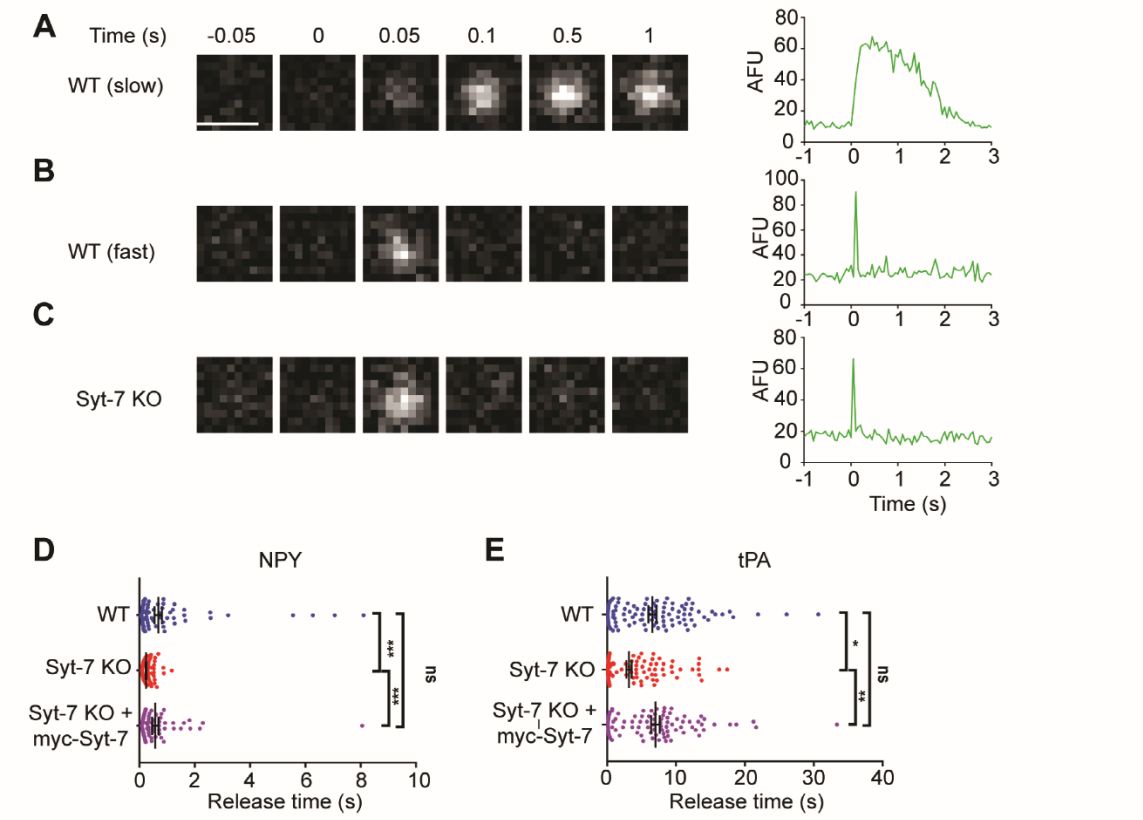

F I G U R E 2.2 Syt-7 slows release of lumenal cargos. WT and Syt-7 KO cells over-expressing pHl-tagged NPY and tPA were stimulated with 100 mM KCl. Fusion events were observed using total internal reflection fluorescence microscopy and cargo release times were measured. (a–c) Representative images showing fusion events of NPY-pHl expressing granules from WT and Syt-7 KO chromaffin cells alongside intensity versus. time curves. Release times in WT cells ranged from fast to slow (a). However, release in Syt-7 KO cells was shifted to faster times (c). (d) Individual times for NPY release are shown in a scatter plot. In WT cells, these ranged from 49 ms to 8.10 s (average time = 0.67 ± 0.13 s; n = 100 events; 3 primary cell preparations). In Syt-7 KO cells, the distribution of the release times was narrower, and ranged from 84 ms to 1.17 s (average time = 0.25 ± 0.17 s; n = 73 events; 3 primary cell preparations). The over-expression of myc-Syt-7 in Syt-7 KO cells restored the broader distribution of release times, which now ranged from 76 ms to 8.05 s (average time = 0.57 ± 0.11 s; n = 77 events; 3 primary cell preparations). (e) Release times for individual tPA events shown in a scatter plot. Secretion events from WT cells show a large distribution of release times ranging from 68 ms to 30.67 s (average time = 6.57 ± 0.59 s; n = 103 events; 3 primary cell preparations). In Syt-7 KO cells, the distribution of the release time was somewhat narrower, and ranged from 84 ms to 17.44 s (average time = 3.16 ± 0.38 s; n = 120 events; 3 primary cell preparations). The over-expression of myc-Syt-7 in the Syt-7 KO cells again restored the broader distribution of release times, which now ranged from 100 ms to 33.4 s (average time = 7.00 ± 0.62 s; n = 89 events; 3 primary cell preparations). *p < .05, **p < .005 Tukey's multiple comparison test

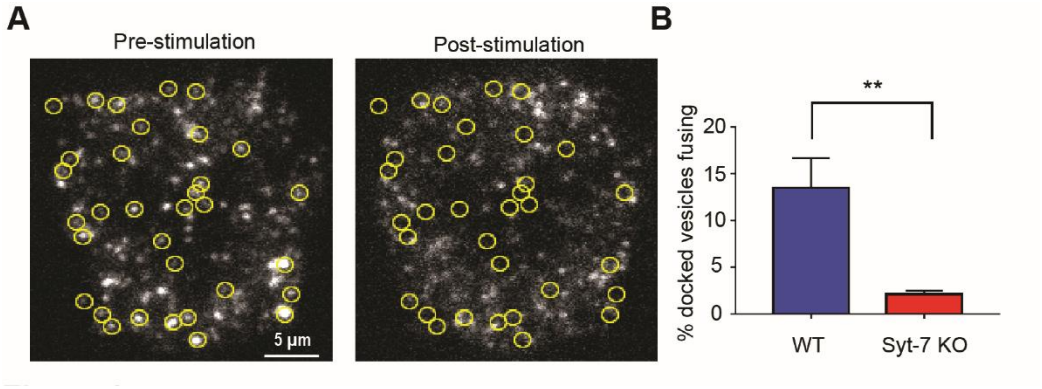

F I G U R E 2.3 Syt-7 endows granules with an increased fusion probability. WT and Syt-7 KO cells over-expressing GFP-tagged NPY were stimulated with 100 mM KCl. Fusion events were observed using total internal reflection fluorescence microscopy (TIRFM). (a) Pre- and post-stimulation images of fluorescent NPY puncta in a WT cell. Yellow circles indicate the position of granules that fused during the stimulation period. (b) Box plot showing the percentage of docked granules that fused in WT (13.49 ± 3.23%; n = 8 cells; 4 primary cell preparations) and Syt-7 KO cells (2.14 ± 0.36 s; n = 5 cells; 4 primary cell preparations). Box dimensions extend from the 25th to the 75th percentiles; whiskers represent the minimum and maximum values; line represents median. ** $p < .005$, Mann–Whitney test, Brown– Forsythe, $p < .05$)

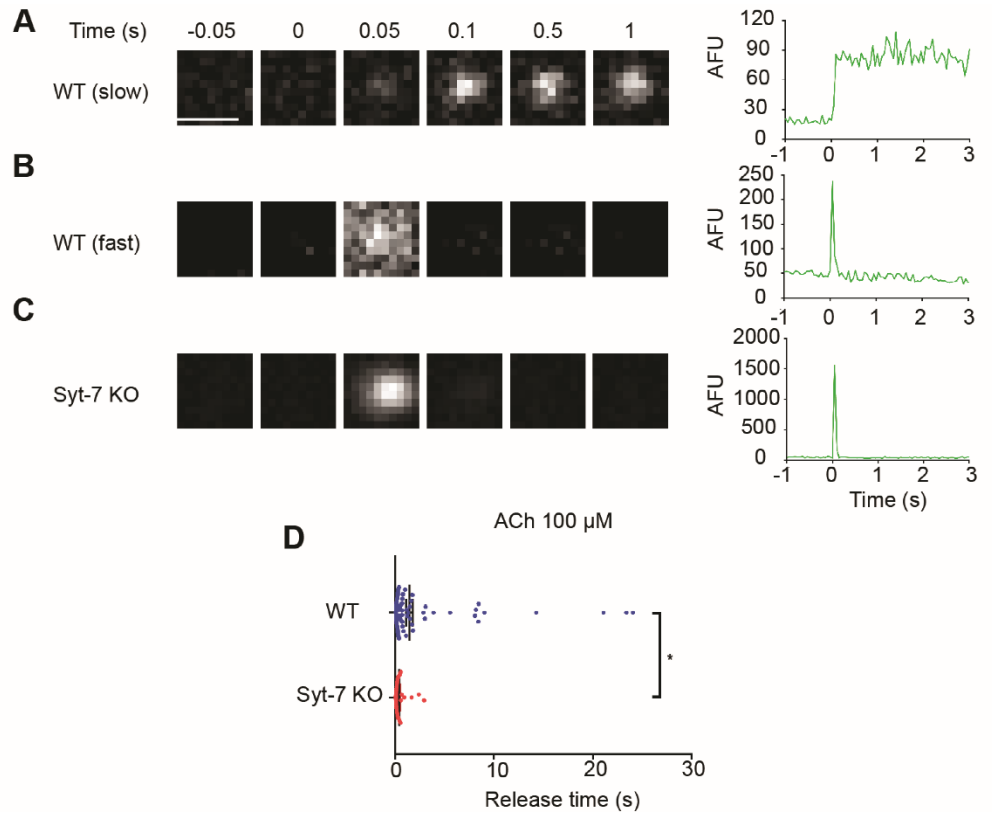

F I G U R E 2.4 Syt-7 slows release of over-expressed NPY in cells stimulated with ACh. WT and Syt-7 KO cells over-expressing NPY were stimulated with 100 µM ACh for 2 min. Fusion events were monitored using total internal reflection fluorescence microscopy (TIRFM) and NPY release times were measured. (a–c) Representative images showing fusion events from WT and Syt-7 KO chromaffin cells alongside intensity versus. time curves. Release times in WT cells ranged from fast to slow (a). Release times in Syt-7 KO cells were typically faster (c). (d) Release times for individual NPY fusion events shown in a scatter plot. Release times in WT cells ranged from 67 ms to 24.05 s (average time = 1.47 ± 0.34 s; n = 130 events, 7 cells; 3 primary cell preparations). In Syt-7 KO cells, the distribution of the release times was narrower and ranged from 70 ms to 2.93 s (average time = 0.44 ± 0.10 s (n = 38 events, 9 cells; 3 primary cell preparations)

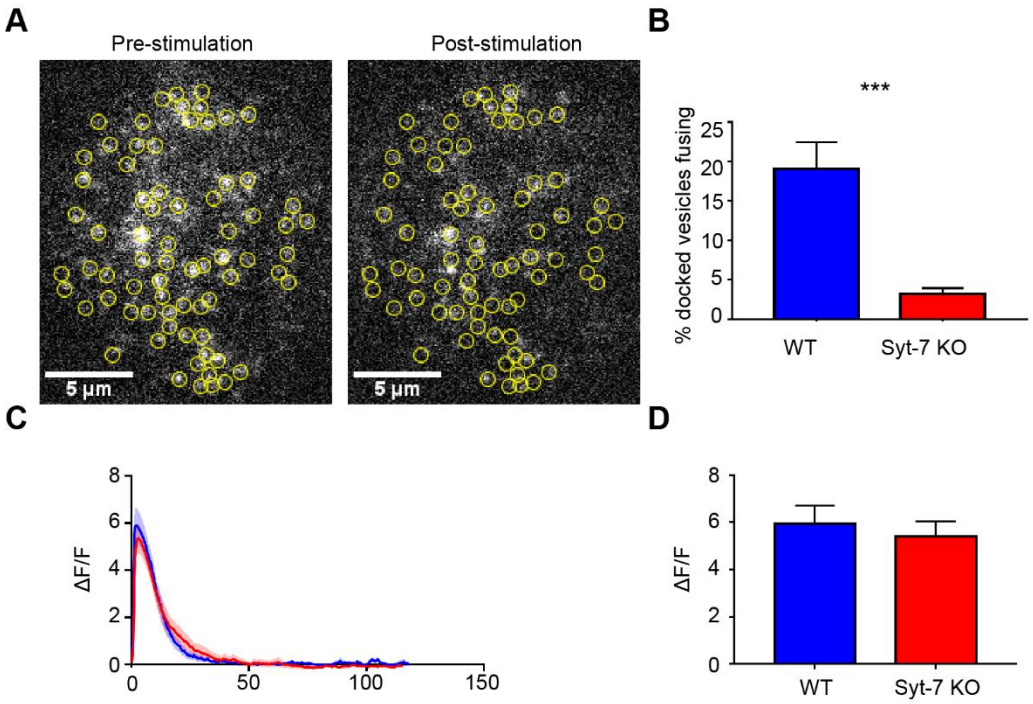

F I G U R E 2.5 Granules in Syt-7 KO cells stimulated by ACh evince a lower fusion probability than those in WT cells. WT and Syt-7 KO cells over-expressing GFP-tagged NPY were stimulated with 100 µM ACh for 2 min. Fusion events were observed using total internal reflection fluorescence microscopy (TIRFM). (a) Pre- and post-stimulation images of fluorescent NPY puncta in a WT cell. Yellow circles indicate the position of granules that fused during the stimulation period. (b) Box plot showing the percentage of docked granules that fused in WT (19.1 ± 3.4%; n = 8 cells; 4 primary cell preparations) and Syt-7 KO cells (3.2 ± 0.7%; n = 7 cells; 4 primary cell preparations). ***p < .005, Mann–Whitney test, Brown-Forsythe, p < .05). (c–d) WT and Syt-7 KO cells transfected with GCaMP5G were stimulated with 100 µM ACh for 2 min. Fluorescence was monitored using TIRFM, with ΔF/F was calculated for each cell. (c) Average ΔF/F versus. time traces in response to ACh stimulation for WT (n = 7 cells, blue; 5 primary cell preparations) and Syt-7 KO (n = 7 cells, red; 5 primary cell preparations) cells. (d) Box plot showing the average value of the peak ΔF/F for WT (5.41 ± 0.62) and Syt-7 KO (5.94 ± 0.76) cells. The average values were not statistically significant (Student's t-test, p > .05). For all box plots, box dimensions extend from the 25th to the 75th percentiles; whiskers represent the minimum and maximum values; line represents median

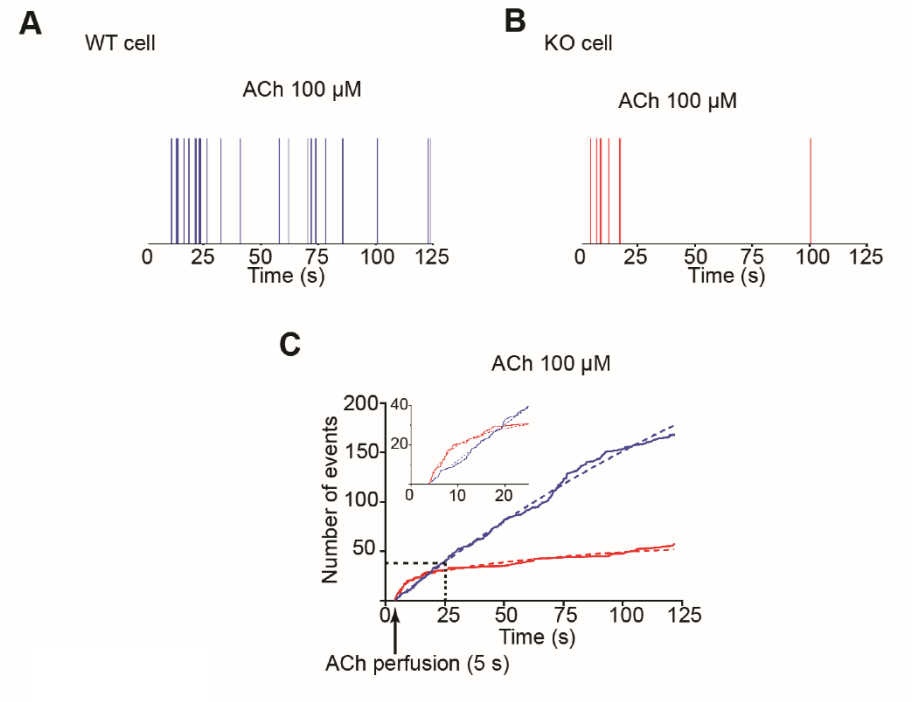

F I G U R E 2.6 Syt-7 is necessary to sustain secretion during prolonged ACh stimulation. NPY-pHl was over-expressed in WT and Syt-7 KO chromaffin cells. Secretion was triggered by local perfusion of 100 µM ACh. (a and b). Time distribution of fusion events in a WT (a) and Syt-7 KO (b) cell. Each vertical line corresponds to the occurrence of a single fusion event during the stimulation period. (c) Cumulative frequency distribution showing the time at which fusion events occurred in WT (blue) and Syt-7 KO (red) cells (n = 7 cells; 4 primary cell preparations for each group). WT cells continue to secrete throughout the course of the stimulation period; secretory activity in Syt-7 KO cells largely ceases after 25 s. Note that in the 5–25 s window (inset), the rate at which fusion events occur is actually higher in the Syt-7 KO cell. Curves were fit by a two phase association function in Prism 7 with $R2 \geq$ 0.99; WT: $k$fast = 1.3 s−1; $k$slow = 4.3 × 10−3 s−1; KO: $k$fast = 0.2 s−1; $k$slow = 1.3 × 10-2s−1

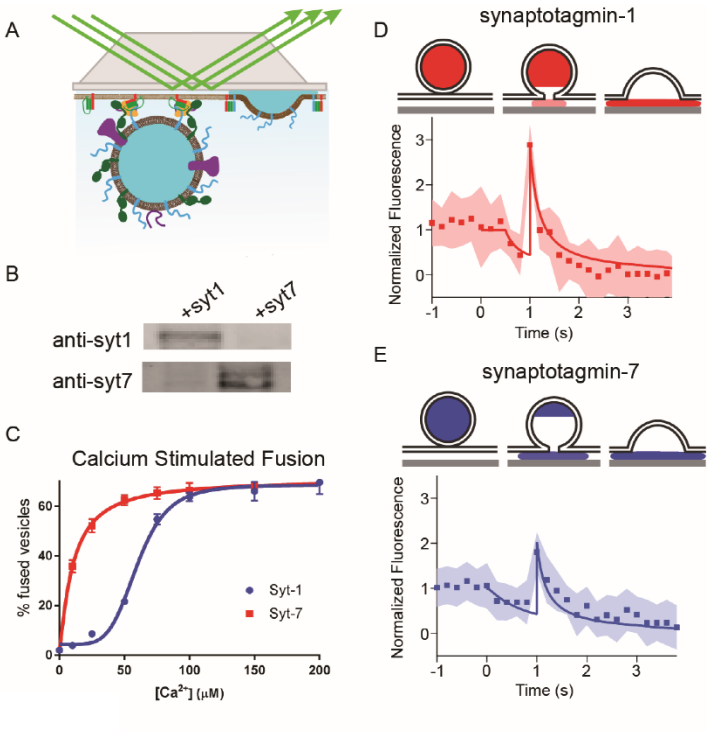

F I G U R E 2.7 In vitro fusion of Syt-7 and Syt-1 granules on planar supported bilayers. (a and b) Fusion of dense core granules containing either Syt-1 or Syt-7 with planar supported bilayers containing syntaxin-1a, dSNAP-25, Munc18, and complexin-1 were examined. As described previously, dense core granules labeled with NPY-mRuby stably dock to the supported bilayer, where fusion is triggered by injection of calcium. (c). The calcium sensitivity of fusion is dependent on the Syt-isoform expressed on purified dense core granules (K1/2 = 63 ± 3 μM for Syt-1 granules and 10 ± 1 μM for Syt-7 granules). Example of a characteristic NPY-mRuby signal (d and e) is observed for fusion. There is an initial decrease in NPY-mRuby fluorescence caused by diffusion of the protein away from the site of fusion under the cleft of the supported bilayer. This is followed by an increase in fluorescence caused by a collapse of the granule into the supported bilayer. This action pulls the remaining lumenal content toward the brightest portion of the evanescent field. Eventually, the fluorescence diminishes as NPY-mRuby diffuses away from the site of fusion. Averaging more than 20 individual traces (d and e) for Syt-1 fusion events, revealed a short delay (d) between the initial decrease in fluorescence and the subsequent increase in fluorescence during granule collapse. The delay time between these phases of the fluorescent signal was prolonged for Syt-7 granule fusion. The average tracings of Syt-7 and Syt-1 events are shown as an overlay (f). The cartoons illustrate the mathematical model (solid line in c and d) used to fit the data

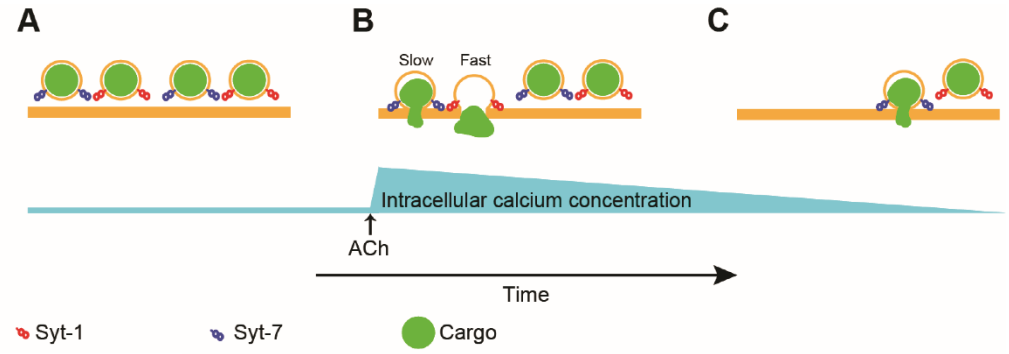

F I G U R E 2.8 Chromaffin cells require Syt-7 for sustained secretory activity during cholinergic stimulation. (a) Chromaffin cell granules harbor Syt-1, Syt-7, or both (not shown). When stimulated with ACh, intracellular calcium concentrations increase rapidly (Figure 2.5c), leading to fusion of Syt-1 and Syt-7 granule populations (b). (c) Prolonged stimulation with ACh causes nicotinic receptor desensitization (Figure S7a). Associated with desensitization is a corresponding decline in intracellular Ca^{2+} which is buffered, sequestered, or otherwise removed from the cytosol. Because Syt-1 has a lower affinity for Ca^{2+} than Syt-7, granules bearing this isoform are less likely to fuse as intracellular Ca^{2+} levels decline. Syt-7-bearing granules continue to fuse in the setting of near-baseline cytosolic Ca^{2+}

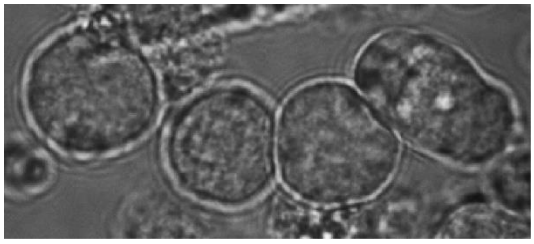

Supplementary Figure 2.1s. **Mouse chromaffin cells 24 hours after plating on Matrigel coated glass bottom dishes.** Healthy, transfected chromaffin cells are selected for TIRFM experiments based on their oblong shape and tendency to cluster.

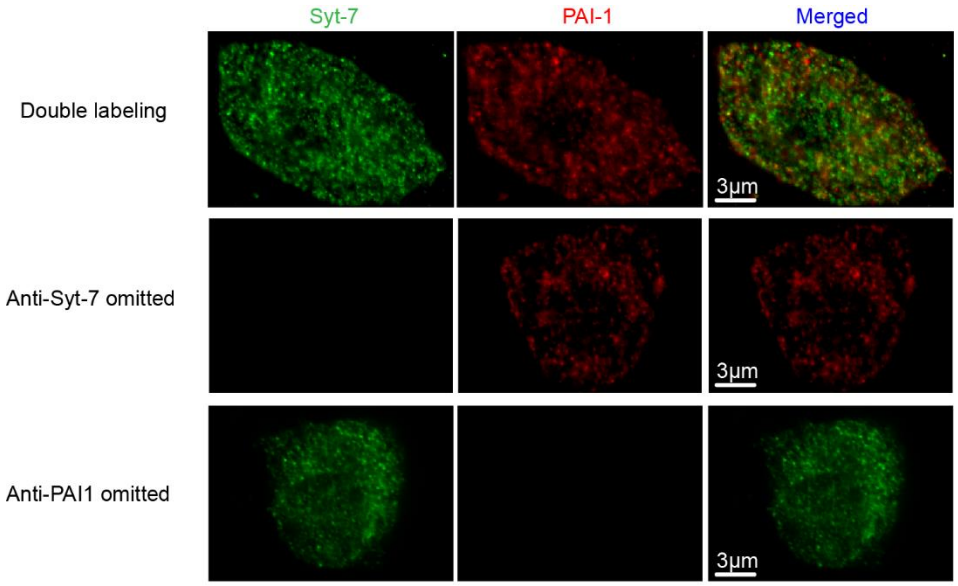

Supplementary Figure 2.2s. **Validation of immunocytochemical-staining method using two primary antibodies raised in rabbit.** Images show double-labeling for Syt-7 and PAI-1 (top row, image from figure 2.1). No labeling was seen for Syt-7 when the antibody was omitted. No labeling for PAI-1 was seen when the antibody was omitted (Syt-7, middle row and PAI-1 bottom row; 1 primary cell preparation).

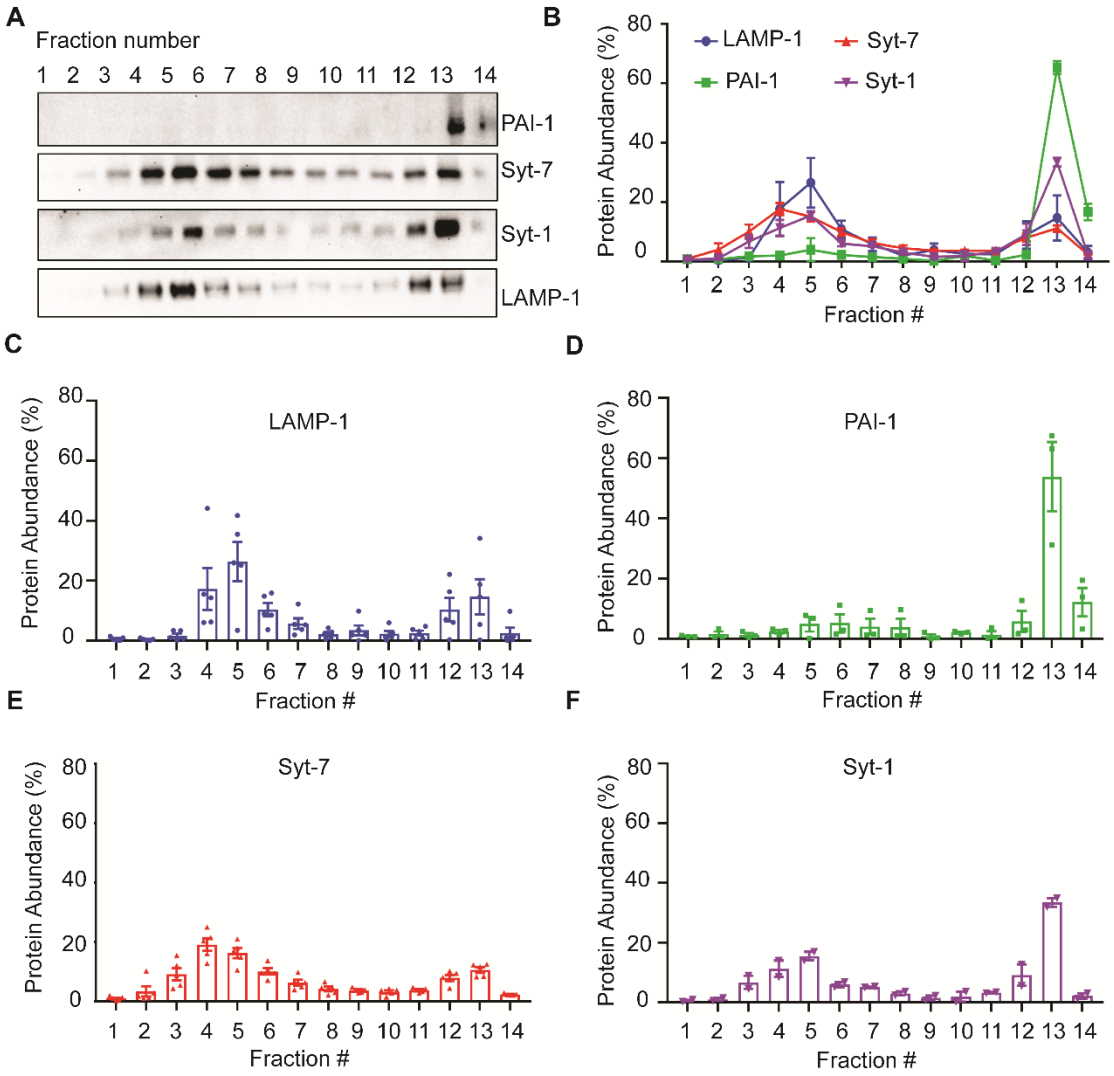

Supplementary Figure 2.3s. A. Representative blot showing bands corresponding to protein of interest (PAI-1: 45 kDa, Syt-7: 45 kDa, Syt-1: 65 kDa, and LAMP-1: 120 kDa). **B.** Expression level of PAI-1 (n = 3), Syt-7 (n = 5), Syt-1 (n = 2), and LAMP-1 (n = 5) shown as percentage of protein abundance in each subcellular fraction of bovine chromaffin cells (n represents individual fractionation experiments; 3 primary bovine cell preparations) **C-F**. Individual scatter box-plot graphs for LAMP-1, PAI-1, Syt-7 and Syt-1 respectively. Data are represented as mean ± SEM.

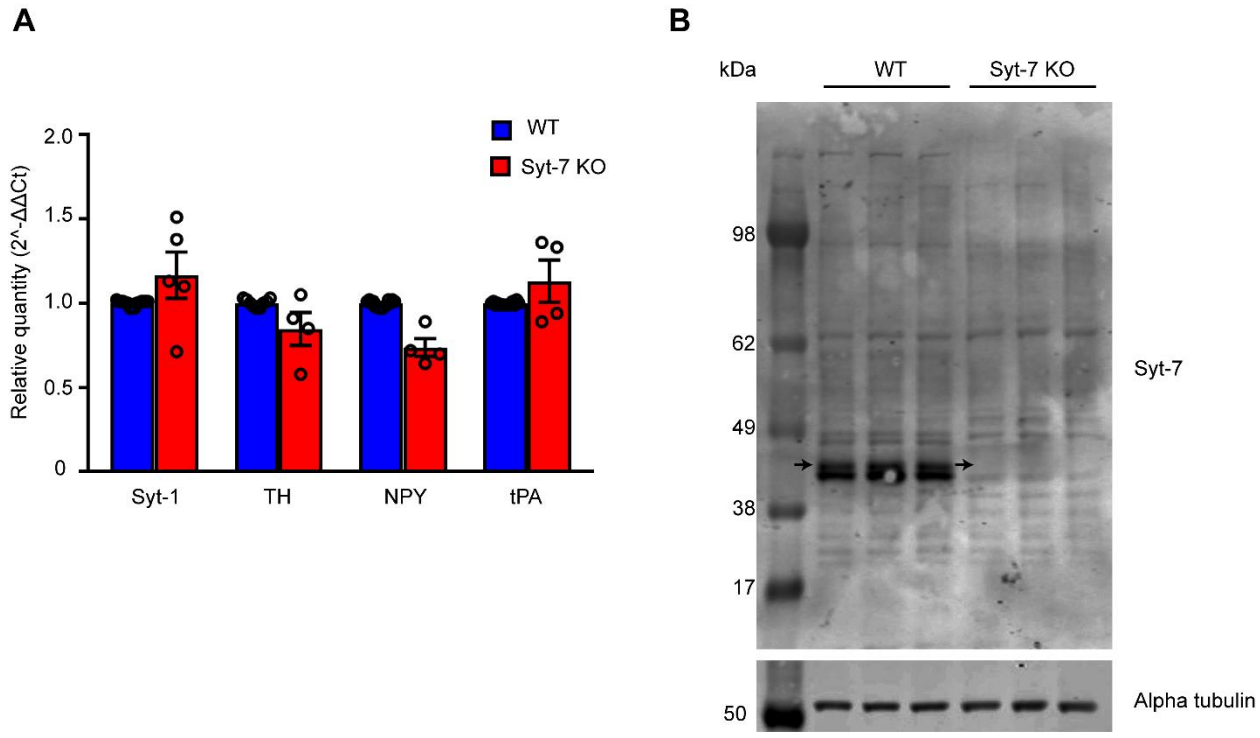

Supplementary Figure 2.4s. A. Expression of Syt-1, TH, NPY and tPA transcripts in WT and Syt-7 KO chromaffin cells. For each individual experiment, 4 WT and 4 KO adrenal medullas were homogenized, mRNA was extracted, and RT-qPCR was performed on the samples for Syt-1 (n = 5), NPY (n = 3), tPA (n = 3), TH (n = 3), and Syt-7 (n = 2; n represents individual experiments for all). Syt-7 transcript was not detected using the primers shown in Table 1. Expression of Syt-1 mRNA was not significantly different in WT and KO cells (Student's t-test, $p > 0.05$). **B.** Western blot analysis was performed on WT and Syt-7 KO adrenal glands. Black arrow indicates the region where the approximately 45 kDa Syt-7 □□variant should be observed (Chakrabarti et al., 2003; Sugita et al., 2001). This band is present in the WT lanes but not in the Syt-7 KO lanes.

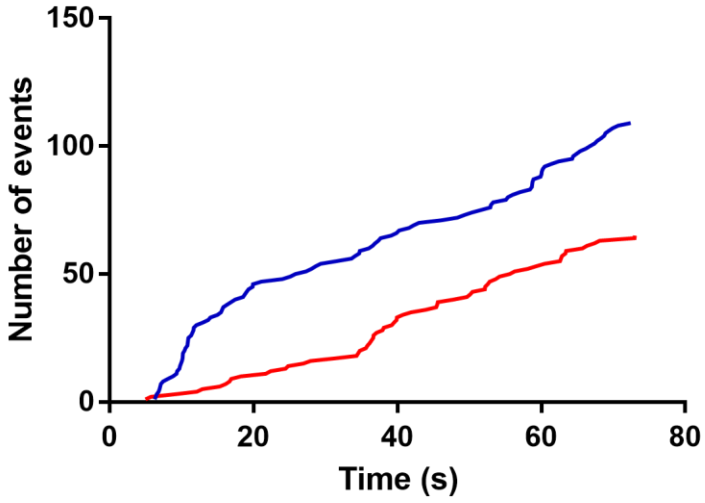

Supplementary Figure 2.5s. NPY-pHl was overexpressed in WT and Syt-7 KO chromaffin cells. Secretion was triggered by local perfusion of 100 mM KCl. Cumulative frequency distribution showing the time at which fusion events occurred in WT (blue) and Syt-7 KO (red) (n=8 cells for WT and n=5 cells for KO; 4 primary cell preparations for both groups). Both WT and KO cells secrete throughout the stimulation period, although the total number of fusion events is greater in WT cells.

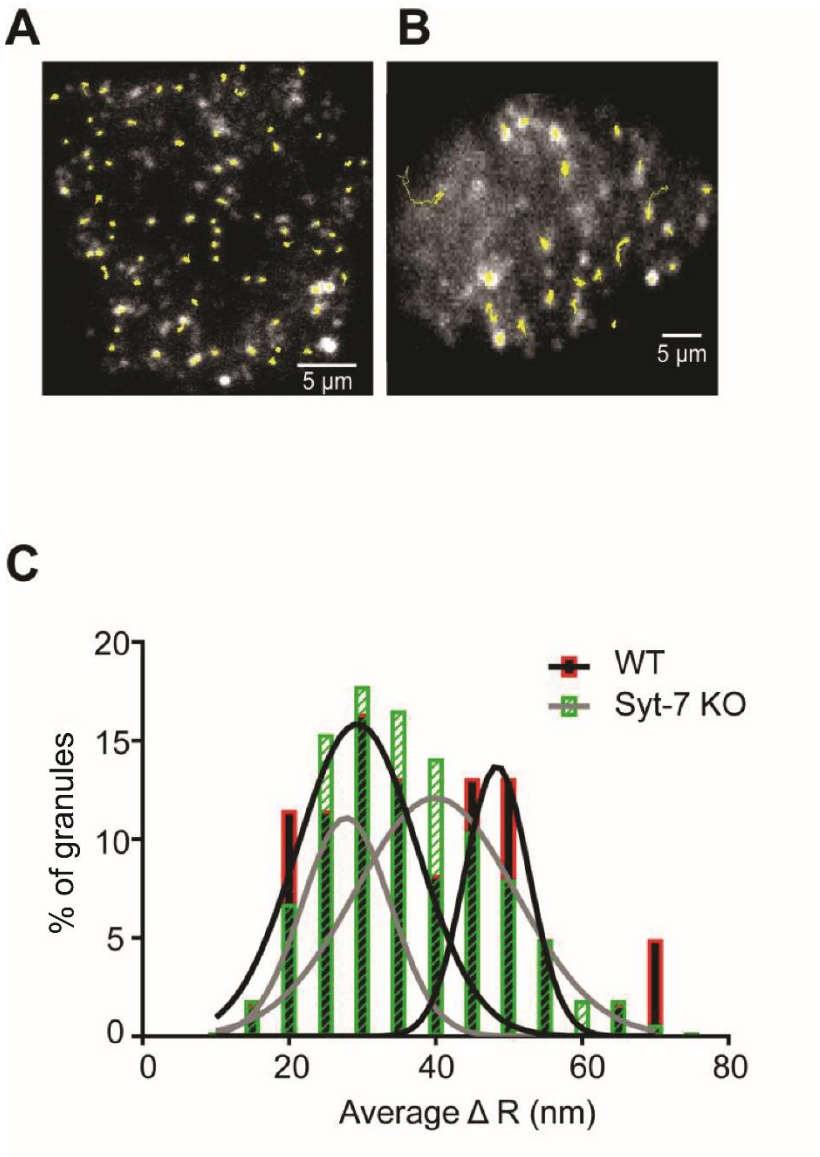

Supplementary Figure 2.6s. An analysis of granule motion in WT and Syt-7 KO cells. A-B. Representative tracks of WT (A) and Syt-7 KO (B) granules. **C.** Average mean frame-to-frame displacement of slower and faster WT granule populations, 29.32 +/- 1.41 nm/frame and 48.39 +/- 1.13 nm respectively, and slower and faster Syt-7 KO granules, 27.82 +/- 0.59 nm/frame, and 39.97 +/- 3.76 nm/frame, respectively.

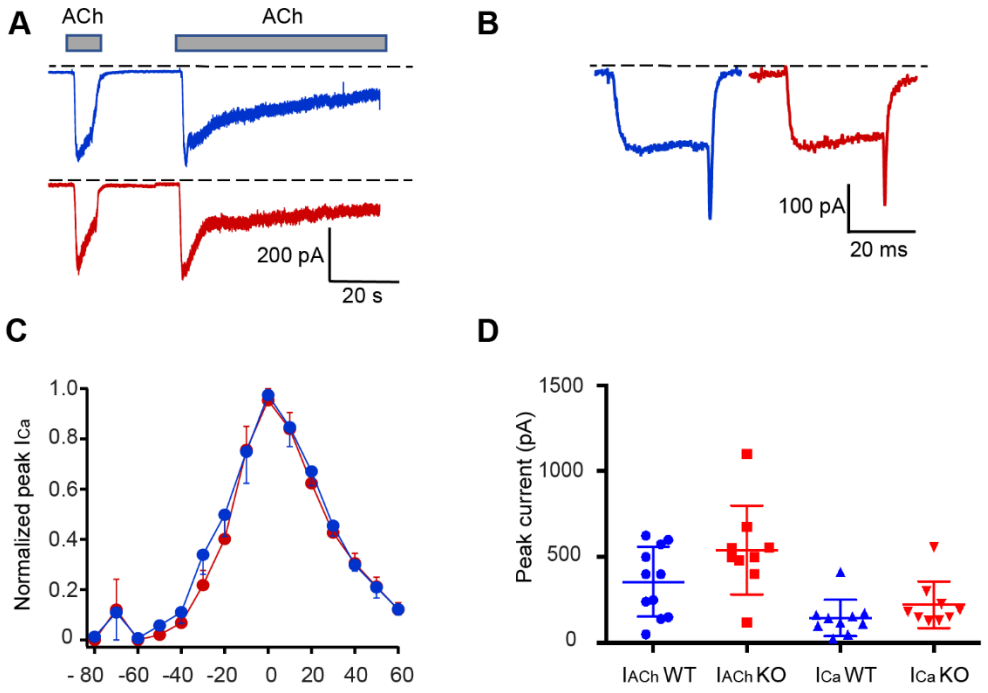

Supplementary Figure 2.7s. Cholinergic currents and depolarization-evoked Ca^{2+} currents are similar in WT and KO cells. Whole-cell patch clamp recordings were performed in WT (blue) and Syt-7 KO (red) cells. **A-B.** Representative cholinergic currents (I_{ACh}) (**A**) and Ca^{2+} currents (I_{Ca}) (**B**). Currents were evoked by application of 100 µM ACh (**A)** or by a 30 ms step-depolarization (**B**) from a holding potential of -90 mV. **C.** Voltage-dependent activation and inactivation of the I_{Ca} in WT and Syt-7 KO cells. Each point represents the mean peak amplitude of the I_{Ca} (n = 7 evoked currents) evoked by a 30 ms step depolarization to test potentials of different amplitudes from a holding potential of -90 mV and normalized to the maximal response of each cell. **D.** A comparison of the mean data and range of peak amplitudes of I_{ACh} and I_{Ca} evoked in WT and Syt-7 KO cells. Mean Syt-7 KO current amplitudes were not altered compared to WT cells (Student's t-test, $p > 0.05$).

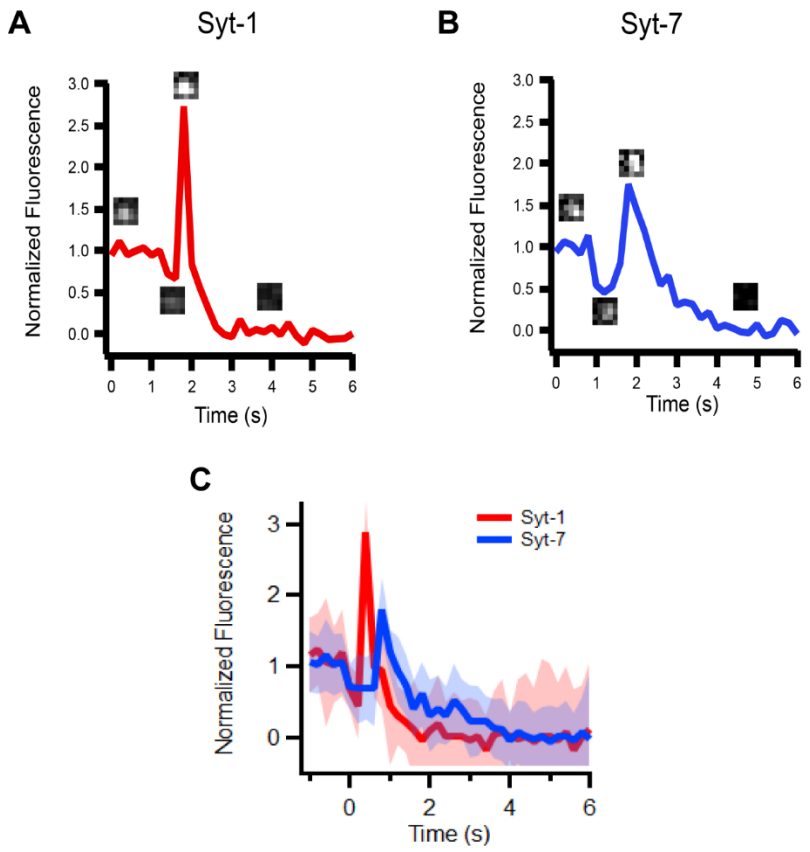

Supplementary Figure 2.8s. **A-B**. Images from individual NPYmRuby release events. **C**. An overlay of the averaged NPYmRuby "line shapes" is shown

References

Abbineni, P.S., D. Axelrod, and R.W. Holz. 2018. Visualization of expanding fusion pores in secretory cells. *J Gen Physiol*.

Anantharam, A., B. Onoa, R.H. Edwards, R.W. Holz, and D. Axelrod. 2010. Localized topological changes of the plasma membrane upon exocytosis visualized by polarized TIRFM. *J Cell Biol*. 188:415428.

Bendahmane, M., K.P. Bohannon, M.M. Bradberry, T.C. Rao, M.W. Schmidtke, P.S. Abbineni, N.L. Chon, S. Tran, H. Lin, E.R. Chapman, J.D. Knight, and A. Anantharam. 2018. The synaptotagmin C2B domain calcium-binding loops modulate the rate of fusion pore expansion. *Molecular Biology of the Cell*. 29:834-845.

Bhalla, A., W.C. Tucker, and E.R. Chapman. 2005. Synaptotagmin isoforms couple distinct ranges of Ca^{2+}, Ba^{2+}, and Sr^{2+} concentration to SNARE-mediated membrane fusion. *Mol Biol Cell*. 16:4755-4764.

Bittner, M.A., and R.W. Holz. 1992. Kinetic analysis of secretion from permeabilized adrenal chromaffin cells reveals distinct components. *Journal of Biological Chemistry*. 267:16219-16225.

Bohannon, K.P., M.A. Bittner, D.A. Lawrence, D. Axelrod, and R.W. Holz. 2017. Slow fusion pore expansion creates a unique reaction chamber for co-packaged cargo. *J Gen Physiol*. 149:921934.

Carmichael, S.W., and H. Winkler. 1985. The adrenal chromaffin cell. *Scientific American*. 253:40-49.

Chakrabarti, S., K.S. Kobayashi, R.A. Flavell, C.B. Marks, K. Miyake, D.R. Liston, K.T. Fowler, F.S. Gorelick, and N.W. Andrews. 2003. Impaired membrane resealing and autoimmune myositis in synaptotagmin VII-deficient mice. *J Cell Biol*. 162:543-549.

de Diego, A.M., L. Gandia, and A.G. Garcia. 2008. A physiological view of the central and peripheral mechanisms that regulate the release of catecholamines at the adrenal medulla. *Acta Physiol (Oxf)*. 192:287-301.

Domanska, M.K., V. Kiessling, A. Stein, D. Fasshauer, and L.K. Tamm. 2009. Single vesicle millisecond fusion kinetics reveals number of SNARE complexes optimal for fast SNARE-mediated membrane fusion. *J Biol Chem*. 284:32158-32166.

Domanska, M.K., V. Kiessling, and L.K. Tamm. 2010. Docking and fast fusion of synaptobrevin vesicles depends on the lipid compositions of the vesicle and the acceptor SNARE complex-containing target membrane. *Biophysical journal*. 99:2936-2946.

Doreian, B.W., T.G. Fulop, and C.B. Smith. 2008. Myosin II Activation and Actin Reorganization Regulate the Mode of Quantal Exocytosis in Mouse Adrenal Chromaffin Cells. *Journal of Neuroscience*. 28:4470-4478.

Douglas, W.W. 1968. Stimulus-secretion coupling: the concept and clues from chromaffin and other cells. *Br J Pharmacol*. 34:451-474.

Douglas, W.W., T. Kanno, and S.R. Sampson. 1967. Influence of the ionic environment on the membrane potential of adrenal chromaffin cells and on the depolarizing effect of acetylcholine. *J.Physiol.(Lond)*. 191:107-121.

Flannery, A.R., C. Czibener, and N.W. Andrews. 2010. Palmitoylation-dependent association with CD63 targets the Ca^{2+} sensor synaptotagmin VII to lysosomes. *J Cell Biol*. 191:599-613.

Fukuda, M., E. Kanno, M. Satoh, C. Saegusa, and A. Yamamoto. 2004. Synaptotagmin VII is targeted to dense-core vesicles and regulates their Ca^{2+} -dependent exocytosis in PC12 cells. *J Biol Chem*. 279:52677-52684.

Fulop, T., B. Doreian, and C. Smith. 2008. Dynamin I plays dual roles in the activity-dependent shift in exocytic mode in mouse adrenal chromaffin cells. *Archives of Biochemistry and Biophysics*. 477:146-154.

Fulop, T., S. Radabaugh, and C. Smith. 2005. Activity-Dependent Differential Transmitter Release in Mouse Adrenal Chromaffin Cells. *Journal of Neuroscience*. 25:7324-7332.

Gucek, A., N.R. Gandasi, M. Omar-Hmeadi, M. Bakke, S.O. Doskeland, A. Tengholm, and S. Barg. 2019. Fusion pore regulation by cAMP/Epac2 controls cargo release during insulin exocytosis. *Elife*. 8.

Han, W., J.S. Rhee, A. Maximov, Y. Lao, T. Mashimo, C. Rosenmund, and T.C. Sudhof. 2004. Nglycosylation is essential for vesicular targeting of synaptotagmin 1. *Neuron*. 41:85-99.

Jackman, S.L., J. Turecek, J.E. Belinsky, and W.G. Regehr. 2016. The calcium sensor synaptotagmin 7 is required for synaptic facilitation. *Nature*. 529:88-91.

Jaiswal, J.K., S. Chakrabarti, N.W. Andrews, and S.M. Simon. 2004. Synaptotagmin VII restricts fusion pore expansion during lysosomal exocytosis. *PLoS Biol*. 2:E233.

Kalb, E., S. Frey, and L.K. Tamm. 1992. Formation of supported planar bilayers by fusion of vesicles to supported phospholipid monolayers. *Biochim Biophys Acta*. 1103:307-316.

Kolski-Andreaco, A., H. Cai, D.S. Currle, K.G. Chandy, and R.H. Chow. 2007. Mouse adrenal chromaffin cell isolation. *Journal of visualized experiments : JoVE*:129.

Kreutzberger, A., V. Kiessling, C. Stroupe, B. Liang, J. Preobraschenski, M. Ganzella, M.A.B. Kreutzberger, R. Nakamoto, R. Jahn, J.D. Castle, and L.K. Tamm. In Press. In vitro fusion of single synaptic and dense core vesicles reproduces key physiological properties. *Nat Commun*.

Kreutzberger, A.J.B., V. Kiessling, B. Liang, P. Seelheim, S. Jakhanwal, R. Jahn, J.D. Castle, and L.K. Tamm. 2017a. Reconstitution of calcium-mediated exocytosis of dense-core vesicles. *Sci Adv*. 3:e1603208.

Kreutzberger, A.J.B., V. Kiessling, B. Liang, S.T. Yang, J.D. Castle, and L.K. Tamm. 2017b. Asymmetric Phosphatidylethanolamine Distribution Controls Fusion Pore Lifetime and Probability. *Biophysical journal*. 113:1912-1915.

Kroeber, S., C. Schomerus, and H.W. Korf. 1998. A specific and sensitive double-immunofluorescence method for the demonstration of S-antigen and serotonin in trout and rat pinealocytes by means of primary antibodies from the same donor species. *Histochem Cell Biol*. 109:309-317.

Kwon, S.E., and E.R. Chapman. 2012. Glycosylation is dispensable for sorting of synaptotagmin 1 but is critical for targeting of SV2 and synaptophysin to recycling synaptic vesicles. *J Biol Chem*. 287:35658-35668.

MacDougall, D.D., Z. Lin, N.L. Chon, S.L. Jackman, H. Lin, J.D. Knight, and A. Anantharam. 2018. The high affinity calcium sensor synaptotagmin-7 serves multiple roles in regulated exocytosis. *J Gen Physiol*. 150:783-807.

Martinez, I., S. Chakrabarti, T. Hellevik, J. Morehead, K. Fowler, and N.W. Andrews. 2000. Synaptotagmin VII regulates Ca($^{2+}$)-dependent exocytosis of lysosomes in fibroblasts. *J Cell Biol*. 148:1141-1149.

Matsuoka, H., K. Harada, J. Nakamura, M. Fukuda, and M. Inoue. 2011. Differential distribution of synaptotagmin-1, -4, -7, and -9 in rat adrenal chromaffin cells. *Cell Tissue Res*. 344:41-50.

Moghadam, P.K., and M.B. Jackson. 2013. The Functional Significance of Synaptotagmin Diversity in Neuroendocrine Secretion. *Frontiers in endocrinology*. 4:124.

Neher, E., and G.J. Augustine. 1992. Calcium gradients and buffers in bovine chromaffin cells. *The Journal of physiology*. 450:273-301.

Perrais, D., I.C. Kleppe, J.W. Taraska, and W. Almers. 2004. Recapture after exocytosis causes differential retention of protein in granules of bovine chromaffin cells. *The Journal of Physiology Online*. 560:413-428.

Rao, T.C., D.R. Passmore, A.R. Peleman, M. Das, E.R. Chapman, and A. Anantharam. 2014. Distinct fusion properties of synaptotagmin-1 and synaptotagmin-7 bearing dense core granules. *Mol Biol Cell*. 25:2416-2427.

Rao, T.C., Z.S. Rodriguez, M.M. Bradberry, A.H. Ranski, P.J. Dahl, M.W. Schmidtke, P.M. Jenkins, D. Axelrod, E.R. Chapman, D.R. Giovannucci, and A. Anantharam. 2017. Synaptotagmin isoforms confer distinct activation kinetics and dynamics to chromaffin cell granules. *Journal of General Physiology*. 149:763-780.

Schonn, J.S., A. Maximov, Y. Lao, T. C. Sudhof, and J.B. Sorensen. 2008. Synaptotagmin-1 and -7 are functionally overlapping Ca^{2+} sensors for exocytosis in adrenal chromaffin cells. *Proc Natl Acad Sci U S A*. 105:3998-4003.

Sugita, S., W. Han, S. Butz, X. Liu, R. Fernandez-Chacon, Y. Lao, and T.C. Sudhof. 2001. Synaptotagmin VII as a plasma membrane Ca($^{2+}$) sensor in exocytosis. *Neuron*. 30:459-473.

Sugita, S., O.H. Shin, W. Han, Y. Lao, and T.C. Sudhof. 2002. Synaptotagmins form a hierarchy of exocytotic Ca($^{2+}$) sensors with distinct Ca($^{2+}$) affinities. *EMBO J*. 21:270-280.

Sugita, S., and T.C. Sudhof. 2000. Specificity of Ca^{2+}-dependent protein interactions mediated by the C2A domains of synaptotagmins. *Biochemistry*. 39:2940-2949.

Tsuboi, T., and M. Fukuda. 2007. Synaptotagmin VII modulates the kinetics of dense-core vesicle exocytosis in PC12 cells. *Genes Cells*. 12:511-519.

Wagner, M.L., and L.K. Tamm. 2001. Reconstituted syntaxin1a/SNAP25 interacts with negatively charged lipids as measured by lateral diffusion in planar supported bilayers. *Biophysical journal*. 81:266275.

Wang, M., Q. Wang, and M.D. Whim. 2016. Fasting induces a form of autonomic synaptic plasticity that prevents hypoglycemia. *Proc Natl Acad Sci U S A*. 113:E3029-3038.

Weber, J.P., T.L. Toft-Bertelsen, R. Mohrmann, I. Delgado-Martinez, and J.B. Sorensen. 2014. Synaptotagmin-7 is an asynchronous calcium sensor for synaptic transmission in neurons expressing SNAP-23. *PLoS One*. 9:e114033.

Weiss, A.N., A. Anantharam, M.A. Bittner, D. Axelrod, and R.W. Holz. 2014. Lumenal protein within secretory granules affects fusion pore expansion. *Biophysical journal*. 107:26-33.

Wu, Q., Q. Zhang, B. Liu, Y. Li, X. Wu, S. Kuo, L. Zheng, C. Wang, F. Zhu, and Z. Zhou. 2019. Dynamin 1 Restrains Vesicular Release to a Subquantal Mode In Mammalian Adrenal Chromaffin Cells. *The Journal of neuroscience : the official journal of the Society for Neuroscience*. 39:199-211.

Zdanowicz, R., A. Kreutzberger, B. Liang, V. Kiessling, L.K. Tamm, and D.S. Cafiso. 2017. Complexin Binding to Membranes and Acceptor t-SNAREs Explains Its Clamping Effect on Fusion. *Biophysical journal*. 113:1235-1250.

Zhang, Q., B. Liu, Q. Wu, B. Liu, Y. Li, S. Sun, Y. Wang, X. Wu, Z. Chai, X. Jiang, X. Liu, M. Hu, Y. Wang, Y. Yang, L. Wang, X. Kang, Y. Xiong, Y. Zhou, X. Chen, L. Zheng, B. Zhang, C. Wang, F. Zhu, and Z. Zhou. 2019. Differential Co-release of Two Neurotransmitters from a Vesicle Fusion Pore in Mammalian Adrenal Chromaffin Cells. *Neuron*. 102:173-183 e174.

Zhang, Z., Y. Wu, Z. Wang, F.M. Dunning, J. Rehfuss, D. Ramanan, E.R. Chapman, and M.B. Jackson. 2011. Release mode of large and small dense-core vesicles specified by different synaptotagmin isoforms in PC12 cells. *Mol Biol Cell*. 22:2324-2336.

Zhao, W.D., E. Hamid, W. Shin, P.J. Wen, E.S. Krystofiak, S.A. Villarreal, H.C. Chiang, B. Kachar, and L.G. Wu. 2016. Hemi-fused structure mediates and controls fusion and fission in live cells. *Nature*. 534:548-552.

Chapter III

Acetylcholine and PACAP Activate Chromaffin Cell Secretion by Signaling Through Unique and Parallel Pathways, Resulting in Phenotypically Different Fusion Events

Alina Morales, Shreeya Bakshi, Ramkumar Mohan, Mounir Bendahmane, Joshua West, John Traynor, Alan Smrcka, Arun Anantharam

Introduction

The term “fight-or-flight” refers to the state of heightened physiological and mental arousal triggered by a physical threat, emotionally charged event, or metabolic disturbance. Although the precise reaction to each stressor may vary, all share some basic characteristics of sympathetic activation. The adrenal medulla is a core effector of the sympathetic nervous system in the periphery (Cannon 1940). When activated, it discharges a cocktail of powerful hormones (epinephrine, norepinephrine, and vasoactive peptides) into the suprarenal vein for circulation throughout the body (Wolf, Zarkua et al. 2016). These hormones modulate cardiac, pulmonary, and metabolic functions in ways that favor survival or preserve internal conditions when they are likely to be disturbed (Cannon 1940, Goldstein and Kopin 2007, Goldstein 2010). Thus, many of the “emergency” measures encompassed in the term fight-or-flight, rely on the adrenal medulla. Secretion from the adrenal medulla is dependent on input from preganglionic, sympathetic fibers which pass into the gland via the splanchnic nerves (De Robertis and Ferreira 1957, Grynszpan-Winograd 1974). The fibers terminate on adrenomedullary chromaffin cells which secrete

hormones contained in dense core granules (Carmichael and Winkler 1985). That chromaffin cell secretion is triggered by presynaptically released ACh has been appreciated for many decades. But whether ACh alone is sufficient to sustain catecholamine release, particularly under conditions where the adrenal medulla is strongly stimulated, is not as clear. Indeed, prior studies have revealed that catecholamine secretion exhibits a dramatic time-dependent decline when medullae are continuously perfused with ACh (Bevington and Radda 1985, Wakade 1988); such a decline is not evident when the medullary secretion is elicited by direct electrical stimulation of the splanchnic nerve (Wakade 1988).

In the last decade, evidence has emerged that pituitary adenylate cyclase activating polypeptide (PACAP), complements and, under specific conditions associated with strong sympathetic activation, supersedes ACh as the principal neurotransmitter at the splanchnic-chromaffin cell synapse (Smith and Eiden 2012, Stroth, Kuri et al. 2013, Eiden, Emery et al. 2018). PACAP was first identified in 1989, when it was described to cause an increase in cAMP in the ovine hypothalamus (Miyata, Arimura et al. 1989). Once PACAP became available as a pharmacological agent, it was applied to perfused adrenal medullae and shown to cause a long-lasting, non-desensitizing form of secretion (Przywara, Guo et al. 1996). Splanchnic nerve terminals have been shown to contain PACAP with chromaffin cells expressing the PAC1 receptor (PAC1R) (Hamelink, Tjurmina et al. 2002, Guerineau 2019). Subsequent studies established the necessity of PACAP for sympathetic adjustments to insulin-induced hypoglycemia – a process regulated by adrenomedullary hormones – but evidence that PACAP was actually released from the nerves innervating the adrenal medulla was lacking. This evidence was eventually provided by Smith and colleagues, who showed that high frequency splanchnic stimulation of an adrenal slice fails to sustain catecholamine secretion when a PAC1R

receptor antagonist, PACAP (6-38), is included in the slice bathing solution (Kuri, Chan et al. 2009, Smith and Eiden 2012).

In comparison to ACh – which causes Na+ entry through nicotinic receptors to depolarize the membrane potential, initiate action potentials, and eventually a Ca^{2+} influx to trigger catecholamine release – the molecular mechanisms by which PACAP acts to stimulate secretion are poorly understood. This is a significant shortcoming given the central role of PACAP in regulating physiological responses to sympathetic stressors. The identity of at least part of the PACAP signaling pathway is encoded in its name; there is strong evidence that, in multiple cell types, exposure to PACAP leads to activation of adenylate cyclase and cAMP production leading to Ca^{2+} entry and exocytosis (Przywara, Guo et al. 1996). However, other reports implicate a $G\alpha_q$-dependent signaling mechanism, whereby the Gα activates phospholipase C β, and subsequent IP_3-stimulated mobilization of Ca^{2+} from intracellular stores for exocytosis (Eiden, Emery et al. 2018). There is also a conspicuous lack of information on the nature of the Ca^{2+} signals, their amplitude and time course, which might provide deeper insights into how PACAP- versus ACh-stimulated elevations in Ca^{2+} are caused and ultimately how that Ca^{2+} drives the secretory response. Finally, whether PACAP and ACh, operating through distinct intracellular effectors, differentially impact the fusion event itself or impinge on the fusion pore to regulate its expansion, has not previously been investigated.

The goal of this study was to elucidate the molecular mechanisms linking PACAP stimulation of chromaffin cells to dense core granule fusion. To this end, high resolution imaging approaches were brought to bear on bovine and mouse adrenal chromaffin cells stimulated with PACAP or ACh and undergoing exocytosis. The data show that PACAP stimulates a form of exocytosis that requires signaling through a $G\alpha_s$, Epac, and PLCε. Little to no cross talk is

evident in the pathways that couple nACh receptor versus PAC1 receptor activation to fusion. The Ca^{2+} transients that follow PACAP stimulation, imaged with genetically-encoded Ca^{2+} indicators, have a small amplitude, fluctuate rapidly, and do not show evidence of desensitization. The data are most consistent with a route of Ca^{2+} entry that is Ni^{2+} sensitive and ostensibly relies on voltage-dependent channels. Exocytotic events stimulated by PACAP and ACh also differ in form and frequency. Both small (<1 kD) and larger (~30 kD) cargos are released more slowly from fusing granules when cells are exposed to PACAP. Granules that fuse in response to PACAP stimulation frequently undergo cavicapture, which demonstrates a PACAP effector-specific action on the fusion pore that not only slows but also reverses pore expansion. In sum, these results indicate that PACAP and ACh stimulate parallel and independent pathways for granule fusion in chromaffin cells. These pathways have presumably evolved to maximize the chromaffin cell secretory response to different stimulation loads.

Materials and Methods

Animals

Animals were obtained from Jackson Labs, Bar Harbor, ME. Syt-7 -/- litters of male and female mice (catalogue # 004950, Jackson labs) (gift of Dr. Joel Swanson; (Chakrabarti, Kobayashi et al. 2003) and Syt-7 +/+ from C5BL/6J background were used for studies. PLCε KO mice were from collaborator Dr. Alan Smrcka, (Wang, Oestreich et al. 2005). Animals were group housed with 2-5 per ventilated cage with a 12hr dark/12 hr light cycle with full access to food and water. All animal procedures and experiments were conducted in accordance with the University of Michigan Institutional Animal Care and Use Committee protocol (PRO00007247 and PRO00009235).

Mouse chromaffin cells preparation and transfection

6-16 week old male or female mice (18-26 g) were gas anesthetized using an isofluorane drop jar technique and sacrificed by cervical dislocation. 3-4 mice were euthanized for 2 plates to ensure proper cell density and health of chromaffin cells. Adrenal glands were removed from mice and moved to dishes containing ice cold mouse buffer (148 mM NaCl, 2.57 mM KCl, 2.2 mM K2HPO4•3H2O, 6.5 mM KH2PO4, 10 mM glucose, 5 mM HEPES free acid, 14.2 mM mannitol). Using a dissection microscope, the cortex was carefully removed using forceps (Dumont Swissmade, Switzerland Cat. # 72891-Bx) and microscissors (World Precision Instruments, 14124-G). The medullae were rinsed 3 times in 75 µL drops of papain enzyme solution (450 units/ml Papain (Worthington Biochemical. #LS003126), 250 µg/ml BSA, and 75 µg/ml dithiothreitol) for 15 minutes at 37 ˚C shaking 140 rpm in 0.5 mL of papain solution. After 15 minutes, the digesting solution was mostly removed and replaced by 0.5 mL of collagenase enzyme solution (250 µg/ml BSA, 0.375% collagenase, 0.15mg/mL DNase). Digestion was continued for another 15 minutes at 37 ˚C shaking 140 rpm. The digestion was stopped by transferring glands into an antibiotic-free culture medium (Dulbecco's Modified Eagle's Medium (DMEM) (ThermoFisher Scientific) supplemented with 10% Fetal Bovine Serum (FBS) (ThermoFisher Scientific). The glands were then triturated by push-pull movement using a 1mL pipette tip (up to 8 times). The suspension containing glands was then spun at 1300x g for 2.5 minutes. Supernatant was discarded and the pellet was resuspended in 300 µL of antibiotic-free medium and triturated again in a 200 µL pipette tip (up to 8 times). The suspension was spun again at 1300 x g for 2.5 minutes. After discarding the supernatant, the pellet was re-suspended in 110 µL of resuspension buffer (Invitrogen, Thermofisher Scientific) for transfection. The desired plasmid was added to the mixture (7ng/ 10^6 cells). The suspended cells were transiently transfected by electroporation with a single pulse (1050 mV, 40ms) using the neon transfection

system (Invitrogen, Thermofisher Scientific). Before digestion step, 35 mm diameter dishes with 14 mm diameter glass-bottom dishes (MatTek Corporation, Ashland, MA. #P35G-1.5-14-C) were pre-coated with Matrigel (Corning, NY, Cat. #356230) diluted in DMEM (1:7) for 1.5 hours after which the dishes were washed with DMEM. After electroporation, 200 µL of antibiotic free medium was added to cells. 150 µL of electroporated cells were then deposited in each dish (2 dishes total per condition). The cells were stored in an incubator (37°C, 5% CO2) for approximately 4 hours. Culture medium with antibiotics was then added to a final volume of 2 mL (DMEM supplemented with 10% FBS, 9.52 unit/ml Penicillin, 9.52 µg/ml Streptomycin and 238 µg/ml Gentamicin (ThermoFisher Scientific). The media was changed the day after plating and experiments were conducted within between 24 and 48 hours after plating. For non-electroporated cells transduced with FFN, the cells were not resuspended in resuspension buffer, but resuspended in 300 µL of antibiotic free medium and plated, 150 uL in each dish (2 dishes per condition). The cells would incubate in 100 µM FFN for 1 hour before imaging experiments, FFN prepared in imaging buffer, basal PSS described in Cell stimulation section of methods.

TIRF microscopy for observation of exocytosis

An Olympus cell TIRF-4line microscope (Olympus, USA) was used to perform TIRF imaging. The microscope utilizes a TIRF oil-immersion objective (NA 1.49) with an additional 2x lens in the emission path between the microscope and electron-multiplying charge-coupled device camera ((iXon 897; Andor Technology). The final pixel size of images was 80 nm. Series of images for FFN and NPY pHluorin studies were acquired at ~ 70Hz with exposure of 14ms and images for GCaMP studies were acquired at ~ 20Hz with exposure of 30ms, EM gain of 100. pHluorin and FFN were excited using a 488 nm laser and syt-7 and PLCε rescue cells were located using 560nm laser.

Cell stimulation

All TIRF experiments were performed between 34-37° C. Physiological salt solution (PSS) buffer was prepared (145 mM NaCl, 5.6 mM KCl, 2.2 mM CaCl2, 0.5 mM MgCl2, 5.6 mM glucose, and 15 mM HEPES, pH 7.4) and prewarmed to 37° C before experiments were performed. Culture medium was replaced with PSS before the experiment and changed after each stimulation protocol. Chromaffin cells were individually stimulated using a needle (100-µm inner diameter) connected to a perfusion system under positive pressure ALA-VM4 (ALA Scientific Instruments, Westbury, NY). During experiments, cells were perfused with basal PSS for 5 seconds and then stimulated with 100uM ACh for 90 seconds, then perfused with basal PSS for 30 seconds and then 1uM PACAP for 120 seconds. For r pH switching studies using NPY-pHluorin, PACAP or ACh were prepared using basal PSS as previously described, or basal PSS pH 5.5 with 0.5uM bafilomycin to slow reacidification of granules (145 mM NaCl, 5.6 mM KCl, 2.2 mM CaCl2, 0.5 mM MgCl2, 5.6 mM glucose, and 15 mM HEPES, pH 5.4) after 30 seconds of stimulation at neutral pH, stims were switched between pH 7.4 and 5.5 for 5 second intervals for ~60 seconds. For low extracellular calcium studies, buffer used was 145 mM NaCl, 5.6 mM KCl, 0.5 mM MgCl2, 5.6 mM glucose, and 15 mM HEPES, 1 mM EGTA, pH 7.4 to ensure minimal amounts of extracellular calcium present.

Image analysis

Fusion events for cells containing either NPY-pHluorin or FFN were identified visually. The abruptness with which the puncta disappear and/or increased cloud of fluorescence followed by disappearing of the puncta is taken as indication that fusion and release of cargo has occurred. Regions of interest (ROIs) were selected using the Time Series Analyzer v3.0 plugin on Fiji software. Manually selected fusion events were selected using ROIs measuring 0.8um diameter.

The intensity of fluorescence was measured for each frame for each ROI. A nearby ROI where no fusion event occurred was selected for background subtraction. Dr. Daniel Axelrod (University of Michigan) wrote a custom program written in Interactive Data Language (IDL; ITT, Broomfield, CO) which was used to background subtract intensity time curves and calculate the duration of cargo release (Bohannon, Bittner et al. 2017, Abbineni, Bittner et al. 2019)

Cells transfected with GCaMP5G (Akerboom, Chen et al. 2012) were analyzed in order to determine the relative amount of calcium in the cell before and after stimulation. Three ROIs measuring 1um in diameter were manually selected at different points within each cell and fluorescence was measured for each ROI for every frame collected. The equation $\Delta F/F$ was calculated for each ROI for each frame collected, then the final values were averaged between the three ROIs, which resulted in the overall $\Delta F/F$ for the whole cell. The values determined were plotted versus time. Cells that were not sufficiently stuck to the dish or responded to control stimulus were excluded for analysis.

Cyclic AMP assay

Cyclic AMP accumulation was measured using the AlphaScreen cAMP kit from Perkin Elmer (Waltham, MA, USA). In brief, adrenal cells were harvested the same day of from mice and incubated with various concentrations of forskolin (Cayman Chemicals) for 30 minutes by an experimenter blinded to the genotype of the cells, prior to lysing with immunoassay buffer. The varying amounts of forskolin were added to stimulate cyclic AMP (cAMP) production, alongside anti-cAMP AlphaScreen Acceptor beads (acceptor beads, emission at 520-620 nm) with the adrenal cells. A mixture of streptavidin coated Alpha Donor beads linked to biotinylated cAMP (donor beads, excited at 680 nm) was then added during the lysing portion of the assay,

included with kit immunoassay buffer. Production of cAMP will disrupt the interaction between donor beads and acceptor beads, decreasing FRET signaling. Data were collected on Varioskan LUX Multimode Microplate Reader (Smrcka Lab thanks). Assays were performed in quadruplicate or triplicate (depending on cell count for that individual day) and averaged. The results presented are the mean ± SEM from one individual assay, derived from 2 mice. All data was analyzed using GraphPad Prism v9.01.

Statistical Analysis

GraphPad prism 8.4.3 was used for all statistical analysis, except for cAMP assay data, which was analyzed using GraphPad Prism v9.01. Data collected for studies utilizing primary chromaffin cells culture were collected using at least 2 cell preparations (more for KO studies) yielding 2 dishes per prep, per condition. When two group averages were compared, a student's t test or Welch's t test was used to determine statistical significance. The choice of using a parametric or non-parametric test was determined by using an F-test of a Brown-Forsythe test which determines if the variances between groups are significantly different. For data comparing averages from more than two groups, an ordinary one-way ANOVA or a Brown-Forsythe and welch ANOVA test. Again, choice of using parametric or non-parametric was determined by using F-test to determine if variances between groups compared were significantly different. cAMP data was analyzed using non-linear regression. All results reported are shown as mean +/- SEM. No sample calculation was performed to determine appropriate sample sizes.

Results

PACAP and ACh trigger distinct fusion modes in chromaffin cells

Catecholamines are released more slowly from chromaffin cells when PACAP rather than ACh is the secretagogue. Ostensibly, it is slow expansion of the early fusion pore which

accounts for the longer duration for catecholamine release. However, chromaffin granules are known to co-release catecholamines and peptides. Thus, the idea was tested that PACAP-stimulated mechanisms act to constrain peptide release, even after the pore has widened to release catecholamines. These experiments were performed in chromaffin cells dissociated from the bovine adrenal medulla, which provide a much greater cell yield. First, bovine chromaffin cells expressing GCaMP5G were stimulated with ACh and PACAP to confirm that Ca^{2+} transients in this system were similar to those measured in mouse chromaffin cells (Figure 3.1A, B). In separate experiments, chromaffin cells expressing Neuropeptide Y (NPY) fused to the pH-sensitive FP, pHluorin, were stimulated with either ACh or PACAP. Release durations were quantified as described in the Methods (Figure 3.1C-E). Fusion events were readily identifiable as localized and sudden stimulus-evoked increases in fluorescence which decayed with a variable time course (Figure 3.1C, D). When many such events from multiple cells were compared, it is clear that the time for complete NPY-pHl release was significantly longer when cells were stimulated by PACAP rather than ACh (Figure 3.1E).

In some cases, it was not possible to know the outcome of the fusion event simply by monitoring changes in NPY-pHl fluorescence. Three such events are shown in Figure 3.2. In figures 2A and B, the center of mass of the fluorescent punctum that appears after PACAP stimulation appears to travel laterally. The dimming of the fluorescence in the I versus time graphs may reflect slow re-acidification of the granule after cavicapture and/or movement of the granule out of the evanescent field. Figure 3.2C shows an event with an exceptionally long release duration. Such an outcome is possible if fusion pore expansion is halted preventing further release of NPY-pHl, or if cavicapture has occurred causing retention of the fluorescent cargo followed by slow-reacidification. To better distinguish between these outcomes, rapid pH

switching of the extracellular pH was performed to differentiate between fusion pores that are narrow and accessible to the extracellular space from those that have resealed during cavicapture. An example of a cavicapture event (red circle) occurring near a fusion event in which pore expansion is halted (red arrow), is shown in Figure 3.2D. Graphs underneath 9D show the sensitivity of the "red arrow" event to continued cycles of low pH perfusion (left); meanwhile, fluorescence of the "red circle" (i.e., cavicapture) event is not sensitive to cycles of low pH. Remarkably, cavicapture events were never observed in chromaffin cells stimulated by ACh. However, in chromaffin cells stimulated by PACAP, 8 cavicapture events were observed (Figure 3.2E). Thus, PACAP, acting through PAC1 receptors, activates an intracellular signaling cascade that causes Ca^{2+} influx and exocytosis; as part of this signaling cascade, mechanisms are stimulated that ultimately impinge on the fusion pore to slow, and in many cases, reverse its expansion.

Ca^{2+} transients evoked by PACAP and ACh have different amplitudes and time courses

To characterize differences in the Ca^{2+} transients elicited by PACAP and ACh stimulation, dissociated chromaffin cells expressing the genetically encoded calcium indicator, GCaMP5G were stimulated with 100 µM ACh and 1 µM PACAP (Akerboom, Chen et al. 2012). In contrast to ACh, PACAP elicits Ca^{2+} transients that are non-desensitizing, have a small amplitude and fluctuate, which distinguishes them from the transients evoked by ACh (Figure 3.3A.

Previous studies suggest that extracellular Ca^{2+} enters chromaffin cells via plasma membrane Ca^{2+} channels that are sensitive to Ni^{2+} (Hill, Chan et al. 2011). Imaging studies shown in Figure 3.2 lend support to this idea. In the presence of Ni^{2+}, the small amplitude fluctuations in Ca^{2+} fluorescence, evoked by PACAP stimulation, largely disappear (Figure 3.3A, B, D). However, there is little to no effect of Ni^{2+} on either the amplitude of the Ca^{2+}

transient evoked by ACh. Thus, while the route of Ca^{2+} entry after PACAP stimulation is strongly Ni^{2+} sensitive, ACh stimulation causes a Ca^{2+} influx that mostly insensitive to the presence of Ni^{2+}.

Electrophysiological studies suggest that Ca^{2+} enters the cell through low voltage gated, T-type Ca^{2+} channels (Cav3.2)(Hill, Chan et al. 2011). To assess whether the PACAP-stimulated Ca^{2+} transients are sensitive to a T-type Ca^{2+} channel blocker, chromaffin cells were incubated with TTA-P2 prior to ACh and PACAP perfusion. The ACh-stimulated Ca^{2+} transients remain largely insensitive to the presence of the Ca^{2+} channel blocker, while Ca^{2+} transients stimulated by PACAP, are strongly reduced (Figure 3.3F, G). These data further strengthen the idea that PACAP causes Ca^{2+} influx through a T-type Ca^{2+} channel in chromaffin cells.

PACAP and ACh utilize separate pathways for Ca^{2+} influx and exocytosis in chromaffin cells

PACAP, through the PAC1 receptor, stimulates adenylate cyclase, leading to elevation of intracellular cAMP, inositol 1,4,5,-trisphosphate (IP_3), and diacylglycerol (DAG) (Hamelink, Lee et al. 2002). Chromaffin cells express Epac1 and Epac 2 proteins which belong to a family of intracellular cAMP receptors which may be responsible for transducing the effects of cAMP in chromaffin cells (Eiden, Emery et al. 2018). In both cases, it is Ca^{2+} influx, rather than its mobilization from intracellular stores, that drives the GCaMP5G fluorescent response (Figure 3.4A, B,C,D).To evaluate the role of Epac in a cAMP-mediated signaling pathway leading to fusion, cells were incubated with an Epac antagonist, ESI-09, during stimulation with PACAP. In the presence of ESI-09, Ca^{2+} transients evoked by PACAP are no longer detected (Figure 3.4E, 3F). Because Ca^{2+} transients evoked by ACh in the presence and absence of the inhibitor

are qualitatively similar (Figure 3.4E, G), it does not appear that secretion stimulated by ACh requires Epac or its downstream effectors.

Epac is a cAMP-guanine nucleotide exchange factor that can activate Rap, which, in turn, binds to and activates phospholipase C epsilon (PLCε)(Smrcka, Brown et al. 2012). PLCε is a phosphoinositide-specific phospholipase which is purported to control processes requiring sustained phosphoinositide hydrolysis, but involving DAG rather than IP_3 as a major product (Smrcka, Brown et al. 2012). The role of PLCε as an effector that links PAC1R and $G\alpha_s$ to membrane fusion, has never previously been investigated. To facilitate these studies, a transgenic mouse line in which PLCε expression is abrogated, was employed.

Ca^{2+} transients evoked by ACh and PACAP were imaged in WT and PLCε KO cells as previously described in Figure 3.1. In response to ACh stimulation, intracellular Ca^{2+} levels increase to comparable levels in WT and KO cells, as measured by increases in GCaMP5G fluorescence, abruptly increase and then decline, ostensibly as a result of nAChR desensitization (Figure 3.5A, B, D). However, no apparent increase in intracellular Ca^{2+} is detected when PLCε KO cells are stimulated with PACAP (Figure 3.5B, 3E). To verify that it is the absence of PLCε and not some other component of the signaling pathway that is responsible for the disruption in Ca^{2+} influx, rescue experiments were also performed (Figure 3.5C, E). The rescue of PLCε resulted in rescue of Ca^{2+} influx after PACAP stimulation.

Next, exocytosis was imaged in chromaffin cells which had been incubated with FFN511 to label secretory granules and stimulated with either ACh or PACAP. FFN511 is a fluorescent molecule which uses the endogenous vesicular monoamine transporter (VMAT) to enter granules (Gubernator, Zhang et al. 2009, Zhang, Gubernator et al. 2009). Because of its

structural similarities as a substrate to dopamine, FFN511 can be effectively utilized as a fluorescent proxy for catecholamine release from fused dense core granules.

FFN511 fusion events are readily detected as sudden, stimulus-evoked decreases in fluorescence intensity (Figure 3.5F). Average release durations between WT, PLCε KO, and PLCε KO (rescue) cell experiments are shown in Figure 3.5B. They indicate that cargos are released more slowly from fusion pores after PACAP stimulation than ACh stimulation. Also show in Figure 3.5 are vertical line graphs which indicate the time at which an event occurs with respect to the start of stimulation (~5 s for all experiments) (Figure 3.5G, F). No fusion events are observed in PLCε KO cells stimulated with PACAP (Figure 3.5H, middle panel). In general, the number of exocytotic events, per unit area, in cells stimulated with PACAP is lower than in cells stimulated with ACh. Moreover, ACh-stimulated release is insensitive to the presence of PLCε; note that the average number of fusion events per unit area in WT and PLCε KO cells is roughly equivalent (Figure 3.5I).

To ensure that changes in responsiveness of PLCε KO cells to PACAP were due principally to the loss of PLCε and not other proteins essential for transducing the effects of PACAP, adrenal medulla mice were probed for expression of PACAP, PAC1, Epac 2, Syt7, and PLCε. Expression of the various target proteins were normalized to expression of α tubulin in chromaffin cells. As shown in Figure 3.6A – H, expression of Epac 2 were roughly unchanged in WT and PLCε KO cells. PAC1R and PACAP expression were slightly increased in the PLCε KO (Figure 3.6E, F). Finally, to ensure that cAMP production was not disrupted in the absence of PLCε, WT and KO cells were exposed to forskolin, lysed, and then subjected to a fluorescence assay that is sensitive to cAMP. As shown in Figure 3.6I, KO cells exposed to a

wide range of forskolin concentrations, do not exhibit any apparent disruption in cAMP production.

PACAP and ACh trigger fusion of overlapping population of Syt-bearing granules

There is a non-uniform distribution of Ca^{2+} sensors on chromaffin cell granules. The two major isoforms of synaptotagmin expressed on chromaffin granules are Syt1 and Syt7. Most granules harbor either Syt1 or Syt7, with a minority of granules harboring both Syt isoforms. Syt7 is characterized by having a substantially higher sensitivity to Ca^{2+} than Syt1; upon fusion, Syt7 pores expand with slower kinetics than Syt1 pores. PACAP causes catecholamine release (i.e., measured by FFN511) to occur with a slower time course than ACh. In addition, Ca^{2+} transients elicited by PACAP stimulation are substantially smaller than those caused by ACh (Figure 3.1). It was therefore reasoned that PACAP might preferentially drive fusion of Syt7 granules, which are sensitive to relatively small changes in intracellular Ca^{2+} and release cargos through pores whose rapid expansion is prevented (Bendahmane, Morales et al. 2020). To test this idea, WT and Syt7 KO chromaffin cells were stimulated with either ACh or PACAP. PACAP generally elicits fusion events from which cargos are released more slowly than fusion events elicited by ACh (Figure5). However, in the absence of Syt7, PACAP-stimulated release occurs with durations that are not significantly different from ACh-stimulated release (Figure 3.7A). However, the more striking outcome was the fact that very few fusion events were recorded at all when Syt7 expression was absent, whether ACh or PACAP was the secretagogue (Figure 3.7B – E). This suggests that both neurotransmitters cause release by triggering fusion of Syt7 granules, and ostensibly, Syt1 granules.

Discussion

In this report, we demonstrate that PLCε is required for PACAP-stimulated secretion and supports the idea that the PAC1 receptor is $G\alpha_s$ coupled. Noticeable differences in fusion pore phenotypes were observed when comparing PACAP to ACh-stimulated secretion, which prompted studies that focused on the PACAP mechanism of secretion. When bovine chromaffin cells transfected with NPY-pHluorin were stimulated with PACAP, the resulting events were significantly longer lived than ACh events (Figure 3.1 E). Moreover, the events that occurred after PACAP stimulated exocytosis were not always interpretable. For example, some events lasted for the length of image acquisition, and other seemed to move after initial fusion and cargo release (Figure 3.2 A,B,C). ACh stimulated events always led to rapid release of cargo and full release of cargo proteins, so we hypothesized that PACAP stimulation may lead to cavicapture events, which are events where the fusion pore opens briefly, and cargo are released partially. NPY-pHluorin was transfected into WT bovine chromaffin cells and we conducted pH switching experiments after PACAP and ACh stimulation to see if cavicapture events were occurring in response to stimulation. PACAP receptor activation led to more cavicapture events than ACh overall and supported the idea that the previously seen events presented in Figure 3 may have been cavicapture events. Because syt-7 has previously been reported to both slow the rate at which cargo is released and allow dense core granule secretion to result in cavicapture events (Rao, Passmore et al. 2014, Rao, Rodriguez et al. 2017, Bendahmane, Morales et al. 2020), we thought that syt-7 may be responsible for driving the bulk of PACAP-stimulated secretion from chromaffin cells. We conducted experiments using syt-7 KO chromaffin cells to determine if syt-7 is indeed responsible for this phenomenon. However, studies revealed that though the lack of syt-7 does effect secretion to a certain extent, it is not absolutely required for PACAP mediated

exocytosis (Figure 3.7). It is notable that the release times between ACh and PACAP in both WT and sty-7 rescue cells are significantly different. Again, we observed that PACAP stimulation tends to prolong fusion events and release of cargo, whereas ACh stimulation largely leads to rapid fusion events. It is possible that there is something constraining the fusion pore that is specific to PACAP stimulated secretion and is in the signaling pathway. However, despite previously conducted research to illuminate PACAP signaling mechanisms (Hamelink, Tjurmina et al. 2002, Smith and Eiden 2012, Stroth, Kuri et al. 2013, Eiden, Emery et al. 2018), the intracellular components that lead to calcium influx which triggers secretion remains unknown.

It has been previously reported that PACAP stimulation can lead to opening of low threshold T-type calcium channels (Hill, Chan et al. 2011), so we used T-type channel blocker TTA-P2 and the non-selective calcium channel blocker $NiCl_2$ to see if cellular calcium levels are hindered after PACAP stimulation of chromaffin cells in the presence of inhibitors (Figure 3.3 A,C,F,G). We did confirm with our studies that PACAP-mediated calcium influx utilizes low threshold T-type channels. T-type calcium channels do not require an action potential to open and allow calcium influx but opens to even mild cellular depolarization. Calcium influx through T-type channels can then further depolarize the cell and allow greater calcium influx (Lukyanetz and Neher 1999). It is possible that because PACAP is released form the splanchnic nerve in response to stress, that the use of T-type channels is to ensure chromaffin cell secretion even if cells are not sufficiently depolarized to elicit an action potential.

To further characterize the intracellular components involved n PACAP stimulated exocytosis, we conducted pharmacological experiments to determine and confirm previous studies that implicated Epac as an intracellular signaling protein in neuroendocrine signaling activation (Emery, Xu et al. 2017) Epac is activated by cAMP, which is produced when a $G\alpha_s$

coupled G-protein receptor is activated and stimulates adenylyl cyclase. When ESI-09, an Epac inhibitor, was applied in the imaging bath solution, no calcium influx was observed after PACAP stimulation. However, ACh-stimulated calcium influx was unhindered by the inhibitor (Figure 3.4 E, F, G). Since ACh most likely primarily activates nACh receptors which are ligand-gated ion channels, we expected no difference in calcium influx even with the presence of ESI-09. To confirm that ACh relies mostly on nACh receptors to elicit the increase of intracellular calcium, we stimulated cells in the presence of scopolamine, a muscarinic receptor blocker. We did not observe any significant differences in calcium influx in response to ACh, confirming that nicotinic receptors drive chromaffin cell secretion after ACh perfusion onto the cell. It is important to note that PACAP and ACh utilize two completely different signaling mechanisms to elicit chromaffin cell exocytosis, ACh depolarizes the cell by activating and opening ligand-gated ion channel receptors, whereas PACAP activates metabolic receptors, which signal through Epac and eventually leads to the opening of low threshold T-type channels, which allow low levels of calcium to enter the cell which elicit cell secretion. We also conducted experiments with low levels of extracellular calcium to determine if intracellular calcium stores were responsible for increased calcium levels after PACAP stimulation. In conditions with low calcium, no rise of calcium levels within the cells after stimulation with ACh or PACAP were observed. This gives us information about the intracellular components involved in the signaling cascade. In the signaling pathway of some GPCRs, the hydrolysis of PIP_2 results in IP_3 and DAG. DAG remains associated to the membrane and is known to activate PKC. IP_3 is released into the cytoplasm, travels to the endoplasmic reticulum and binds to IP_3 receptors, which free intracellular stores of calcium (Dillon, Murray et al. 1987, Wong, Hadjiyanni et al. 2005, Taylor and Tovey 2010). The result that we observed confirms that IP_3 is not involved in the PACAP

mechanism of chromaffin cell secretion, since extracellular calcium is solely responsible for increased calcium levels after PACAP and ACh stimulation. This tells us that DAG is likely what is responsible for activating PKC which then eventually leads to calcium influx. Future work will likely focus on testing this hypothesis.

Having made the observation that Epac is involved in the intracellular pathway and that the calcium is coming from the extracellular space, we then explored what is downstream of Epac. It has recently been shown that Epac can activate PLCε, which can then enhance calcium induced calcium release through a PKC dependent mechanism. (Oestreich, Wang et al. 2007, Oestreich, Malik et al. 2009). So, through a collaboration, we used PLCε KO mouse chromaffin cells to study the effect that a lack of PLCε has on PACAP-stimulated secretion. There was no difference between WT and PLCε KO cells after cholinergic stimulation of the cell (Figure 3.5, A, B,D,G,I), however there was no calcium influx or release events after PACAP stimulation in PLCε KO cells. By transfecting PLCε KO cells with a plasmid encoding PLCε, we were able to rescue normal cellular response. The results of these experiments show that PACAP-stimulated calcium influx and chromaffin cell secretion are reliant on PLCε signaling. To confirm that the lack of calcium influx and chromaffin cell secretion was due to the knockout of PLCε and not a difference in the cells ability to produce cAMP, we conducted cAMP assays with WT and PLCε KO cells. The results showed that both cell types were able to produce cAMP at comparable levels in response to forskolin (Figure 3.6 I)

The evidence collected in this project support the hypothesis that the PAC1 receptor is $G\alpha_s$ coupled, not $G\alpha_q$ coupled. We attempted to use a $G\alpha_q$ inhibitor to confirm this hypothesis further. When 100nM $G\alpha_q$ inhibitor was used, lower amounts of calcium entering the cell were observed after PACAP perfusion onto the cells (data not shown). We initially thought that this

might mean that both receptor types were present. However, after further research, we found that the $G\alpha_q$ inhibitor that we used was not truly selective, but also was shown to inhibit $G\alpha_s$ (Peng and Shen 2019). Until there are more selective G protein inhibitors, we will not be able to directly test which G protein is involved, however based on the data presented, the hypothesis that the PAC1 receptor is $G\alpha_s$ coupled is supported. Having said that, we know that Epac and PLCε are required for PACAP stimulated secretion, which strongly support that hypothesis that the PAC1 receptor is $G\alpha_s$ coupled. Altogether, this work provides novel insight into the intracellular pathway involved in PACAP-stimulated secretion which has not been previously determined.

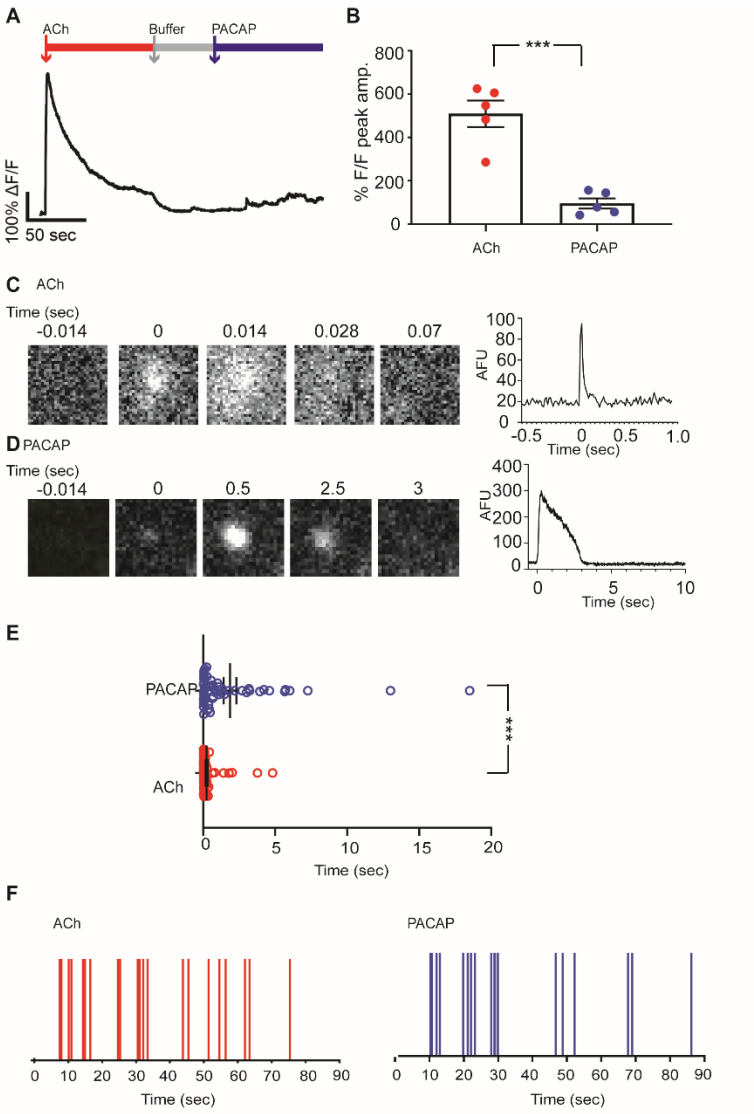

Figure 3.1. PACAP stimulation prolongs fusion time compared to ACh stimulation. Bovine cells transfected with GCaMP were stimulated using ACh and PACAP. A An example trace of relative calcium influx, shown as ΔF/F, after stimulation with ACh and PACAP. **B**. The graph shows the ΔF/F after stimulation with ACh (509.8 ΔF/F +/- 61.16) and PACAP (95.84 ΔF/F +/- 23.29). The difference in peak amplitude is significantly different, $p < 0.0005$. C. Panels represent single event from bovine cell transfected with NPY pHluorin after ACh stimulation. Fluorescence rapidly dissipates after initial fusion. **D.** Panels represent single after PACAP stimulation. Fluorescence does not dissipate until after ~2.5sec. **E.** Duration of release for individual events after either ACh or PACAP perfusion for all cells was analyzed. PACAP elicited events are prolonged compared to ACh-stimulated events which occur rapidly. Using a Welch's t test, we saw a significant difference between ACh (0.2305 sec +/- 0.06982) and PACAP elicited events (1.857 sec +/- 0.4452) $p < 0.001$.

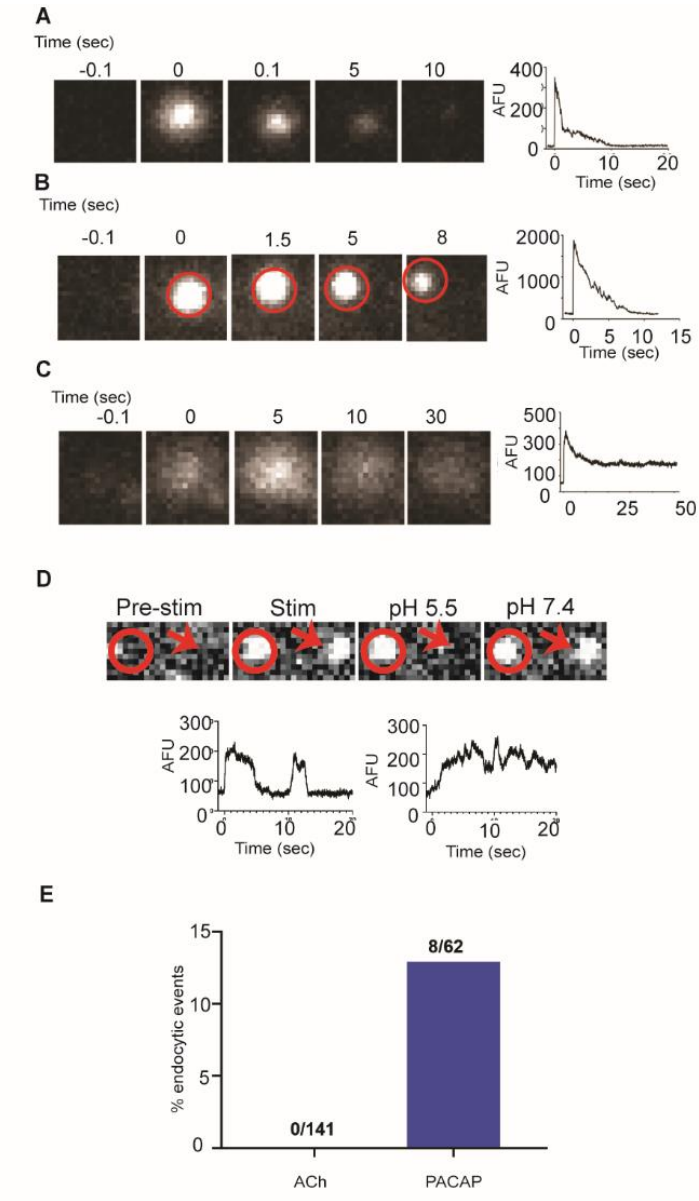

Figure 3.2. PACAP stimulation led to more cavicapture events than ACh stimulation. In bovine cells transfected with NPY-pHluorin, PACAP stimulated events were phenotypically different from ACh. **A**. Panels show a long-lived event after PACAP stim, which could represent cavicapture or slowed cargo release. **B**. Panels show an event that moves laterally after initial fusion, which may possibly mean that the event was endocytosed after fusion but remained near the membrane. **C**. Panels show event where the fluorescence, after initial granule fusion, does not go back down to baseline during the entire course of perfusion and image acquisition. This may also represent an endocytic event or slow release of cargo. **D**. pH switching experiments were conducted to determine if cavicapture was occurring after PACAP stimulation. pH was switched every 5 seconds between pH 5.5 and pH 7.4 during continuous perfusion with ACh or PACAP. Panel shows an event that is fused to the membrane during the course of cargo release (arrow) and an endocytic event that is endocytosed but remains near the membrane after initial fusion. The panel at pH 5.5 shows the fluorescent cargo of the non-endocytic event being quenched by the acidic environment. However, the fluorescent cargo in the endocytic event is not quenched. **E**. PACAP stimulation led to some cavicapture events, but ACh activation resulted in no endocytic events.

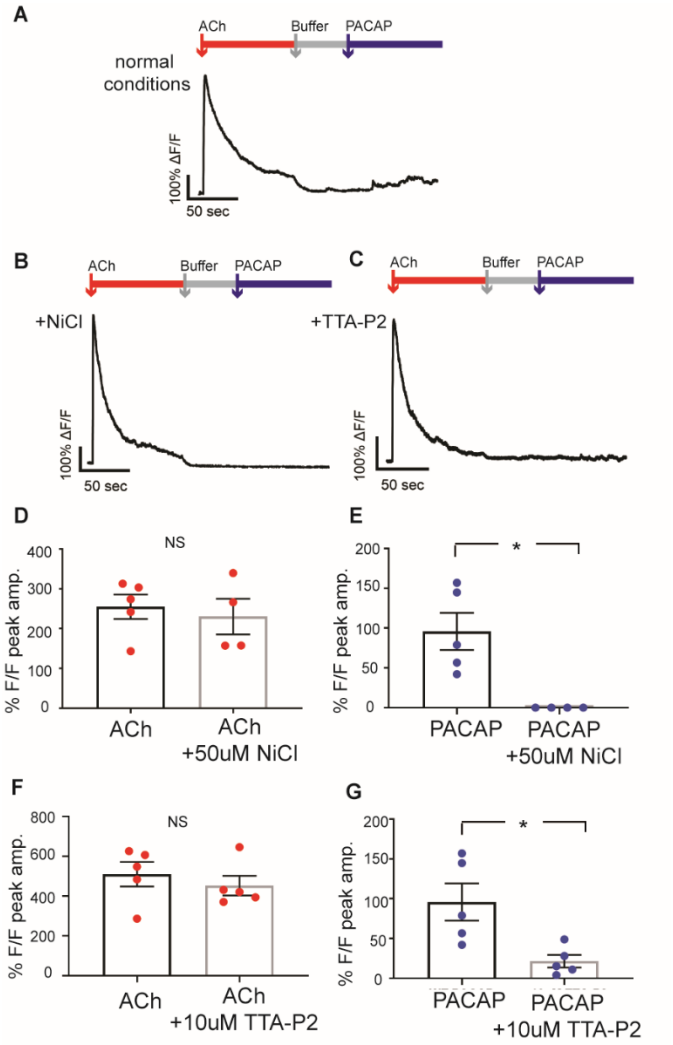

Figure 3.3. PACAP-stimulated calcium influx utilizes low voltage gated T-type channels. Bovine cells were transfected with GCaMP5G to observe the amount of calcium entering the cell after stimulation **A.** The tracing shows the relative calcium influx after ACh and PACAP stimulation in normal conditions. **B.** Tracing of calcium influx in the presence of nickel which, non-selectively blocks calcium channels **C**. Tracing of calcium influx in the presence of T-type channel blocker TTA-P2 **D**. The addition of 50 uM NiCl also had no significant effect on ACh-induced calcium influx (509.8 ΔF/F +/- 61.16 normal conditions; 460.2 ΔF/F +/- 89.09 with inhibitor), however (**E**) The presence of nickel significantly lowered the amount of calcium entering the cell after perfusion with PACAP, $p < 0.05$ (95.84 ΔF/F +/- 23.29 normal conditions; 0.00 with inhibitor). ACh data was analyzed using a student's t test and PACAP data was analyzed using a Welch's corrected t test since group variance was significant. **F.** The addition of the T-type channel inhibitor TTA-P2 (10uM) had no effect on the level of calcium influx after ACh stimulation (509.8 ΔF/F +/- 61.16 normal conditions; 452 ΔF/F +/- 49.44 with inhibitor) however (**G**) TTA-P2 significantly lowered the amount of calcium entering the cell after PACAP stimulation, $p < 0.05$ (95.84 ΔF/F +/- 23.29 normal conditions; 21.51 ΔF/F +/- 7.902 with inhibitor).

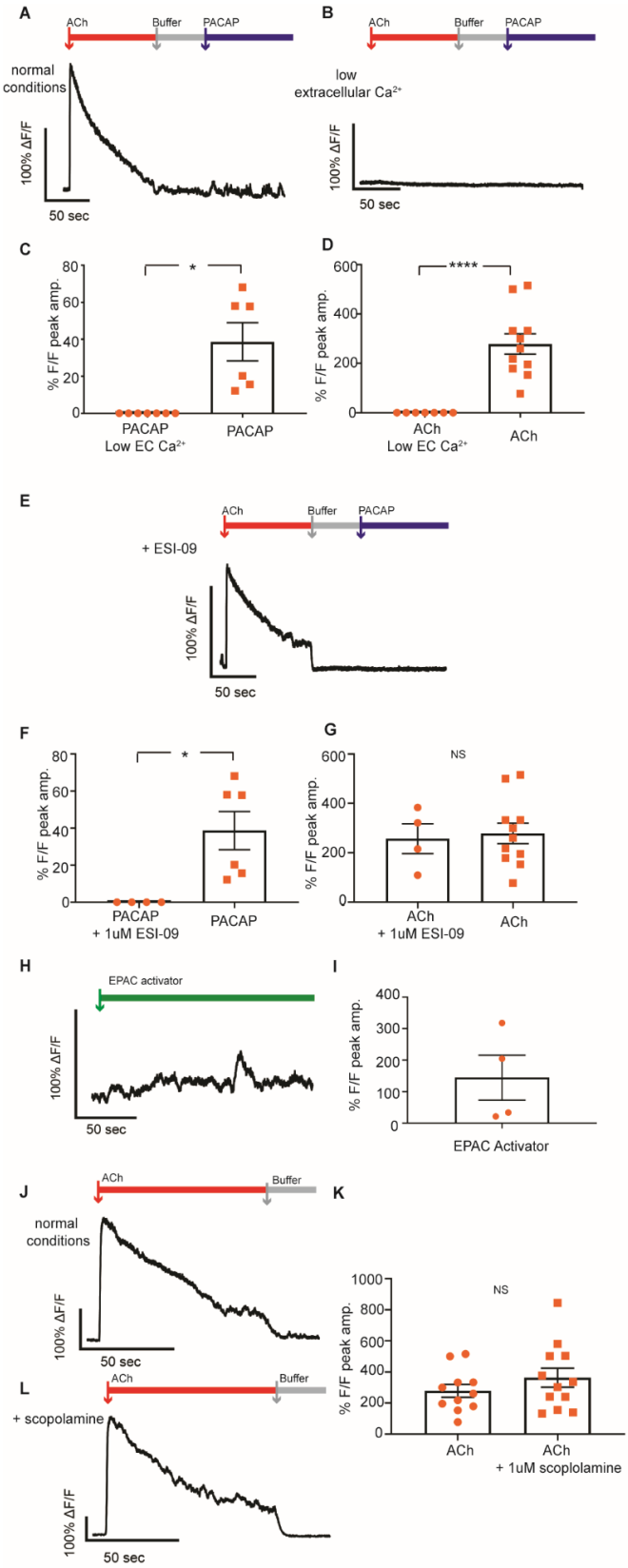

Figure 3.4. PACAP stimulated increase n calcium levels rely on extracellular calcium influx and EPAC signaling. Mouse chromaffin cells were transfected with GCaMP5G to determine EPAC's involvement in the PACAP signaling pathway. **A.** Tracing of a WT cell stimulated with ACh and PACAP. B. Trace of cellular levels of calcium in low calcium environment (+ 1uM EGTA). **C**. The % of ΔF/F peak amplitude are for multiple cells were analyzed using a Welch's t test. In low extracellular calcium conditions, there was no calcium seen after PACAP stimulation (0.00) however in normal conditions, calcium influx was observed after PACAP perfusion (38.64 ΔF/F +/- 10.29), p <0.05**. E**. Trace representing calcium level in cell after ACh and PACAP in the presence of EPAC inhibitor, ESI-09. **F**. Influx of calcium did not occur in the presence of ESI-09 after PACAP stimulation, p< 0.05 (0.00 ΔF/F with inhibitor; 38.64 ΔF/F +/- 10.29 normal conditions. The data were analyzed using a Welch's t test since variances between groups were significantly different. **G.** In the presence of ESI-09, there was no difference in peak amplitude after ACh stimulation (257.3 Δ F/F +/- 60.36 with inhibitor; 278.4 ΔF/F +/- 41.42 normal conditions). The data were analyzed using a student's t test. **H, I** EPAC activator was perfused onto cells and resulted in calcium entrance. **J, K, L**. In the presence of 1uM scopolamine, there was no statistical difference between ACh-stimulated calcium influx compared to normal conditions (362.6 ΔF/F +/- 61.53 with inhibitor; 278.4 ΔF/F +/- 41.42 normal conditions).

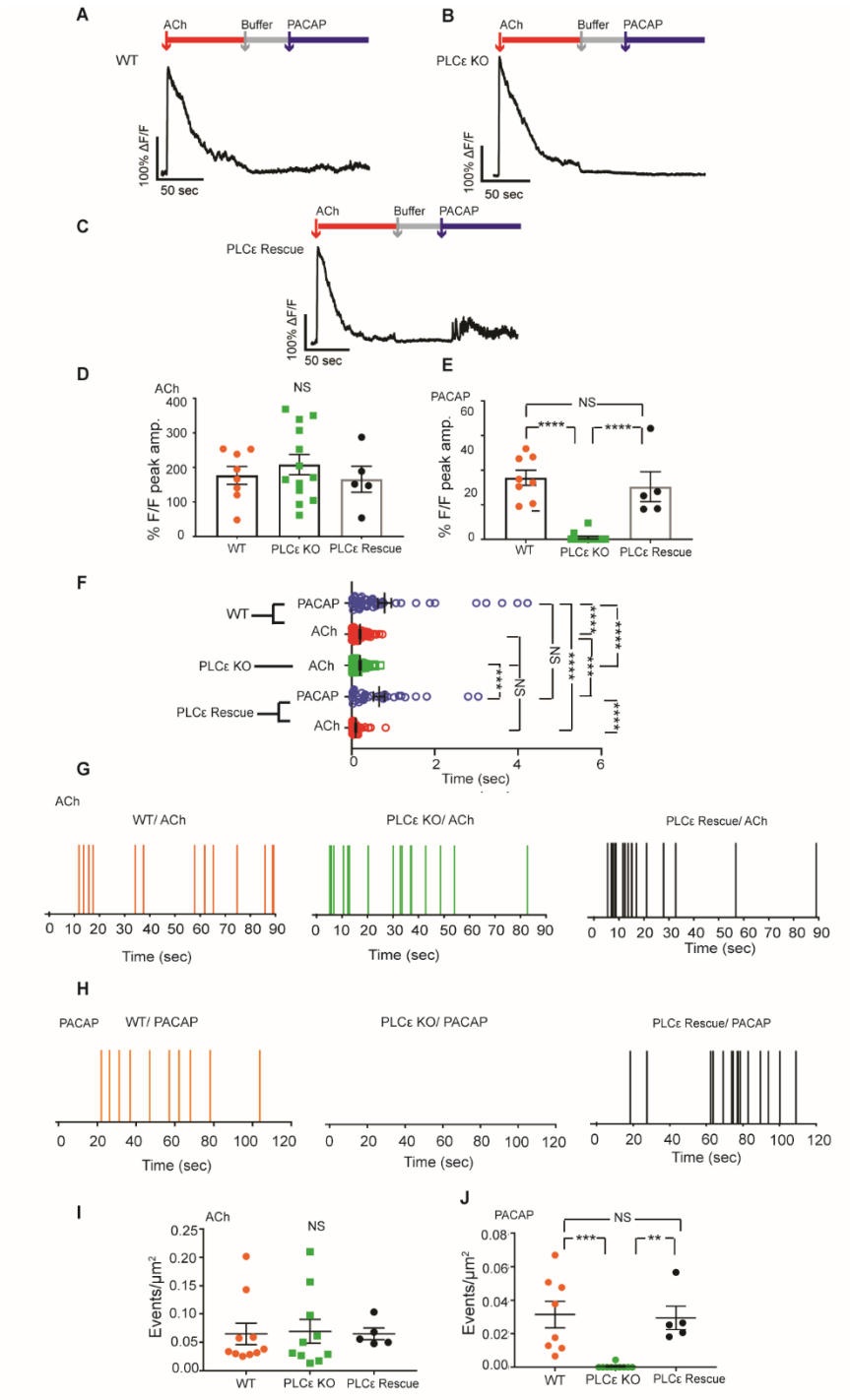

Figure 3.5. PLCε is required for PACAP stimulated calcium influx and ultimately, chromaffin cell exocytosis. Mouse chromaffin cells were transfected with GCaMP. **A**. Trace represents calcium influx after WT cell was stimulated with ACh and PACAP. **B**. Calcium Trace from PLCε KO cell stimulated with ACh and PACAP**. C**. Trace of calcium influx in PLCε KO cell transfected with PLCε plasmid. **D.** GCaMP data was analyzed using an ordinary one-way anova and a Tukey's multiple comparisons test. Data were analyzed using ordinary one-way anova and a Tukey's multiple comparisons test. ACh GCaMP amplitudes were not significantly different from one another. For WT ACh, the average peak amplitude was 176.8 +/- 25.73, PLCε KO average peak amplitude was 208.1 +/- 29.10 and PLCε Rescue was 165.8 +/- 37.69. **E**. PACAP GCaMP peak values were statistically significant between WT and PLCε KO values ($p<0.0001$) and PLCε Rescue and PLCε KO ($p<0.0001$), however were not statistically significant between WT and PLCε rescue. The peak average for WT were 35.57 +/- 4.396, PLCε KO average was 1.0008 +/- 0.7557 and PLCε rescue average was 30.40 +/- 8.664. **F.** The graph represents duration of individual events from each cell analyzed. The duration of ACh-stimulated events for WT, PLCε KO and PLCε rescue were not significantly different from each other, and the duration of PACAP stimulated events for WT and PLCε rescue were not significantly different from each other. However, multiple comparisons test revealed that ACh stimulated events were all significantly different from PACAP stimulated events regardless of the genotype of cell. Values are as follows: WT PACAP vs. WT ACh, $p< 0.0001$ (0.7925 sec +/- 0.1588; 0.2005 sec +/- 0.01688), WT PACAP vs. PLCε KO ACh, $p<0.0001$, (0.07925 sec +/- 0.1588; 0.2021 sec +/- 0.02193), WT PACAP vs. PLCε rescue ACh, $p< 0.0001$ (0.07925 sec +/- 0. 0.09900 sec +/- 0.01745), PLCε rescue PACAP vs. WT ACh, $p<0.001$ (0.6603 sec +/- 0.1312; 0.2005 sec +/- 0.1688) and PLCε rescue PACAP vs, PLCε KO ACh, $p<0.001$ and finally PLCε rescue PACAP vs. PLCε rescue ACh, $p < 0.0001$. The graph represents the amount of events per surface area of the cell in um2. Data was analyzed using an ordinary

one-way anova and a Tukey's multiple comparisons test. ACh-elicited events per um2 were not significantly different between WT, PLCε KO or PLCε rescued. The average value for WT ACh-stimulated events was 0.06490 +/- 0.01877, for PLCε KO the average value was 0.6933 +/- 0.02091 and for the PLCε rescue, the average was 0.06500 +/- 0.01024. PACAP-stimulated events per um2 was significantly different between WT and PLCε KO ($p<0.005$) and significantly different between PLCε rescue and PLCε KO ($p<0.05$). The average amount of events per um2 for WT was 0.03147 +/- 0.007875, for PLCε KO the average value was 0.0004436 +/- 0.00004436 and the average event/um2 for PLCε rescued was 0.02948 +/- 0.006958.

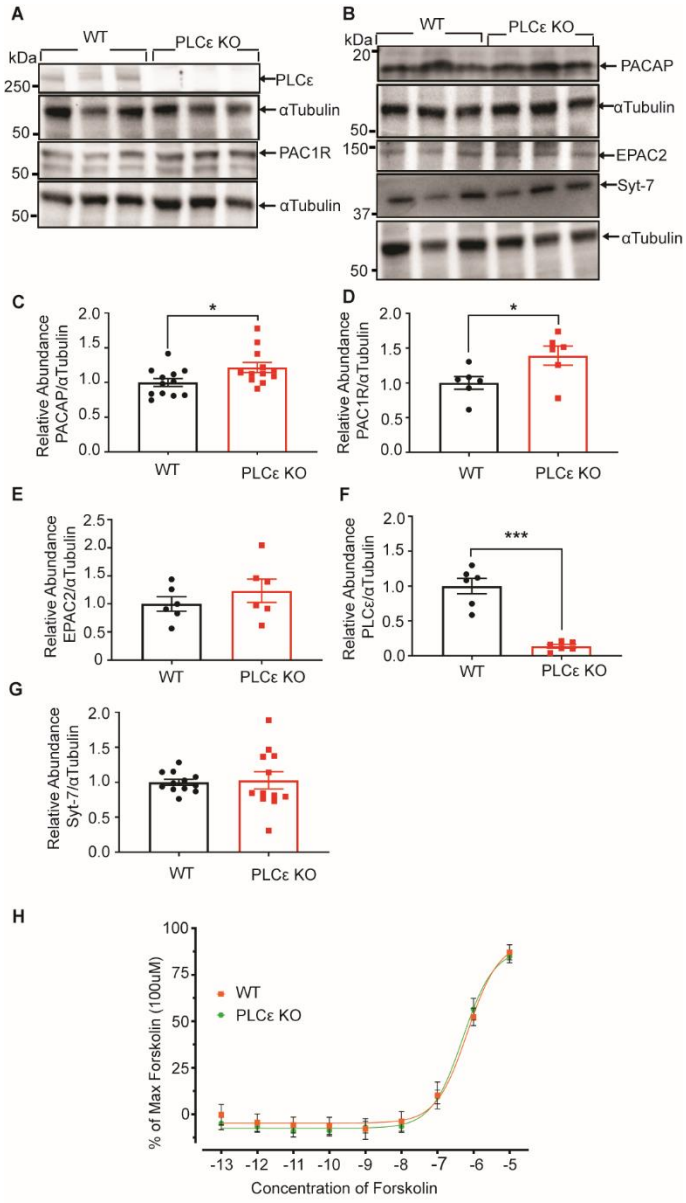

Figure 3.6 Expression levels and cAMP production of WT and PLCε KO cells. A,B. Western blot analysis was performed on WT and PLCε KO adrenal medullas to compare protein expression levels. **C.** Data were analyzed using a Welch's t-test. PLCε KO cells had significantly high levels of expression for PACAP than WT cells. **D**. PLCε KO cells had significantly more PAC1R receptor, possibly a compensatory expression change. **E,**. Both EPAC 2 is expressed in WT and PLCε KO cells at similar levels. **F**. PLCε KO cells are indeed knockout cells, compared to WT which express high levels of PLCε **G**. Expression of Syt-7 was also comparable in WT and PLCε KO cells. **H.** cAMP assay was conducted with PLCε and WT chromaffin cells to compare the cAMP production after forskolin activation. Two mice were used per condition and assay, 3 assays total. Each experiment yielded similar results between WT and PLCε KO cells, no significant difference in cAMP production. Nonlinear regression

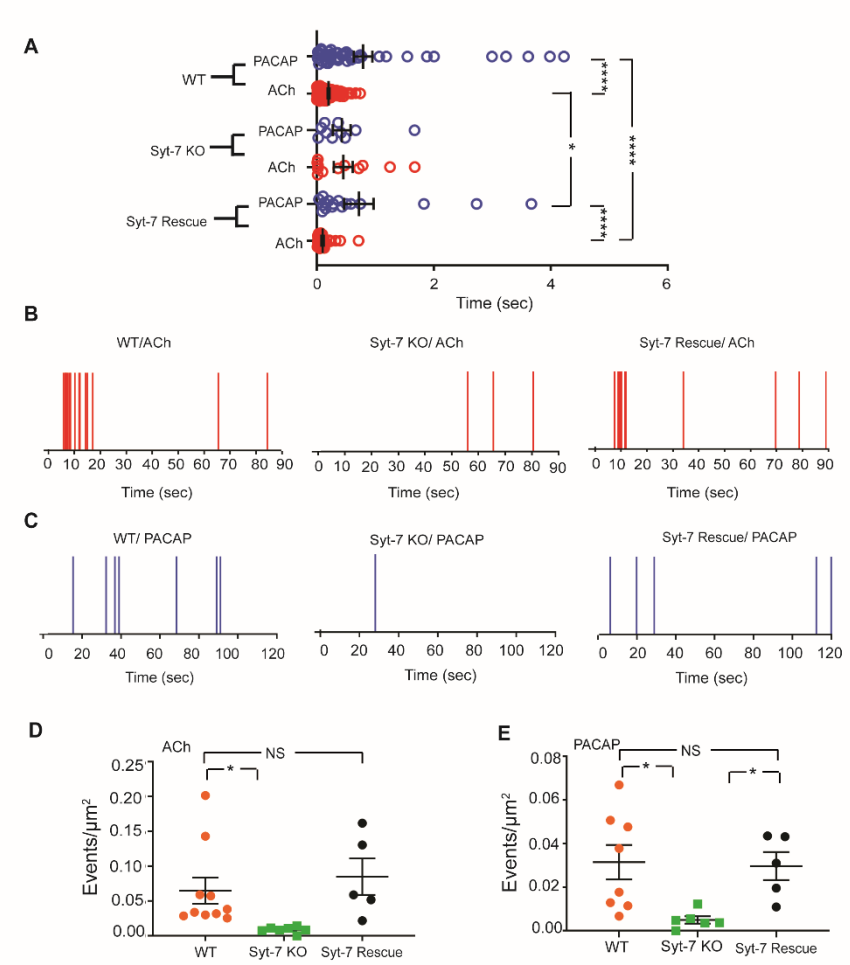

Figure 3.7. Lack of Syt-7 hinders cholinergic and PACAP-stimulated secretion A. The graph represents the duration of each individual event for each genotype and perfusion condition. The data was analyzed using an ordinary one-way anova with a Tukey's multiple comparisons test. The duration of release after ACh stimulate was not statistically significant between WT, Syt-7 KO or Syt-7 rescue. The duration of release after PACAP stimulation was also not statistically significant between WT, Syt-7 KO or Syt-7 rescue. However, there was a significant difference between WT PACAP and WT ACh stimulated events, p< 0.0001 (0.7925 sec +/- 0.1588; 0.2005 sec +/- 0.01688). There was also a significant difference between the Syt-7 rescue PACAP and Syt-7 rescue ACh duration of release, p <0.05 (0.7205 sec +/- 0.2514; 0.09838 sec +/- 0.01847). There was no significant difference between Syt-7 KO ACh and Syt-7 KO PACAP averages (0.4356 +/- 0.1604; 0.4272 +/- 0.1517), Syt-7 KO ACh and PACAP averages were also not significantly different from WT ACh, WT PACAP, Syt-7 rescue ACh or Syt-7 PACAP values, though this may be due to low number of events that occurred after perfusion in KO cells and a smaller sample size. The remaining duration comparisons between groups are as follows: WT PACAP vs. Syt-7 rescue ACh, p <0.0001, WT ACh vs. Syt-7 rescue PACAP, p < 0.05. **B.** Vertical line graphs show time of events for individual WT, PLCε KO and PLCε rescue cells. **C**. Vertical line graphs representing time that events occurred for individual WT, PLCε KO and PLCε rescue cells. **D.** The graph represents the amount of events per surface area of the cell in um2. Data was analyzed using a Brown-Forsythe and Welch Anova test with multiple comparisons. The events per um2 after ACh perfusion was not statistically different between WT and Syt-7 rescue cells (0.06490 um2 +/- 0.01877; 0.08494 um2 +/- 0.02623). There was also no statistical difference between Syt-7 rescue and Syt-7 KO (0.08494 um2 +/- 0.02623; 0.008586 um2 +/- 0.001688), however WT and Syt-7 KO values were statistically different, p <0.05. **E.** The amount of events/um2 for all cell types after PACAP perfusion were statistically different between WT and Syt-7 KO cells (p<0.05) and Syt-7 KO and rescue cells (p<0.05) . The average values for WT, Syt-7 KO and Syt-7 rescue are as follows: 0.03147 um2 +/- 0.007875, 0.004975 um2 +/- 0.001646 and 0.02964 um2 +/- 0.006434.

References

Abbineni, P. S., M. A. Bittner, D. Axelrod and R. W. Holz (2019). "Chromogranin A, the major lumenal protein in chromaffin granules, controls fusion pore expansion." J Gen Physiol **151**(2): 118-130.

Akerboom, J., T. W. Chen, T. J. Wardill, L. Tian, J. S. Marvin, S. Mutlu, N. C. Calderon, F. Esposti, B. G. Borghuis, X. R. Sun, A. Gordus, M. B. Orger, R. Portugues, F. Engert, J. J. Macklin, A. Filosa, A. Aggarwal, R. A. Kerr, R. Takagi, S. Kracun, E. Shigetomi, B. S. Khakh, H. Baier, L. Lagnado, S. S. Wang, C. I. Bargmann, B. E. Kimmel, V. Jayaraman, K. Svoboda, D. S. Kim, E. R. Schreiter and L. L. Looger (2012). "Optimization of a GCaMP calcium indicator for neural activity imaging." J Neurosci **32**(40): 13819-13840.

Bendahmane, M., A. Morales, A. J. B. Kreutzberger, N. A. Schenk, R. Mohan, S. Bakshi, J. M. Philippe, S. Zhang, V. Kiessling, L. K. Tamm, D. R. Giovannucci, P. M. Jenkins and A. Anantharam (2020). "Synaptotagmin-7 enhances calcium-sensing of chromaffin cell granules and slows discharge of granule cargos." J Neurochem.

Bevington, A. and G. K. Radda (1985). "Declining catecholamine secretion in adrenal medulla on prolonged stimulation with acetylcholine." Biochem Pharmacol **34**(9): 1497-1500.

Bohannon, K. P., M. A. Bittner, D. A. Lawrence, D. Axelrod and R. W. Holz (2017). "Slow fusion pore expansion creates a unique reaction chamber for co-packaged cargo." J Gen Physiol **149**(10): 921-934.

Cannon, W. B. (1940). "The Adrenal Medulla." Bull N Y Acad Med **16**(1): 3-13.

Carmichael, S. W. and H. Winkler (1985). "The adrenal chromaffin cell." Sci Am **253**(2): 40-49.

Chakrabarti, S., K. S. Kobayashi, R. A. Flavell, C. B. Marks, K. Miyake, D. R. Liston, K. T. Fowler, F. S. Gorelick and N. W. Andrews (2003). "Impaired membrane resealing and autoimmune myositis in synaptotagmin VII-deficient mice." J Cell Biol **162**(4): 543-549.

De Robertis, E. and A. V. Ferreira (1957). "Submicroscopic changes of the nerve endings in the adrenal medulla after stimulation of the splanchnic nerve." J Biophys Biochem Cytol **3**(4): 611-614.

Dillon, S. B., J. J. Murray, R. J. Uhing and R. Snyderman (1987). "Regulation of inositol phospholipid and inositol phosphate metabolism in chemoattractant-activated human polymorphonuclear leukocytes." J Cell Biochem **35**(4): 345-359.

Eiden, L. E., A. C. Emery, L. Zhang and C. B. Smith (2018). "PACAP signaling in stress: insights from the chromaffin cell." Pflugers Arch **470**(1): 79-88.

Emery, A. C., W. Xu, M. V. Eiden and L. E. Eiden (2017). "Guanine nucleotide exchange factor Epac2-dependent activation of the GTP-binding protein Rap2A mediates cAMP-dependent growth arrest in neuroendocrine cells." J Biol Chem **292**(29): 12220-12231.

Goldstein, D. S. (2010). "Adrenal responses to stress." Cell Mol Neurobiol **30**(8): 1433-1440.

Goldstein, D. S. and I. J. Kopin (2007). "Evolution of concepts of stress." Stress **10**(2): 109-120.
Grynszpan-Winograd, O. (1974). "Adrenaline and noradrenaline cells in the adrenal medulla of the hamster: a morphological study of their innervation." J Neurocytol **3**(3): 341-361.

Gubernator, N. G., H. Zhang, R. G. Staal, E. V. Mosharov, D. B. Pereira, M. Yue, V. Balsanek, P. A. Vadola, B. Mukherjee, R. H. Edwards, D. Sulzer and D. Sames (2009). "Fluorescent false neurotransmitters visualize dopamine release from individual presynaptic terminals." Science **324**(5933): 1441-1444.

Guerineau, N. C. (2019). "Cholinergic and peptidergic neurotransmission in the adrenal medulla: A dynamic control of stimulus-secretion coupling." IUBMB Life.

Hamelink, C., H. W. Lee, Y. Chen, M. Grimaldi and L. E. Eiden (2002). "Coincident elevation of cAMP and calcium influx by PACAP-27 synergistically regulates vasoactive intestinal polypeptide gene transcription through a novel PKA-independent signaling pathway." J Neurosci **22**(13): 5310-5320.

Hamelink, C., O. Tjurmina, R. Damadzic, W. S. Young, E. Weihe, H. W. Lee and L. E. Eiden (2002). "Pituitary adenylate cyclase-activating polypeptide is a sympathoadrenal neurotransmitter involved in catecholamine regulation and glucohomeostasis." Proc Natl Acad Sci U S A **99**(1): 461-466.

Hill, J., S. A. Chan, B. Kuri and C. Smith (2011). "Pituitary adenylate cyclase-activating peptide (PACAP) recruits low voltage-activated T-type calcium influx under acute sympathetic stimulation in mouse adrenal chromaffin cells." J Biol Chem **286**(49): 42459-42469.

Kuri, B. A., S. A. Chan and C. B. Smith (2009). "PACAP regulates immediate catecholamine release from adrenal chromaffin cells in an activity-dependent manner through a protein kinase C-dependent pathway." J Neurochem **110**(4): 1214-1225.

Lukyanetz, E. A. and E. Neher (1999). "Different types of calcium channels and secretion from bovine chromaffin cells." Eur J Neurosci **11**(8): 2865-2873.

Miyata, A., A. Arimura, R. R. Dahl, N. Minamino, A. Uehara, L. Jiang, M. D. Culler and D. H. Coy (1989). "Isolation of a novel 38 residue-hypothalamic polypeptide which stimulates adenylate cyclase in pituitary cells." Biochem Biophys Res Commun **164**(1): 567-574.

Oestreich, E. A., S. Malik, S. A. Goonasekera, B. C. Blaxall, G. G. Kelley, R. T. Dirksen and A. V. Smrcka (2009). "Epac and phospholipase Cepsilon regulate Ca^{2+} release in the heart by

activation of protein kinase Cepsilon and calcium-calmodulin kinase II." J Biol Chem **284**(3): 1514-1522.

Oestreich, E. A., H. Wang, S. Malik, K. A. Kaproth-Joslin, B. C. Blaxall, G. G. Kelley, R. T. Dirksen and A. V. Smrcka (2007). "Epac-mediated activation of phospholipase C(epsilon) plays a critical role in beta-adrenergic receptor-dependent enhancement of Ca^{2+} mobilization in cardiac myocytes." J Biol Chem **282**(8): 5488-5495.

Peng, Q. and J. Shen (2019). "YM-254890 is a General Inhibitor of G Proteins." The FASEB Journal **33**(S1): 503.507-503.507.

Przywara, D. A., X. Guo, M. L. Angelilli, T. D. Wakade and A. R. Wakade (1996). "A non-cholinergic transmitter, pituitary adenylate cyclase-activating polypeptide, utilizes a novel mechanism to evoke catecholamine secretion in rat adreanl chromaffin cells." Journal of Biological Chemistry **271**: 10545-10550.

Rao, T. C., D. R. Passmore, A. R. Peleman, M. Das, E. R. Chapman and A. Anantharam (2014). "Distinct fusion properties of synaptotagmin-1 and synaptotagmin-7 bearing dense core granules." Mol Biol Cell **25**(16): 2416-2427.

Rao, T. C., Z. S. Rodriguez, M. M. Bradberry, A. H. Ranski, P. J. Dahl, M. W. Schmidtke, P. M. Jenkins, D. Axelrod, E. R. Chapman, D. R. Giovannucci and A. Anantharam (2017). "Synaptotagmin isoforms confer distinct activation kinetics and dynamics to chromaffin cell granules." Journal of General Physiology **149**(8): 763-780.

Smith, C. B. and L. E. Eiden (2012). "Is PACAP the major neurotransmitter for stress transduction at the adrenomedullary synapse?" J Mol Neurosci **48**(2): 403-412.

Smrcka, A. V., J. H. Brown and G. G. Holz (2012). "Role of phospholipase Cepsilon in physiological phosphoinositide signaling networks." Cell Signal **24**(6): 1333-1343.

Stroth, N., B. A. Kuri, T. Mustafa, S. A. Chan, C. B. Smith and L. E. Eiden (2013). "PACAP controls adrenomedullary catecholamine secretion and expression of catecholamine biosynthetic enzymes at high splanchnic nerve firing rates characteristic of stress transduction in male mice." Endocrinology **154**(1): 330-339.

Taylor, C. W. and S. C. Tovey (2010). "IP(3) receptors: toward understanding their activation." Cold Spring Harbor perspectives in biology **2**(12): a004010-a004010.

Wakade, A. R. (1988). "Noncholinergic transmitter(s) maintains secretion of catecholamines from rat adrenal medulla for several hours of continuous stimulation of splanchnic neurons." J Neurochem **50**(4): 1302-1308.

Wang, H., E. A. Oestreich, N. Maekawa, T. A. Bullard, K. L. Vikstrom, R. T. Dirksen, G. G. Kelley, B. C. Blaxall and A. V. Smrcka (2005). "Phospholipase C epsilon modulates beta-

adrenergic receptor-dependent cardiac contraction and inhibits cardiac hypertrophy." Circ Res **97**(12): 1305-1313.

Wolf, K., G. Zarkua, S. A. Chan, A. Sridhar and C. Smith (2016). "Spatial and activity-dependent catecholamine release in rat adrenal medulla under native neuronal stimulation." Physiol Rep **4**(17).

Wong, R., I. Hadjiyanni, H. C. Wei, G. Polevoy, R. McBride, K. P. Sem and J. A. Brill (2005). "PIP2 hydrolysis and calcium release are required for cytokinesis in Drosophila spermatocytes." Curr Biol **15**(15): 1401-1406.

Zhang, H., N. G. Gubernator, M. Yue, R. G. Staal, E. V. Mosharov, D. Pereira, V. Balsanek, P. A. Vadola, B. Mukherjee, R. H. Edwards, D. Sulzer and D. Sames (2009). "Dopamine release at individual presynaptic terminals visualized with FFNs." J Vis Exp(30).

Chapter IV

General Discussion

The experimental studies described in this thesis were motivated by the lack of clarity involving both pre- and post-synaptic regulators of the adrenomedullary synapse. Specifically, it was unknown how the calcium sensing proteins, synaptotagmins, regulate chromaffin cell secretion. Also, their location in chromaffin cells has not been determined. It was unknown whether synaptotagmins were located at the plasma membrane (Sugita, Han et al. 2001, Weber, Toft-Bertelsen et al. 2014, Jackman, Turecek et al. 2016) or dense core granules (Fukuda 2004, Zhang, Wu et al. 2011, Rao, Passmore et al. 2014). Additionally, it has not been elucidated how exactly the splanchnic nerve can drive the fight-or-flight response by secreting PACAP onto cells (Eiden and Jiang 2018). PACAP-stimulation induces chromaffin cell secretion via G-coupled protein mediated calcium influx; however, it is unknown which G-protein the receptor is coupled to. The goal of this thesis was to illuminate the intracellular signaling pathway of PACAP stimulated secretion and uncover the underlying regulation of synaptotagmins in chromaffin cell exocytosis.

Regulation of dense core granule secretion in chromaffin cells

Previous studies have shown that syt-7 acts on dense core granules by increasing the rate of fusion pore cargo release (Zhang, Liu et al. 2019), though our lab's previous work supports the idea that syt-7 constrains fusion pore expansion and results in a slower release of cargo (Rao, Passmore et al. 2014) Chapter II of this thesis describes studies that were focused on the location,

kinetic profile, and calcium affinity of synaptotagmins 1 and 7 using syt-7 KO mouse chromaffin cells. Using immunocytochemistry, we determined that syt-7 and syt-1 are sorted to organelles, and differentially sorted to dense core granules. This discovery prompted more questions as to what functional value did differential expression of synaptotagmins endow to dense core granules? Imaging studies using WT and syt-7 KO mouse chromaffin cells transfected with fluorescent cargo proteins, NPY-GFP, NPY- or tPA-pHluorin were conducted to study the effects of syt-7 on cargo release. After stimulation with KCl or ACh, cargo release was significantly more rapid when syt-7 was not present in the system; whereas when the full complement of synaptotagmins were expressed in WT, the cargo release times spanned a broader distribution. When syt-7 was rescued in syt-7 KO chromaffin cells the longer-lived events were rescued. This indicates that the spectrum of slow and fast release of cargo from chromaffin cells are dependent on expression of both synaptotagmins 1 and 7. Dense core granule fusion characteristics, specifically cargo release kinetics, are at least partially controlled by which synaptotagmin is expressed. This was an important observation because it had not previously been determined what the utility of expressing more than one form of synaptotagmin in this system had. These studies have shown that in the adrenomedullary system, chromaffin cell secretion of neuropeptides and catecholamines, is regulated by differentially sorted syts. Future studies should focus on determining the whole-body physiological effects of synaptotagmin regulation. For example, the stress response is partially responsible for triggering gluconeogenesis during times of starvation or fasting, allowing the body to maintain normal blood glucose levels (Watts and Donovan 2010). Injecting syt-7 KO and WT mice with insulin, or starving them for a short period of time, would induce metabolic stress and trigger the stress response. Measuring catecholamine secretion after this experiment would tell us if syt-7 is

important for this process and may link a physiologically important role to the effects that syt-7 has on chromaffin cell secretion.

Other groups have postulated that syt-7 acts by promoting fusion pore expansion (Zhang et al, 2019), which is not supported by the data presented in this thesis. In our studies, we observed that secretion was slowed when syt-7 was expressed in chromaffin cells. We concluded that syt-7 must restrict the fusion pore during exocytosis, resulting in longer lived events and slower cargo release. Previous studies in the lab also support this hypothesis (Rao, Passmore et al. 2014, Rao, Rodriguez et al. 2017). These discrepancies in the literature should be addressed and prompts future work to study, in more detail, the effects that syt-7 has on the fusion pore during chromaffin cell exocytosis. Future experiments could utilize polarized TIRF (P-TIRF) microscopy to directly monitor the membrane curvature during live cell imaging. The use of syt-7 KO mice would allow us to see the effects of syt-1 on the fusion pore. Unfortunately, global syt-1 knockout mice are not viable, so we would not be able to isolate syt-7 granule cells with currently available transgenic mouse lines. However, it is possible to generate a Cre-knockout of syt-1 in the adrenal medulla. Generating this line of mice would allow us to selectively study syt-7 release mechanisms using P-TIRF without overexpression of the protein.

PACAP-stimulated chromaffin cell exocytosis

Chapter II of this thesis focuses on regulation via synaptotagmins after cholinergic stimulation. However, we know that PACAP is also secreted onto chromaffin cells from the splanchnic nerves and prompts a distinct form of sustained chromaffin cell exocytosis (Wakade 1988, Hamelink, Tjurmina et al. 2002). Because of this, we were interested in defining the effects that PACAP had on the fusion pore during chromaffin cell secretion.

When bovine chromaffin cells were transfected with NPY-pHluorin and stimulated with ACh or PACAP to induce secretion, we saw a significant difference in duration of release depending on which secretagogue was perfused onto the cell. ACh-elicited events were more rapid and the cloud of fluorescence that occurred during cargo release dissipated rapidly. In contrast, PACAP-stimulated events were prolonged and could last up to the end of perfusion. The phenotype of the fusion events was unique from ACh events. Some events in response to PACAP stimulation moved laterally away from the initial site of release during the event. We hypothesized that "traveling" events might represent cavicapture events. Cavicapture events are when the granule initially fuses but is endocytosed before full cargo release. Using pH switching studies and a fluorescent pH-sensitive cargo protein, experiments were conducted to determine if cavicapture was occurring during PACAP stimulation compared to cholinergic stimulation. ACh stimulation resulted in no cavicapture events whereas PACAP elicited events were roughly 13% cavicapture. Since PACAP is secreted in response to high frequency firing of the splanchnic nerve (Eiden, Emery et al. 2018), we wondered what physiological utility cavicapture events had for the fight or flight response.

It was previously shown by Smith and Colleagues, using electrophysiological techniques, that chromaffin cell release is activity dependent. When basal firing rates were used to activate chromaffin cell secretion, catecholamines were selectively secreted. However, when under conditions that match acute stress, chromaffin cells secrete both catecholamines and neuropeptides in a stepwise fashion. For example, catecholamines are secreted first, and secretion of neuropeptides followed. They hypothesized that because catecholamines are smaller in size, the fusion pore may be restricted initially an then fully expand, allowing the much larger neuropeptides to be released. (Fulop, Radabaugh et al. 2005) The same group also showed later

that the amount of catecholamines secreted after stress conditions were increased compared to at basal firing rates (Wolf, Zarkua et al. 2016). Because PACAP is released during stress and is known to increase catecholamine release after application to chromaffin cells (Hamelink, Tjurmina et al. 2002), it is possible that the phenotypically unique and cavicapture events that we observed after PACAP stimulation are selective secretion size exclusion events.

A future direction for this project would be to study the effects that PACAP and ACh have on the fusion pore. Additionally, we could study if PACAP is associated with selective, stepwise secretion of catecholamines and neuropeptides. We previously hypothesized that if we transfected the cells catecholamines and neuropeptides, that we may see selective secretion of the catecholamines after stimulation to confirm the size exclusion hypothesis. During this study, we designed an experiment where cells were transfected with NPY-pHluorin and transduced with FFN. I then stimulated the cells with ACh or PACAP. Though the cells were able to secrete, we did not observe any fusion events that co-released the two cargos. This may be due to the use of electroporation for transfection which is harsh on the cells. Transfection using electroporation has been shown to alter fusion pore lifetimes and expression of luminal cargos (Abbineni, Bittner et al. 2019). It is possible that the granules that contained the NPY-pHluorin were unable to either take up the FFN or secrete the FFN in addition to the overexpressed cargo.

A potential way to avoid electroporation transfection would be to use a gentler way to transfect the cells with higher efficiency, such as Beckman transfection. If this technique is successful, then we could co-transfect the cells and monitor secretion after PACAP or ACh stimulation to determine fusion characteristics. Specifically, we could monitor secretion and observe if granules selectively retain neuropeptides but release catecholamines or if it is a stepwise release, where catecholamines are released first followed by neuropeptide secretion.

These experiments could potentially provide a direct role to PACAP verses ACh secretion and bridge the gap of knowledge of what secretagogue is directly responsible for selective secretion.

Regulation of PACAP mediated fusion pore expansion

The effect that PACAP secretion has on the fusion pore has not been directly studied. Using P-TIRF we would be able to monitor membrane curvature and determine if PACAP stimulation restricts fusion pore expansion compared to ACh. We could also directly measure if PACAP secretion and ACh secretion result in different fusion pore openings, allowing for selective secretion of catecholamines, and or neuropeptides.

Due to previous reports showing that syt-7 can restrict fusion pore expansion (Rao, Rodriguez et al. 2017, Bendahmane, Morales et al. 2020), we also hypothesized that syt-7 may be the main driver of fusion pore restriction in response to PACAP stimulation. In this study, we observed that in syt-7 KO cells containing FFN, the time of duration between PACAP and ACh-elicited events were not significantly different, with very few slow-release events. This may be due to the low number events that occurred in syt-7 KO cells. However, it is possible that syt-7 may at least be partially responsible for the long lived PACAP events. To determine the level of involvement that syt-7 has in modifying the fusion pore in PACAP secreted events, we could use P-TIRF and syt-7 KO chromaffin cells. If syt-7 is responsible for the restricted fusion pore, we would see mostly full expansion events and possibly, no selective secretion. If we find that syt-7 is not responsible for the restriction of the fusion pore after PACAP stimulation, there are other proteins that have been implicated in slowing fusion pore expansion, such as SNARE zippering rate and the endocytic protein, dynamin. (Bretou, Anne et al. 2008, Wu, Zhang et al. 2019). If this is the case, then we would explore further if these mechanisms were responsible for the ability of PACAP to slow cargo release.

Intracellular mechanism of PACAP stimulated secretion

Thanks to recent work, we know that PACAP stimulates chromaffin cell secretion during times of stress in a PKC-dependent manor. (Kuri, Chan et al. 2009). The PAC1 receptor expressed by chromaffin cells is a GPCR, however the G protein for which the receptor is coupled is unknown in this system. Therefore, another goal of this study was to determine the intracellular mechanism involved in PACAP-stimulated chromaffin cell secretion and ultimately, what Gα subunit is coupled to the PAC1 receptor.

To evaluate the intracellular proteins involved in the signaling cascade of PACAP and ACh, we addressed three main questions: First, was the rise of intracellular calcium after PACAP stimulation from extracellular or intracellular stores? Second, is the PACAP signaling pathway reliant on the expression of Epac and if so, what is downstream that elicits calcium-mediated chromaffin cell secretion? And third, are the muscarinic receptors activated by ACh at all responsible for calcium influx and chromaffin cell exocytosis; specifically, do PACAP and ACh signal through completely unique pathways, one of which is solely controlled by ligand gated ion channels and the other, signals solely through metabolic receptors?

Based on data that showed the involvement of EPAC in the PACAP signaling pathway (Emery, Xu et al. 2017), we conducted several pharmacological experiments to confirm EPAC as an intracellular signaling protein. Imaging experiments using the calcium indicator GCaMP5G to measure calcium levels after perfusion of ACh and PACAP were performed. The data showed that EPAC is required for PACAP stimulated calcium influx. We then focused on illuminating what was downstream of EPAC to determine how the cell was being prompted to open calcium channels. It has recently come to light that EPAC can activate PLCε and enhance calcium mobilization in a PKC dependent manner (Oestreich, Wang et al. 2007, Oestreich, Malik et al.

2009). This novel pathway and role for PLCε motivated our interest in investigating if PLCε is downstream of EPAC. Luckily, the Smrcka lab, who created the PLCε KO transgenic mouse line and discovered the novel PLCε pathway mentioned previously, collaborated with us, and allowed us access to the KO mice (Wang, 2005). Using the PLCε KO mice and TIRF imaging, we concluded that PLCε is absolutely necessary for PACAP stimulated exocytosis.

The studies described in chapter III of this thesis have answered the lingering question as to what G-protein the PAC1 receptor is coupled to. The discovery that PLCε is part of the intracellular signaling mechanism of PACAP stimulated secretion supports the claim that the PAC1 receptor is $G_{\alpha s}$ coupled. Additionally, we determined that the calcium responsible for triggering exocytosis is extracellular and not released from intracellular stores. Though this study has progressed our knowledge of how chromaffin cell secretion occurs after PACAP stimulation, there are still unanswered questions that must be addressed. For example, what is downstream of PLCε? We know that phospholipases can cleave PIP_2, resulting in IP_3 and DAG. Based on our data showing that the rise of calcium after PACAP stimulation is caused by extracellular calcium influx, we suspect that DAG is the main signaling molecule involved in PACAP mediated effects and not IP_3. PKC, which has been previously shown to be required in PACAP mediated secretion, (Kuri, Chan et al. 2009) can be activated by DAG. The next steps in illuminating the PACAP pathway should focus on determining if DAG is indeed the next step of the pathway connecting PLCε and PKC activity. Repeating similar experiments as described in this study while using pharmacological techniques, such as DAG kinase inhibitors or activators, would be sufficient to show the role of DAG in PACAP-stimulated chromaffin cell secretion.

Conclusions

This thesis has described different levels of splanchnic nerve activity that are able to activate independent and parallel pathways that result in different fusion modes (Figure 4.1). One that signals through nicotinic ACh receptors and causes largely rapid release of granules that result in all the cargo to be released. The other signals through PLCε and causes a variety of fusion modes that seems to restrict the fusion pore in some way and promote either full or partial secretion of the cargo. Moreover, that synaptotagmins act as regulators of the system by endowing the granules that express either syt-1 or syt-7, with distinct fusion properties. Future work will be to characterize and determine the cause of the variety of fusion modes and what exactly is working in the PACAP pathway to slow cargo release and evoke cavicapture events.

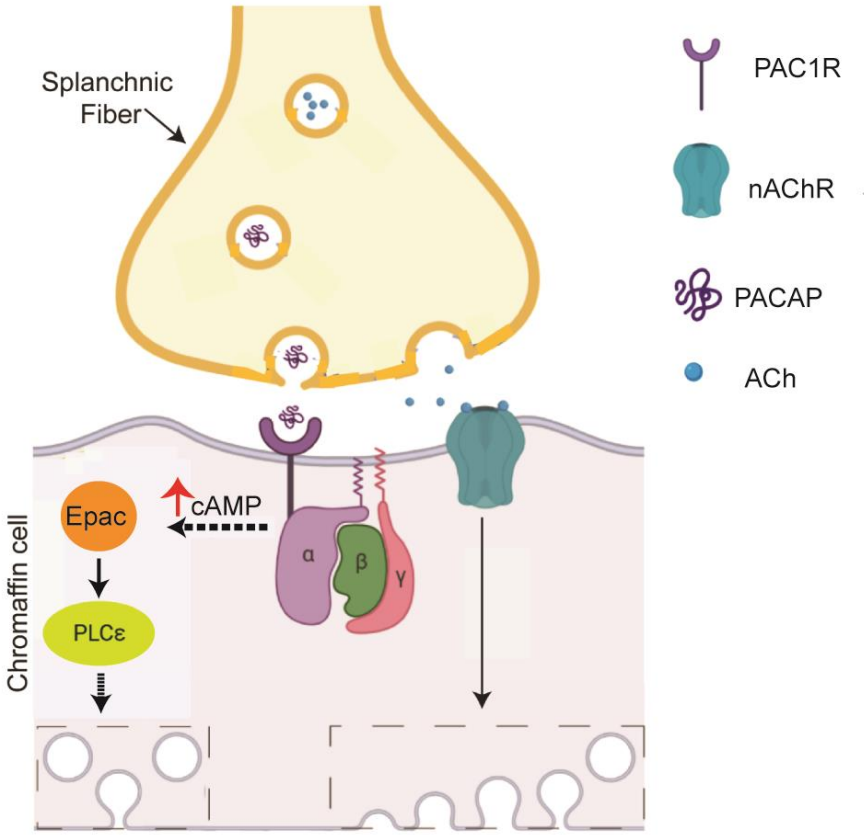

Figure 4.1. Signaling Summary figure. ACh and PACAP signal through independent and parallel pathways to elicit secretion from chromaffin cells. PACAP activates the PAC1 receptor, which is a GPCR. This PACAP signals through EPAC and PLCε which results in events where either all or partial release of cargo proteins. ACh binds and activates nACh receptors, which lead to full release events.

References

Abbineni, P. S., M. A. Bittner, D. Axelrod and R. W. Holz (2019). "Chromogranin A, the major lumenal protein in chromaffin granules, controls fusion pore expansion." J Gen Physiol **151**(2): 118-130.

Bendahmane, M., A. Morales, A. J. B. Kreutzberger, N. A. Schenk, R. Mohan, S. Bakshi, J. M. Philippe, S. Zhang, V. Kiessling, L. K. Tamm, D. R. Giovannucci, P. M. Jenkins and A. Anantharam (2020). "Synaptotagmin-7 enhances calcium-sensing of chromaffin cell granules and slows discharge of granule cargos." J Neurochem.

Bretou, M., C. Anne and F. Darchen (2008). "A fast mode of membrane fusion dependent on tight SNARE zippering." J Neurosci **28**(34): 8470-8476.

Eiden, L. E., A. C. Emery, L. Zhang and C. B. Smith (2018). "PACAP signaling in stress: insights from the chromaffin cell." Pflugers Arch **470**(1): 79-88.

Eiden, L. E. and S. Z. Jiang (2018). "What's New in Endocrinology: The Chromaffin Cell." Front Endocrinol (Lausanne) **9**: 711.

Emery, A. C., W. Xu, M. V. Eiden and L. E. Eiden (2017). "Guanine nucleotide exchange factor Epac2-dependent activation of the GTP-binding protein Rap2A mediates cAMP-dependent growth arrest in neuroendocrine cells." J Biol Chem **292**(29): 12220-12231.

Fukuda, M. (2004). "RNA interference-mediated silencing of synaptotagmin IX, but not synaptotagmin I, inhibits dense-core vesicle exocytosis in PC12 cells." Biochem J **In press**.
Fulop, T., S. Radabaugh and C. Smith (2005). "Activity-Dependent Differential Transmitter Release in Mouse Adrenal Chromaffin Cells." Journal of Neuroscience **25**(32): 7324-7332.

Hamelink, C., O. Tjurmina, R. Damadzic, W. S. Young, E. Weihe, H. W. Lee and L. E. Eiden (2002). "Pituitary adenylate cyclase-activating polypeptide is a sympathoadrenal neurotransmitter involved in catecholamine regulation and glucohomeostasis." Proc Natl Acad Sci U S A **99**(1): 461-466.

Jackman, S. L., J. Turecek, J. E. Belinsky and W. G. Regehr (2016). "The calcium sensor synaptotagmin 7 is required for synaptic facilitation." Nature **529**(7584): 88-91.

Kuri, B. A., S. A. Chan and C. B. Smith (2009). "PACAP regulates immediate catecholamine release from adrenal chromaffin cells in an activity-dependent manner through a protein kinase C-dependent pathway." J Neurochem **110**(4): 1214-1225.

Oestreich, E. A., S. Malik, S. A. Goonasekera, B. C. Blaxall, G. G. Kelley, R. T. Dirksen and A. V. Smrcka (2009). "Epac and phospholipase Cepsilon regulate Ca2+ release in the heart by activation of protein kinase Cepsilon and calcium-calmodulin kinase II." J Biol Chem **284**(3): 1514-1522.

Oestreich, E. A., H. Wang, S. Malik, K. A. Kaproth-Joslin, B. C. Blaxall, G. G. Kelley, R. T. Dirksen and A. V. Smrcka (2007). "Epac-mediated activation of phospholipase C(epsilon) plays a critical role in beta-adrenergic receptor-dependent enhancement of Ca2+ mobilization in cardiac myocytes." J Biol Chem **282**(8): 5488-5495.

Rao, T. C., D. R. Passmore, A. R. Peleman, M. Das, E. R. Chapman and A. Anantharam (2014). "Distinct fusion properties of synaptotagmin-1 and synaptotagmin-7 bearing dense core granules." Mol Biol Cell **25**(16): 2416-2427.

Rao, T. C., Z. S. Rodriguez, M. M. Bradberry, A. H. Ranski, P. J. Dahl, M. W. Schmidtke, P. M. Jenkins, D. Axelrod, E. R. Chapman, D. R. Giovannucci and A. Anantharam (2017). "Synaptotagmin isoforms confer distinct activation kinetics and dynamics to chromaffin cell granules." Journal of General Physiology **149**(8): 763-780.

Sugita, S., W. Han, S. Butz, X. Liu, R. Fernandez-Chacon, Y. Lao and T. C. Sudhof (2001). "Synaptotagmin VII as a plasma membrane Ca(2+) sensor in exocytosis." Neuron **30**(2): 459-473.

Wakade, A. R. (1988). "Noncholinergic transmitter(s) maintains secretion of catecholamines from rat adrenal medulla for several hours of continuous stimulation of splanchnic neurons." J Neurochem **50**(4): 1302-1308.

Watts, A. G. and C. M. Donovan (2010). "Sweet talk in the brain: glucosensing, neural networks, and hypoglycemic counterregulation." Front Neuroendocrinol **31**(1): 32-43.

Weber, J. P., T. L. Toft-Bertelsen, R. Mohrmann, I. Delgado-Martinez and J. B. Sorensen (2014). "Synaptotagmin-7 is an asynchronous calcium sensor for synaptic transmission in neurons expressing SNAP-23." PLoS One **9**(11): e114033.

Wolf, K., G. Zarkua, S. A. Chan, A. Sridhar and C. Smith (2016). "Spatial and activity-dependent catecholamine release in rat adrenal medulla under native neuronal stimulation." Physiol Rep **4**(17).

Wu, Q., Q. Zhang, B. Liu, Y. Li, X. Wu, S. Kuo, L. Zheng, C. Wang, F. Zhu and Z. Zhou (2019). "Dynamin 1 Restrains Vesicular Release to a Subquantal Mode In Mammalian Adrenal Chromaffin Cells." J Neurosci **39**(2): 199-211.

Zhang, Q., B. Liu, Q. Wu, B. Liu, Y. Li, S. Sun, Y. Wang, X. Wu, Z. Chai, X. Jiang, X. Liu, M. Hu, Y. Wang, Y. Yang, L. Wang, X. Kang, Y. Xiong, Y. Zhou, X. Chen, L. Zheng, B. Zhang, C. Wang, F. Zhu and Z. Zhou (2019). "Differential Co-release of Two Neurotransmitters from a Vesicle Fusion Pore in Mammalian Adrenal Chromaffin Cells." Neuron **102**(1): 173-183 e174.

Zhang, Z., Y. Wu, Z. Wang, F. M. Dunning, J. Rehfuss, D. Ramanan, E. R. Chapman and M. B. Jackson (2011). "Release mode of large and small dense-core vesicles specified by different synaptotagmin isoforms in PC12 cells." Mol Biol Cell **22**(13): 2324-2336.